PERFORMANCE OF VARIOUS GRINDING WHEELS IN GRINDING HARDENED STEELS

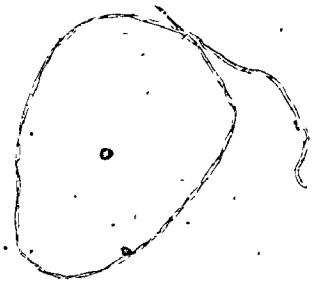

TO MY PARENTS

PERFORMANCE OF VARIOUS GRINDING WHEELS IN GRINDING HARDENED STEELS

by

SAMIR BADRAWY SHALABY, B.Sc., MECH. ENG.

A Thesis

Submitted to the School of Graduate Studies

in Partial Fulfilment of the Requirements

for the Degree

Master of Engineering

McMaster University

April, 1977

MASTER OF ENGINEERING (1977) McMASTER UNIVERSITY
(Mechanical Engineering) Hamilton, Ontario.

TITLE: Performance of Various Grinding Wheels in Grinding Hardened Steels

AUTHOR: Samir Badrawy Shalaby, B.Sc. (Alexandria University)
Production Engineering

SUPERVISOR: Professor J. Tlusty

NUMBER OF PAGES: xiv, 132

ABSTRACT

In this thesis an attempt is made to study the grinding wheel wear phenomena by analyzing the cutting force patterns, wheel wear and wear particles removed from the wheel.

Results of measurements of grinding forces and wheel wear, in addition to the scanning electron microscope observations, are presented for grinding hardened M_2 tool steel and 52100 bearing steel. Plunge-type surface grinding tests were performed with different grade hardness wheels of aluminum oxide grains in vitrified bond.

Contrary to common belief, all wheels tested were found to maintain their grinding capability, during a long grinding operation. The method proposed, for evaluating the performance of grinding wheels from force pattern and grinding wheel wear, appears to present a clear picture of the wear phenomenon. And the method could be adopted for the selection of grinding wheels.

ACKNOWLEDGEMENTS

The author welcomes this opportunity to express his gratitude to Professor J. Tlusty for his supervision of this thesis and his continual interest and encouragement.

Special note of thanks is due to Dr. I. Nesterov and Dr. M. Younis for their practical assistance in the experimental program.

The financial assistance from the National Research Council of Canada and McMaster University is acknowledged.

The excellent and patient typing by Ms. BettyAnne Bedell and Ms. Lorraine Oneschuk is greatly appreciated.

Finally the author would like to thank his family for their support and assistance.

TABLE OF CONTENTS

LIST OF FIGURES

LIST OF TABLES

LIST OF SYMBOLS

Symbol	Description	Dimensions
V_w	Work speed	ft/min.
V_s	Wheel speed	ft/min.
a	Depth of cut	in.
D	Equivalent wheel diameter	in.
d_s	Wheel diameter	in.
d_w	Work diameter	in.
G	Grinding ratio	$in.^3/in.^3$
F_n	Normal force	lbs.
$\overline{F_n}$	Specific normal force	lb/in.
F_t	Tangential force	lbs.
$\overline{F_t}$	Specific tangential force	lb/in.
W	The cutting width	in.
$\overline{Z}$	Metal removal rate	$in.^3/min/in.$
v_m	Volume of metal removed	$in.^3$
v_w	Volume of wheel wear	$in.^3$
ΔR	Radius wear	in.
$\overline{h}$	The average value of the maximum undeformed chip thickness	in.
$\overline{\ell}_{sp}$	The average chip length	in.

CHAPTER 1

INTRODUCTION

Over the years the grinding process has commanded an ever increasing position in industry, until today it is one of the most productive material removal operations. The grinding process is ordinarily accompanied by small or large amounts of wear of grinding wheels, and the degree of wear is significant in controlling the grinding performance. Wheel wear has an important effect on the economics of the grinding process. It affects the shape and size of the work piece, grinding force, work surface roughness, and wheel life time before redressing. The criterion for grinding wheel selection is normally based on the optimum wear behaviour for the operation in question.

Very few investigations have been conducted so far on hardened tool steels and bearing steels. Also, investigations carried out so far on the above mentioned steels have been with the grinding operation for a short period of time under non-severe conditions. These factors have been taken care of in the work presented in this thesis.

The aim of this work is to investigate the wear phenomena by analysing the cutting forces, wheel wear and particles removed from the wheel.

The experimental techniques adopted in this work fall

into three categories: firstly, scanning electron microscopy (ESM) to examine the grinding wheel surface, the geometrical nature of grains and formed chips; secondly, measurements of the cutting forces while increasing down feed; thirdly measurements of the grinding wheel wear, grinding ratio and corresponding forces during a longer grinding operation at a constant down feed.

The results of the experimental work are presented and discussed in Chapters 4 and 5.

Knowledge of ~~the~~ geometry of the cutting grains, the surface topography of the grinding wheels, and the form of chips was obtained and discussed in Chapter 4.

In Chapter 5, a detailed investigation into the cutting ability of the grinding wheels are described using the results of the first test.

The measurements of the grinding wheel wear and corresponding forces during the second test, provided the opportunity to explain the accompanying changes in wheel wear rate and in grinding forces.

Performance of the grinding wheels tested were evaluated in terms of grinding ratio and wheel life, so that the most suitable wheel could be recommended.

The effect of wheel hardness on both the grinding forces and grinding ratio was studied. Also the influence of dressing on the performance of grinding wheels was identified.

Conclusions obtained in each subsection are presented in Chapter 6.

CHAPTER 2

LITERATURE SURVEY

2.1 General

2.1.1 Grinding Process

During the last three decades grinding technology is developing from a finishing process for hard materials to a metal removing process by which a large amount of metal can be removed.

In precision production grinding operations, the objective is to produce work pieces to a close tolerance, with a uniform surface finish and closely controlled surface integrity in the minimum time with the minimum cost, which requires effective control of the many variables involved.

2.1.2 Grinding Wheels

The grinding wheel is a bonded abrasive body consisting usually of Al_2O_3 or SiC abrasive grain in a matrix of ceramic, resinoid, or rubber bond (Figure 1). Only the ceramic (vitrified) bonded wheels will be discussed in this project as it is the type of wheel used in the large majority of precision grinding operations. The grinding wheel may be regarded as a multipoint cutting tool with a cutting action similar to that of a milling cutter except that the cutting points are irregularly shaped and randomly

distributed over the active face of the wheel. Those grains at the surface of the wheel that actually perform the cutting operation are called active grains. In peripheral grinding each active grain removes a chip of gradually increasing thickness in a way that is similar to the action of a tooth on a slab milling cutter. The character of the chips formed varies greatly depending upon the geometry of the grit which forms them, as well as other physical considerations.

Wheels are available in different grit sizes and type and in different wheel grades and structures, that is, amounts of bond and porosity, both of which affect the performance and wear characteristics of the wheel.

Information concerning the basic structure and properties of a grinding wheel is given on the wheel itself or on the wheel washer in the form of a code which takes the following form:

Type of Abrasive	Nature of Abrasive	Grain Size	Grade	Structure	Nature of Bond	Manufacturer's Record

2.1.3 Different Factors Affecting the Grinding Process

Ramachandran and Yanathan [2] discussed the different factors affecting the grinding operation (Figure 2). The quality of the grinding wheel is one of the most important factors with respect to surface roughness, dimensional accuracy and shape of the work piece and wheel life. The

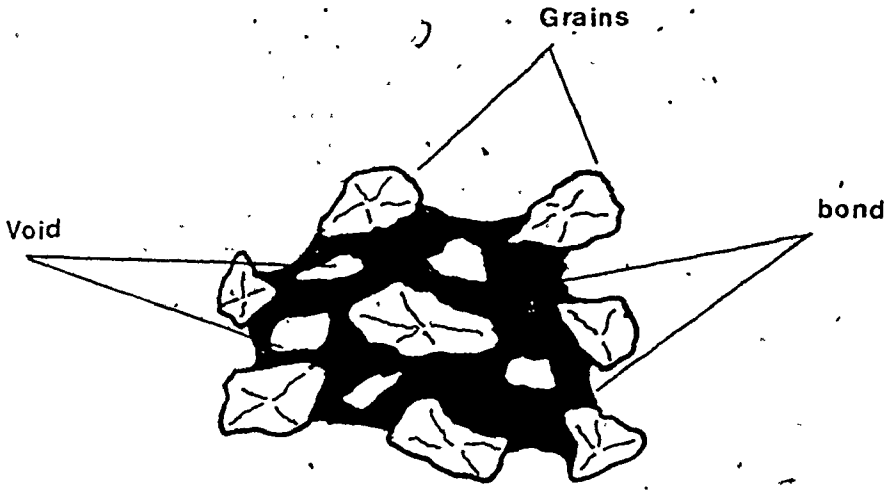

Figure 1. Grinding wheel structure.

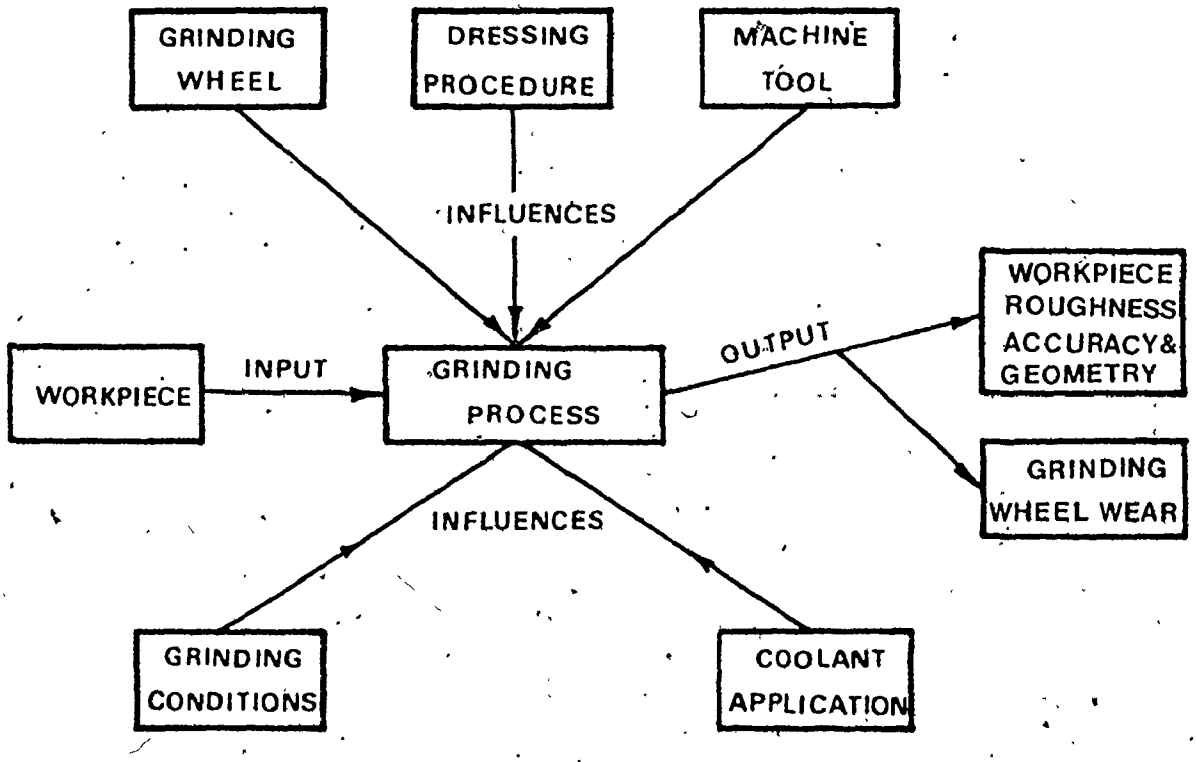

Figure 2. Factors affecting the grinding process [12].

grinding operation also depends on the correct choice of grinding wheel, the quality of which is determined by its physical and chemical properties. In addition, the grinding operation is affected by the number, shape and roughness of abrasive particles. Machine rigidity and grinding conditions affect the quality of the work piece. Grinding wheel wear may be considered as one of the measures of estimating the effectiveness of the grinding process.

2.1.4 Grinding Wheel Wear

Abrasive grains are secured within a wheel in random positions. Each active grain should act as a simple cutting tool and those which, at the beginning of a grinding operation, are not suitably shaped or positioned are either pulled bodily from the wheel or fractured as the grinding operation progresses. The grain fracturing process may convert an initially ineffective grain into an effective cutting tool.

During a grinding operation, the working face of the wheel wears away at a rate of about one million times that of a more conventional cutting tool [3]. The significance of wear is entirely different for grinding than for other cutting tool operations in which wear leads to a progressive deterioration of the tool.

In grinding, wear is an integral part of the process and, a wear rate that is too slow can be more undesirable in

its consequences than a too rapid one.

A curve relating the volume of wheel wear with the volume of metal removed in (Figure 3) is found [3] to be similar to the wear curve of any cutting tool. The curve has the usual pattern of primary, secondary and tertiary stages of wear. At the beginning of the process, the rate of wear is extremely high, but during the secondary stage the wear rate remains constant. As grinding proceeds the abrasive grains make repeated contact with the work piece; sharp edges are worn away producing flat areas on the grain. As this process continues further the flat area of the grain increases, the force on the grain also increases until it becomes sufficient to cause grain fracture producing new cutting points or rupture of the bond post throwing the grain out of the wheel.

Grindability is a term which is used to describe the ease with which a material may be ground to the required size and shape with an acceptable surface finish and surface quality. One measure of grindability is the grinding ratio 'G' and is defined as the volume of work piece material ground away per unit volume of wear worn away. By definition G is the reciprocal of the slope of the wheel wear curve in Region II.

2.1.5 Wheel Wear Mechanisms

The overall wear process is thought [4] to consist

of three simultaneous processes in (Figure 4), namely,

A) Grain dulling B) Grain chipping

C) Grain pull-out.

A) Grain dulling (attritious, abrasive or chemical wear)

Grain dulling is caused by processes which simply wear away the grain material without producing new cutting edges. Abrasive wear occurs when an abrasive work piece material (and the chips produced) simply wears away the grain. Chemical "wear" occurs when the work piece and grain materials have an affinity to each other. These forms of wear are generally undesirable as large grain plateaux (flank wear areas) are produced and new sharp cutting edges are not created. When dull grains exist at the wheel surface in sufficiently large numbers, the wheel has a glazed appearance.

B) Grain chipping (grain fracture or fragmentation)

Fracture wear occurs when stresses induced in the grain material exceed its rupture stress. These stresses may be due to mechanical loading or they may be thermally induced stresses. Grain fracture on a scale comparable with uncut chip thickness is beneficial as new cutting edges are created and a grinding operation may proceed in an efficient manner. This is often called the "self-dressing action".

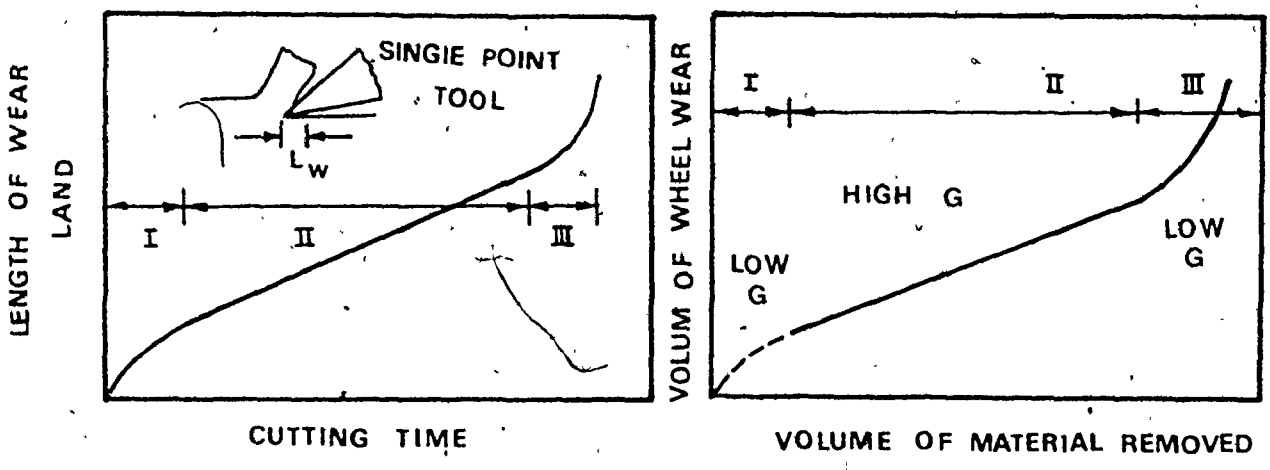

Figure 3. Variation of volume of wheel wear with volume of material removed [3].

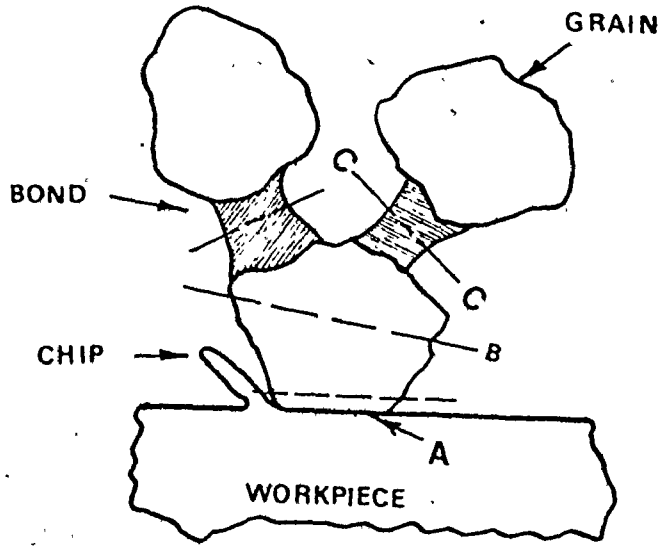

Figure 4. Illustration of the three types of wear [4].

C) Grain pull-out (Break-out or shelling)

Wheel wear also occurs when bond bridges fail and grains are simply pulled or flung from the wheel. The pull-out of complete grain, which is likely to occur when soft wheels or severe grinding conditions are employed, is a drawback particularly in the case of precision grinding. In harder wheels only a small portion of the original grain may be left when it is finally released by failure of the bond posts.

The wear mechanisms can be summerized in (Figure 5).

2.1.6 Factors Affecting Wheel Wear

The Wheel Grade (Hardness)

If for an otherwise fixed set of grinding conditions, only the wheel grade is changed, the grinding ratio tends, at first, to increase with the wheel hardness but then to reach a peak and thereafter decrease with further increase in wheel hardness [5].

Grinding Conditions

The active grains on a wheel will wear away at greater rates when they are subjected to more severe loading conditions.

Wheel Dressing Technique

The dressing technique employed to prepare a wheel for a grinding operation is known to have a significant

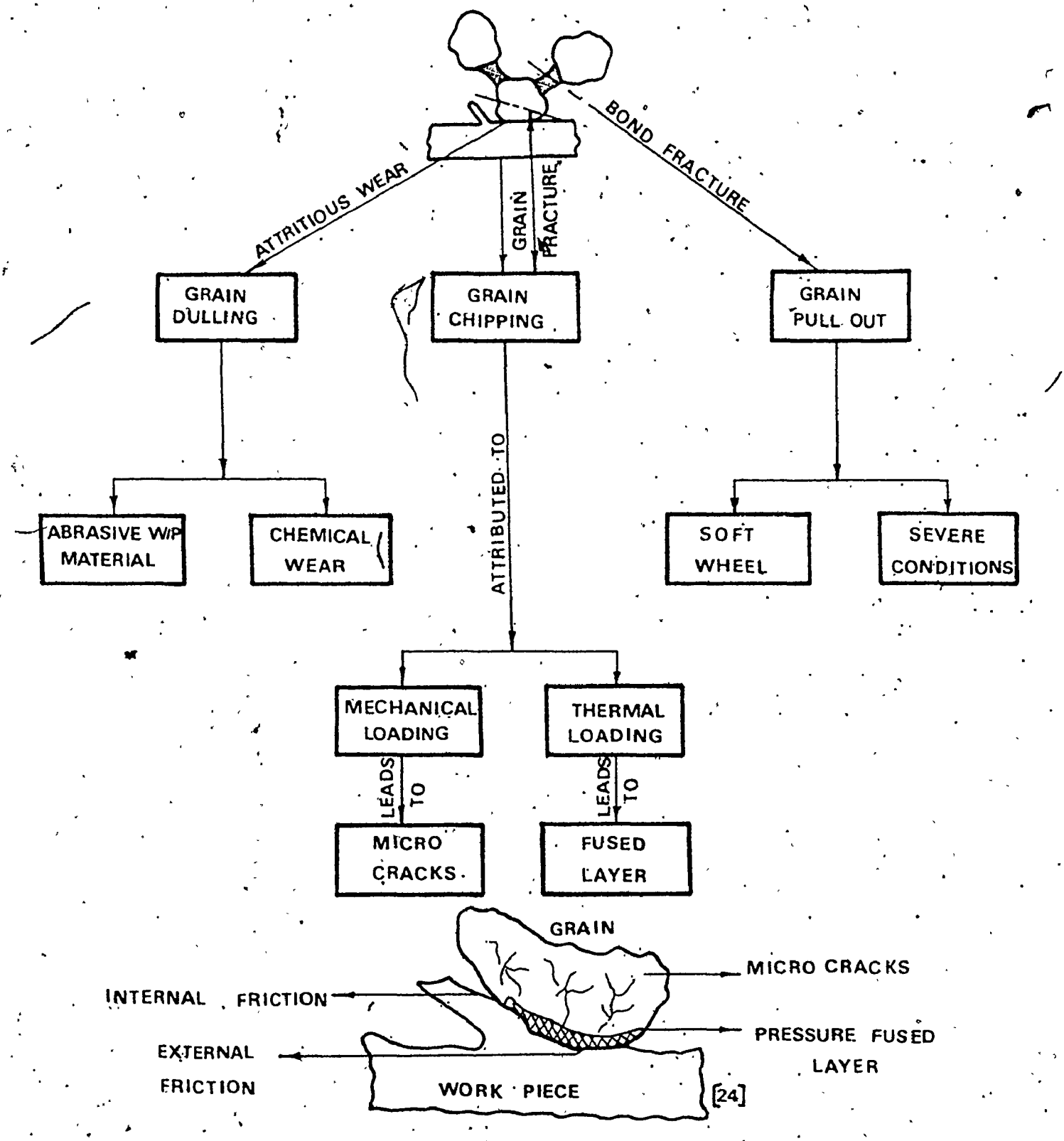

Figure 5. Wheel wear mechanisms.

effect on the initial condition of the wheel working surface.

Work piece material properties

The grinding wheel wear appears to be affected by the chemical affinity between the material of work piece and the kind of grains used as well as by the hardness of the material, specifically by the amount and size of tough carbide grains in the steel.

2.2 Bibliography

2.2.1 Wheel Wear

In grinding, wear is an integral part of the process. The criterion for grinding wheel selection is normally based on the optimum wear behaviour for the operation in question. This wear is both physical and chemical in nature. The relative significance of each of these types of wear depends upon the grinding conditions and the wheel work piece combination.

The nature of grinding wheel wear has been the subject of numerous investigations. In 1963 Yoshikawa and Sata [6] classified the wheel wear as:

1) Attritious wear of grains
2) Mechanical fracture of grains
3) Fracture of bond bridges.

Their research was concerned with the fracture of bond bridges, and with the clarification of the effect of

grinding conditions on the wear characteristics of the grinding wheel.

The effect of grinding time and force on the rate of bond fracture was verified experimentally and obtained for weakly bonded wheels (F-grade). Wear-fragments from the grinding wheel were collected by a special collector together with chips from work material which were speparated by magnet afterward. The wear fragments were screened by a set of sieves and weighed. The size distribution of wear fragments for the soft grade wheel is shown in (Figure 6) together with that of the original grains used in production of the wheel.

With a soft wheel such as this, the average wheel wear particles are only slightly smaller than the grains used in the wheel production. Virtually all the wear is due to bond fracture. In 1967 Yoshikawa [7] also attempted to generalize this approach for harder grades of wheels. The overall wear was analytically determined as the sum of grain fracture and bond fracture particles. The predictions were partially supported by experiments using grinding wheels of different grades.

In 1971 investigation of the mechanisms of grinding wheel wear and their relative importance to the grinding process was presented in two papers by Malkin and Cook [8,9]. Wheel wear was attributed to attrition, grain fracture, and

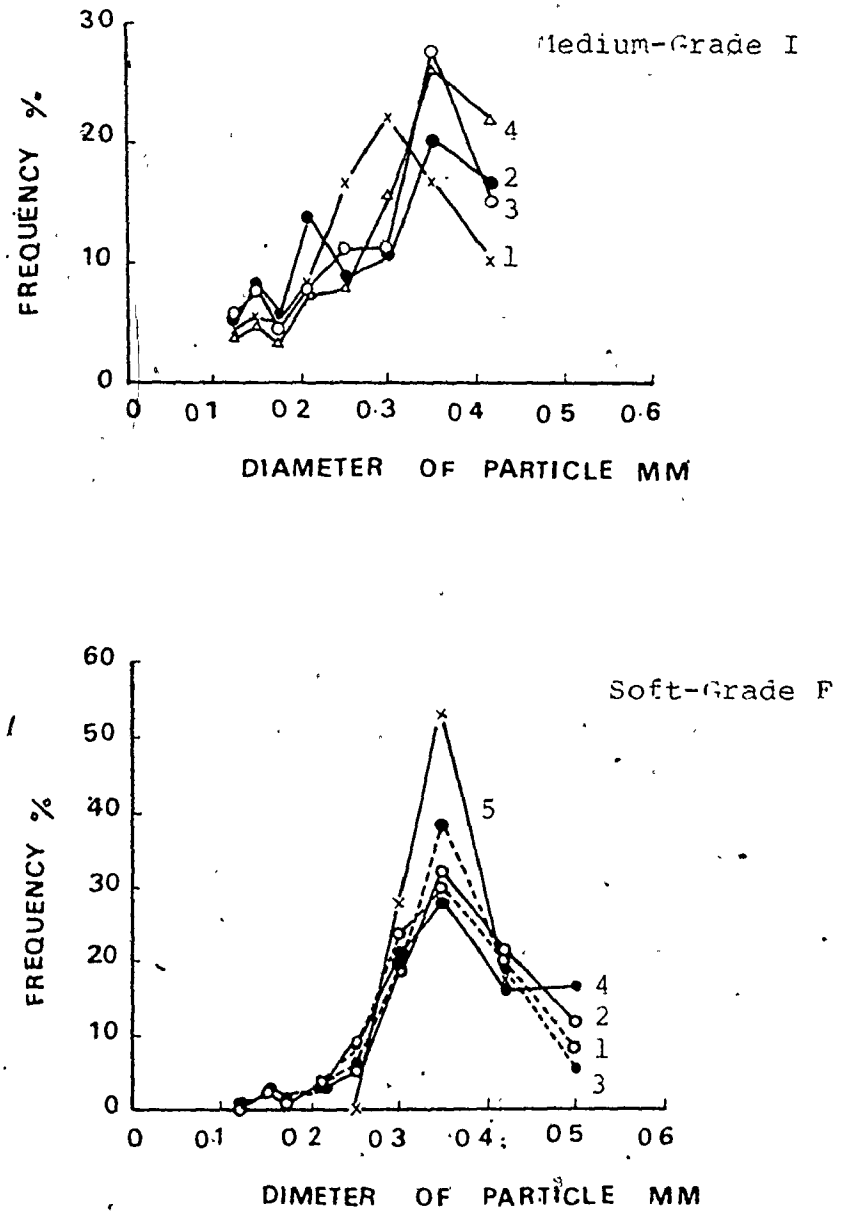

1, 2, 3, 4 Fragments under different grinding conditions. 5 size distribution of grains used in production.

Figure 6. Size distribution of wear fragments [6].

bond fracture. Attrition results in the development and growth of wear flats which are analogous to the wear land on a cutting tool. Straight line relationships were found between the grinding force components and the measured wear flat area for a given grinding condition using different dressing procedures and wheels of different grades, (Figures 7, 8, 9, 10). Finer wheel dressing or harder wheel grades resulted in larger wear flat areas and consequently gave larger grinding forces. When grinding steel, work piece burn was observed when a critical wear flat area was reached and the grinding forces increased at a faster rate with wear flat areas larger than the critical value.

The relative amount of grinding wear occurring by attrition, grain fracture and bond fracture was obtained from a statistical analysis of the size distribution of wheel wear particles collected. With soft wheel as it was proved by Yoshikawa and Sato [6], almost all the wear occurred by bond fracture, and with harder wheels, this was reduced to about half. A probabilistic analysis was developed whereby the rate of fracture wear was related to the grinding forces on each active grain. It was found that the attritious wear constitutes a negligible portion of the total wear volume, but is the most important form of wear, especially in precision grinding, because it directly controls the grinding forces and the grinding wheel tool life as limited by work.

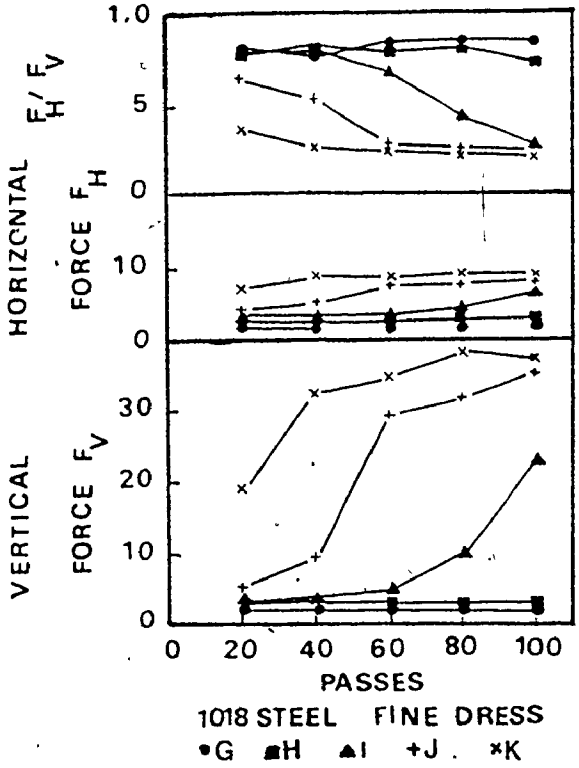

Figure 7. Grinding forces and force ratio versus number of passes (1018 steel, fine dress) [8].

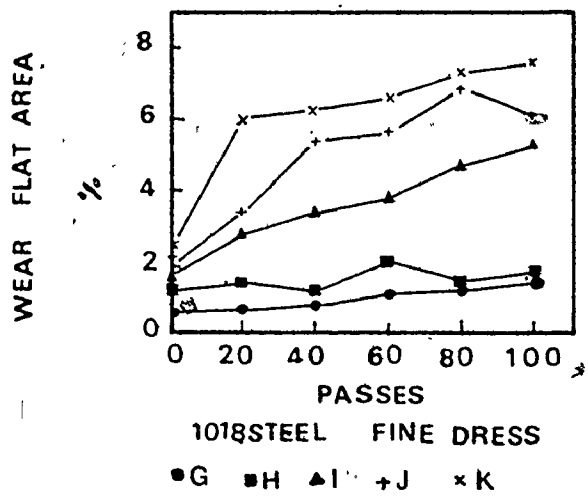

Figure 8. Wear flat area versus number of passes (1018 steel, fine dress) [8].

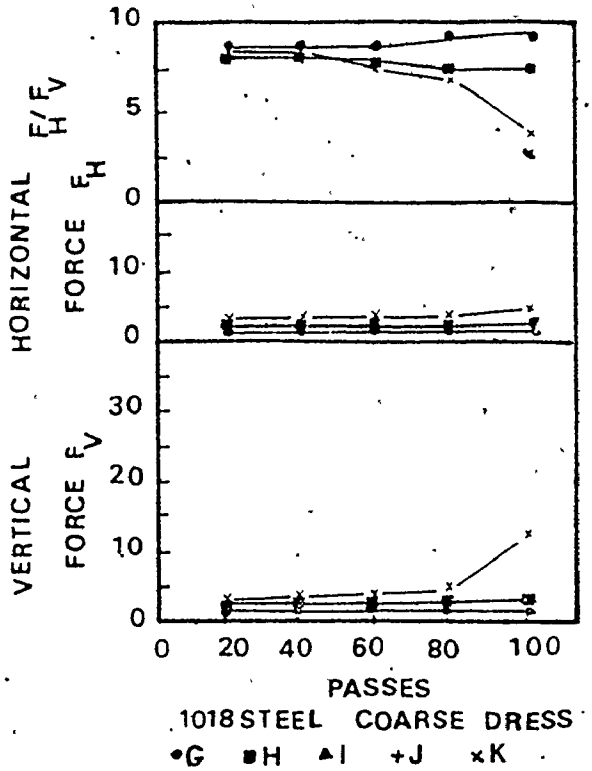

Figure 9. Grinding forces and force ratios versus number of passes (1018 steel, coarse dress) [8].

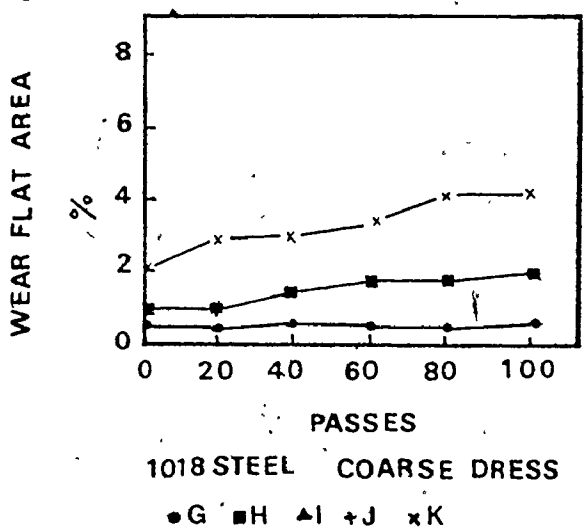

Figure 10. Wear flat area versus number of passes (1018 steel, coarse dress) [8].

piece burn.

The results obtained by Malkin and Cook [8] for the relationship between grinding forces and wear flat area in (Figures 11, 12) were also used to separate the grinding forces into their more basic components. The force intercept at zero wear flat area was attributed to cutting. The forces in excess of this at any wear flat area were attributed to sliding between the wear flats and the work piece.

The experimental results for the force versus wear flat area were used to propose a mathematical model of grinding, whereby the forces are considered to arise from ship formation, plowing and sliding process. Both the vertical and horizontal grinding forces consist of two components, one due to cutting and one due to sliding on the wear flats.

$$F_V = F_{VC} + F_{VS}$$

$$F_H = F_{HC} + F_{HS}$$

This is illustrated in (Figure 13). The linear increase of the vertical force with wear flat area, only up to transition of steels, indicates that the average contact pressure $\bar{P}$ between the wear flats and work piece is constant. Since the horizontal force also increased linearly with wear flat area, the coefficient of sliding friction u is also constant. Defining a_R as the real area of contact

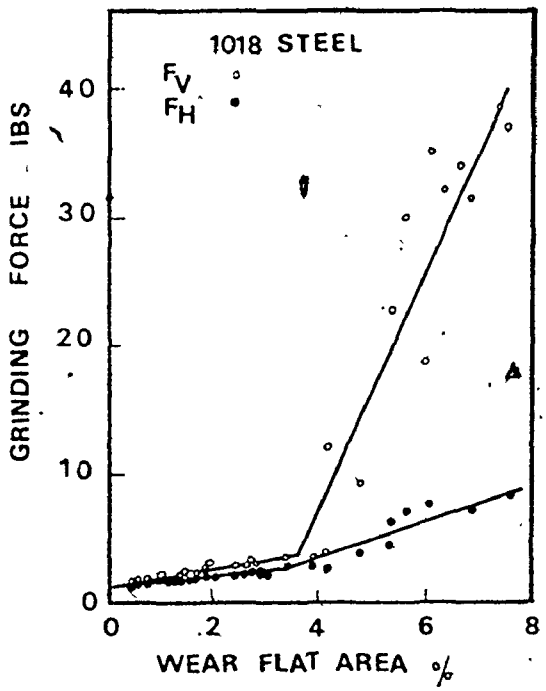

Figure 11. Grinding forces versus wear flat area for 1018 steel [8].

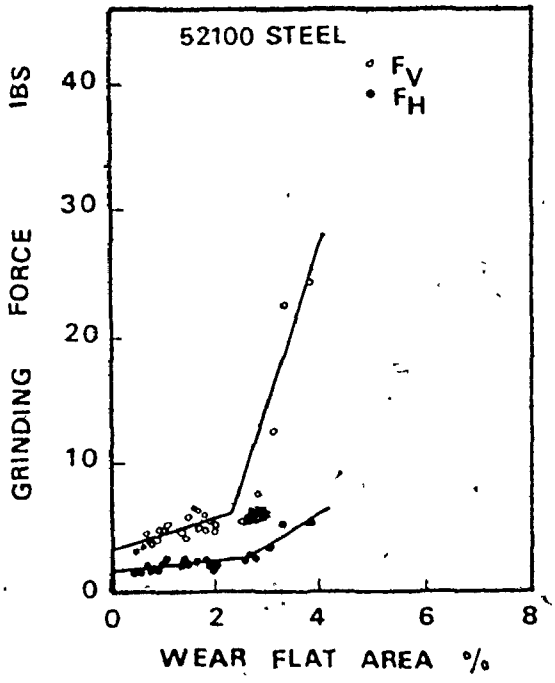

Figure 12. Grinding forces versus wear flat area for 52100 steel [8].

between the wheel and the work piece, the equations mentioned above become

$$F_V = F_{VC} + a_R \bar{P}$$

$$F_H = F_{HC} + \mu a_R \bar{P}$$

The actual wear flat pressure is equal to the slope dF_V/da_R. This is obtained by dividing the slope dF_V/d_A by the apparent grinding area.

From (Figure 14), the apparent grinding area a_A is given by the expression $a_A = bl_C$ where l_C is equal to the undeformed chip length

$$l_C = (Dd)^{\frac{1}{2}}$$

and b is the width of work piece.

The average pressure $\bar{P}$ is then

$$\bar{P} = \frac{dF_V}{da_R} = \frac{dF_V/d_A}{bl_C}$$

The friction coefficient μ is given by

$$\mu = \frac{FH_S}{FV_S} = \frac{dF_H/d_A}{dF_V/d_A}$$

Kannappan and Malkin [10] extended these experiments to cover a wide range of operating parameters and grain sizes. From their results the specific cutting energy in surface grinding, which is the total grinding energy minus the sliding energy per unit volume of metal removed, and which is obtained from using the power force component at zero wear flat area, was independent of grain size and generally decreases with an

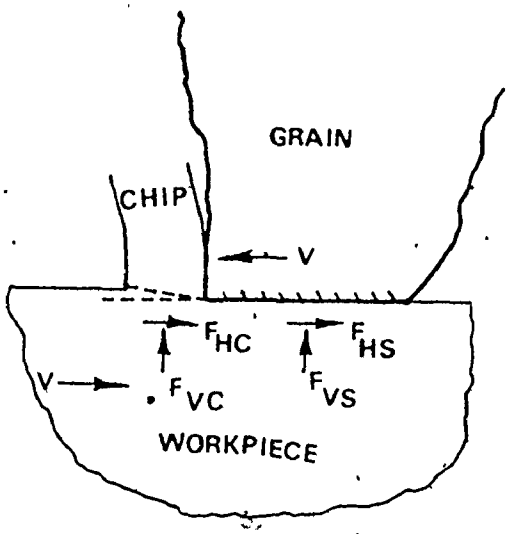

Figure 13. Illustration of chip formation and the cutting and sliding force components [8].

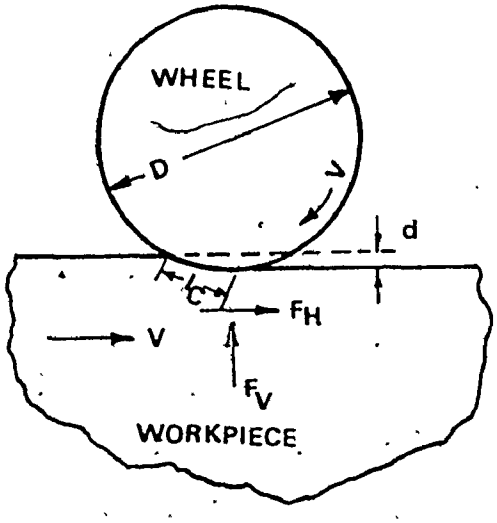

Figure 14. Grinding geometry [8].

increase in table speed and down feed. This is explained by considereing the specific cutting energy to consist of plowing energy and chip forming energy. The specific chip formation energy was found to be constant while the plowing energy decreased with work piece velocity and depth of cut. Additional results were presented which show the effect of the operating parameters and grain size on the G-ratio, the number of grinding passes prior to burning, the critical wear flat area and the energy input rate at the start of burning, and the surface finish.

In 1972, Lal and Shaw [11] studied the wear of single abrasive grains using a fly milling apparatus (Figure 15). The main purpose of this investigation was to study the overall wear behaviour of grinding wheels by observing the behaviour of single grains. Wear rates of a single grain were found to be directly proportional to the cutting length and to increase with increasing values of work piece hardness, wheel speeds, and undeformed chip thickness. The larger wear rates observed with hard abrasive grains was contrary to what is found by precision grinding. This is attributed to the differences in the thermal cycle which a grain undergoes in actual grinding and in fly milling.

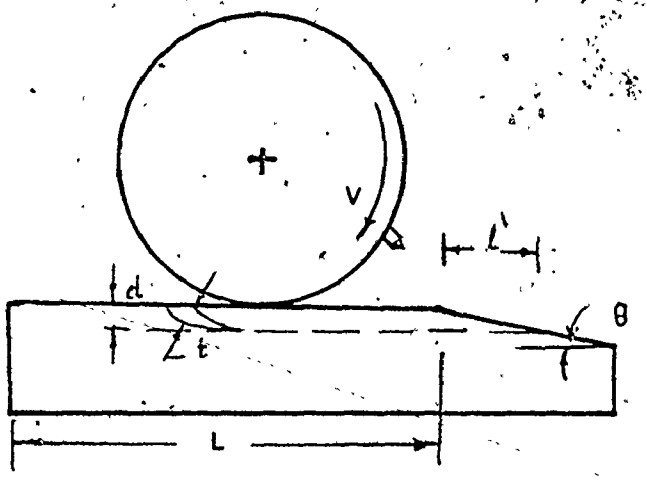

Figure 15. Test arrangement for over cut fly milling operation [11].

In 1975 Pande and Lal [12] investigated wear phenomena accompanying dry surface grinding of mild steel under plunge cut condition. Wheel wear estimates were obtained from the amount of abrasive grains collected during grinding. The abrasive grains separated from the debris were sieved and weighed and the particle size distribution was compared with the grain size distribution on the wheel to obtain the type of wear that was occurring during grinding. Wheel life estimates were estimated from the force pattern as shown in (Figure 16).

The same approach was taken by Stetiu and Lal [13] to investigate the wear phenomena accompanying cylindrical grinding from the wheel particles removed from the wheel and they were succeeded to identify the self-dressing mechanism from the wear particle size distribution.

2.2.2 Grinding Ratio

Most experimental studies of rinding wheel wear consist of measuring the G-ratio and the specific energy (Power Consumed/metal removed) for a particular grinding condition [4]. It was noticed that a small change in grinding conditions often leads to large unexplainable differences in G-ratio.

Backer and Merchant [4] used experimental evidence to show the dependence of grinding mechanics on the length and cross sectional area of the undeformed chip, and the cutting speed. They attempted to correlate the grinding ratio with these variables and their attempts were unsuccessful.

G. B. Lurie [5] found that the grinding ratio tends at first, to increase with the wheel hardness but then to reach a peak and thereafter decrease with further increase in wheel hardness. This change is thought to be brought about as a result of work piece (chip), bond interference as the quantity of the latter in the wheel structure increases, (Figure 17).

2.2.3 Cutting Capability of Grinding Wheels

H. Kaliszer and G. Trmal [16] analyzed the wheel motion relative to the work piece due to the wheel unbalance and its effect on surface topography and waviness in particular. They divided the vibration during grinding into three

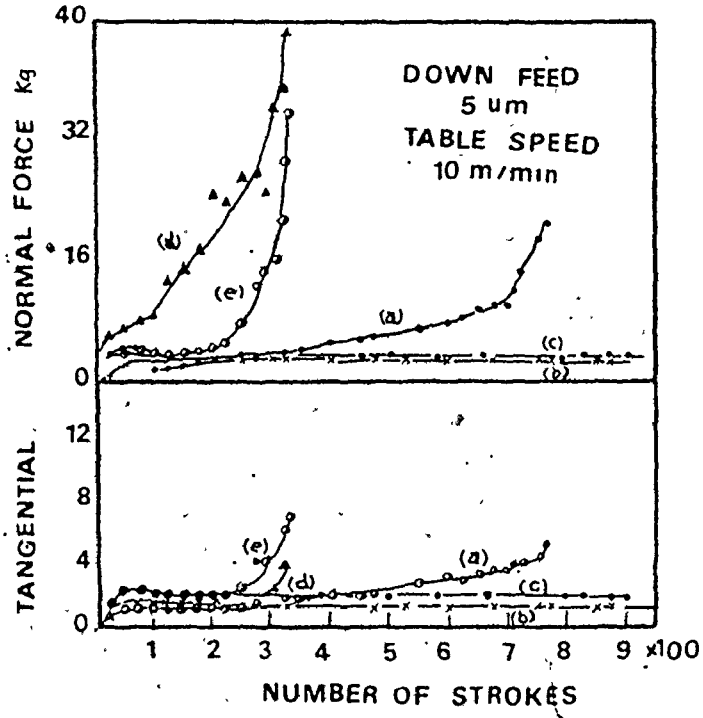

Figure 16. Variation of forces during dry grinding for various grades of wheel hardness [12].

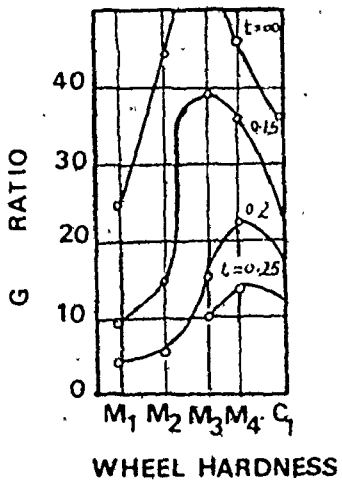

Figure 17. The Relationship between grinding ratio and wheel hardness for various in-feeds [5].

groups:

a) Forced vibration of the machine tool structure or its various parts caused by the action of known excitation forces which is mostly connected with the grinding wheel unbalance.

b) "Passive" vibrations transmitted through foundations from other machines or resulting from random changes in the work piece material, non-uniform wheel rate.

c) Self-excited vibration (or chatter) generated by the internal forces formed by the cutting action itself, without the presence of any external periodic forces. S. Shiozaki, M. Miyshita and Y. Furukaw [17] compared the self-excited vibration in grinding with that in turning by identifying the following characteristics of chatter in grinding:

A) The amplitude of vibrations grows up gradually.

B) Its growing up speed differs according to the giving grinding condition.

Kaczmark and Kornberger [18] discussed the various symptoms of deterioration of cutting capability of grinding wheels. They stated that these symptoms may appear: (1) on the work piece in the form of burns, changes of roughness, changes of waviness, changes of residual stresses and changes of the work size; (2) on the grinding wheel itself in a form of changes of the size of a wear flat area; (3) may accompany the grinding such as the grinding temperature, the grinding horsepower, the grinding forces, (and the vibration) and the

vibration and the sound accompanying the grinding.

Experimental results were presented to illustrate changes in residual tensile stresses and vibration amplitude which occur during grinding. The vibration was sensed by means of a piezo electric unit, applied to the front bearing of the grinding wheel spindle. (Figure 18) illustrates the relationship between the vibration amplitude and cutting time.

2.2.4 Dressing Influence

Malkin and Anderson [19] analyzed the relationship between the size distribution of abrasive particles removed from grinding wheels by dressing and the number of active grains per unit area on the wheel for different grain sizes and wheel grades. Relatively, more bond fracture was found with wheels of softer grades and finer abrasive grain sizes. With more bond fracture, relatively fewer grains are left near enough to the wheel periphary to take part in the grinding operation.

Tsuwa and Yasui [26] showed that the tips of abrasive grains left on the wheel surface are highly fragmented. During initial grinding, this fragile surface layer on the grain is removed leaving behind a surface which is rougher on a microscopic scale. The slight reduction in wear flat area (cutting edge ratio and grinding forces which is often found at the start of grinding was attributed to the removal of this weakly held abrasive layer. As grinding continues, the wear flat

area increases and the tip of the abrasive grain becomes smoother.

Figure 19 shows the muddy white layer disappears in the primary grinding process and afterwards the micro-unevenness appears on the surface of the cutting edges. Furthermore, as the grinding process proceeds, the worn surface increases on the cutting edge. Therefore, the fragile layer does not always affect grinding, although the layer is considered to influence the grinding force in the initial stage of grinding.

Pacitti and Rubenstein [21] studied the influence of the dressing depth of cut on the performance of a single point diamond dressed alumina grinding wheel. It was generally found that increasing the dressing depth resulted in a longer working life of the grinding wheel. This result can be attributed to increased bond fracture during dressing whereby a rougher wheel surface was generated and fewer active grains were presented. With fewer grains, the wear flat area which controls the grinding forces and wheel life should be less after a given amount of grinding. The desirability of using a more severe dressing procedure to enhance wheel life may be offset by the rougher surface finish to be expected.

Besuyen and Verkerk [22] observed the abrasive grains on the surface of a grinding wheel using a scanning electron microscope. For these observations, a segmented wheel was used whereby a section could be removed for direct observation.

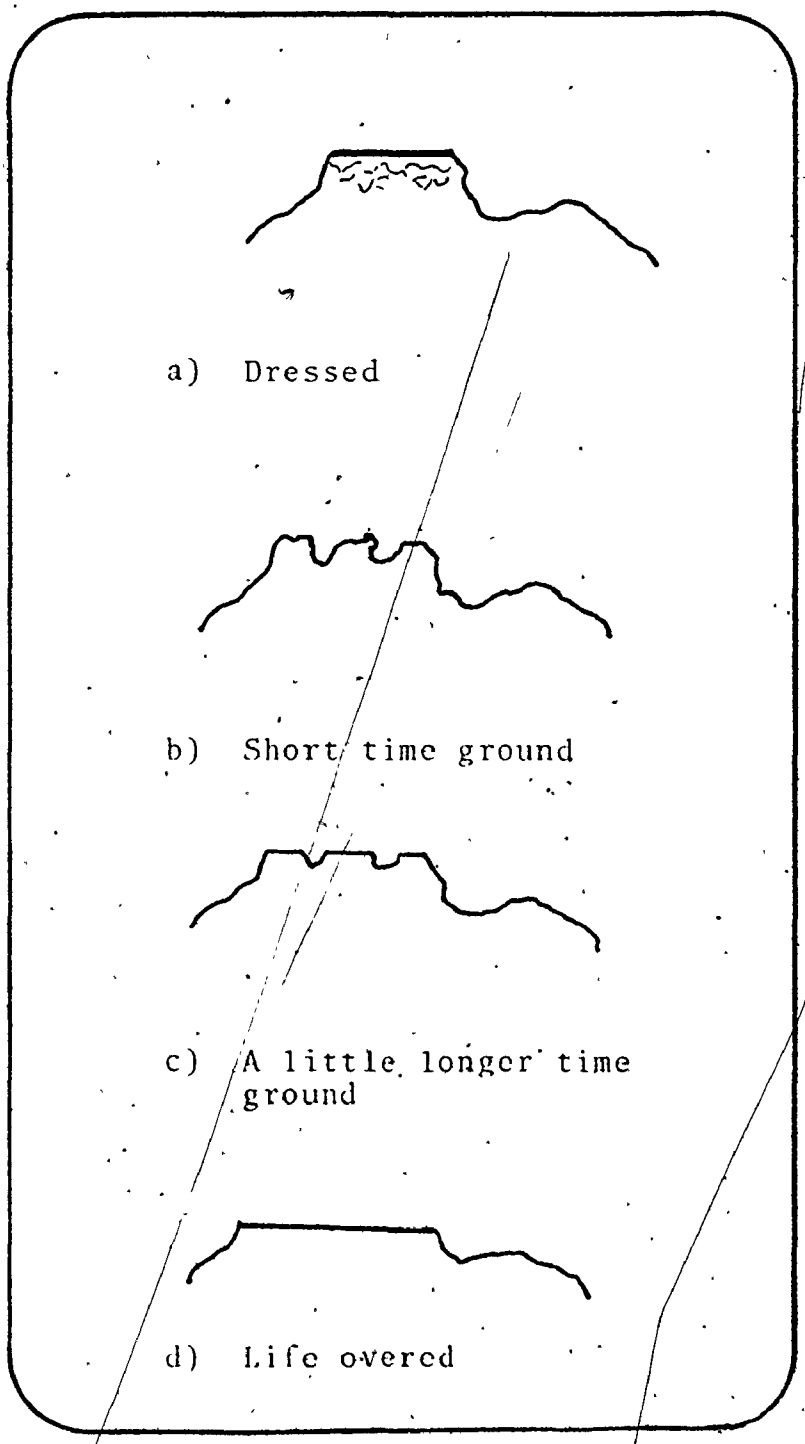

Figure 19. Schematicl representation of the wear process of the cutting edge [20].

A scanning electron microscope clearly showed the development of striated wear flats on the tips of the abrasive grains which appear to consist of a layer of work piece metal over the abrasive. Komanduri and Shaw [23] proposed a simple non-destructive method of investigating the changing aspects of abrasive grain topography in a grinding wheel. The technique involved the use of the familiar replicating technique commonly employed in transmission electron microscopy (TEM).

2.2.5 Kinematic Characteristics of the Grinding Process

H. Optiz, W. Konig, G. Werner [24] described a new method to determine the three-dimensional edge distribution in the wheel surface. Using a stylus and measuring in the circumference direction, the number of edges touched in a certain tracing depth was put into relation to the tracing length, which yields the number of edges per unit of length S static as function of depth Z under the wheel surface. Figure 20 shows this relation between the number of edges per unit length and the tracing depth. Considering the average edge shape perpendicular to the circumference direction of the wheel, it was possible to determine mathematically the three-dimensional number of edges per unit of wheel surface and tracing depth, deriving from the two-dimensional number of edge per unit of length.

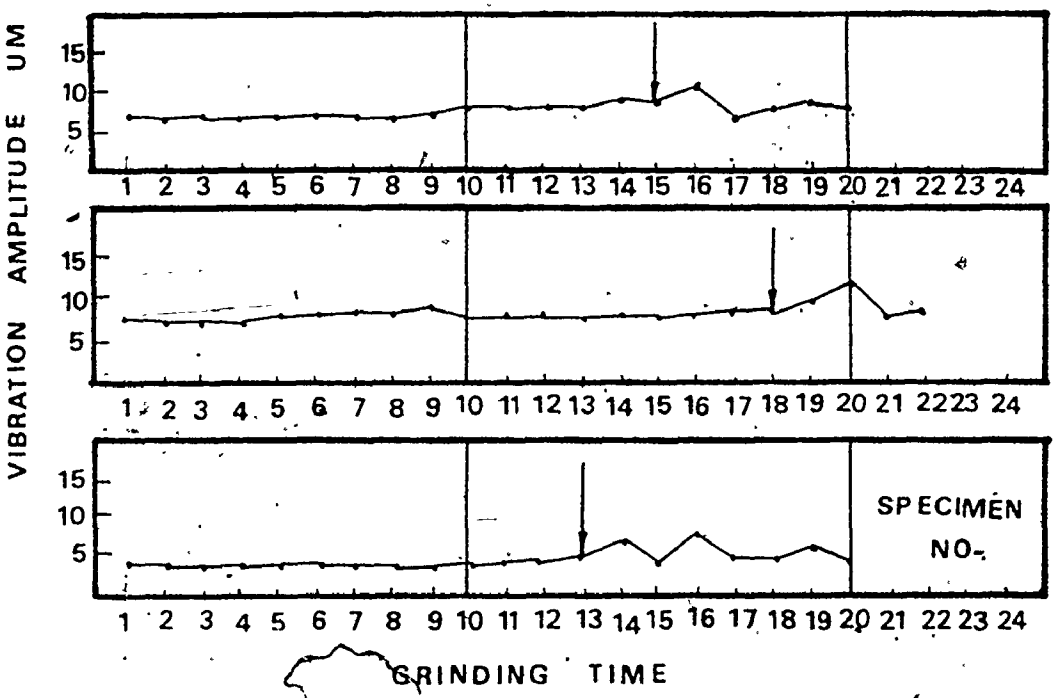

Figure 18. Relationship between vibration amplitude and the grinding time [18].

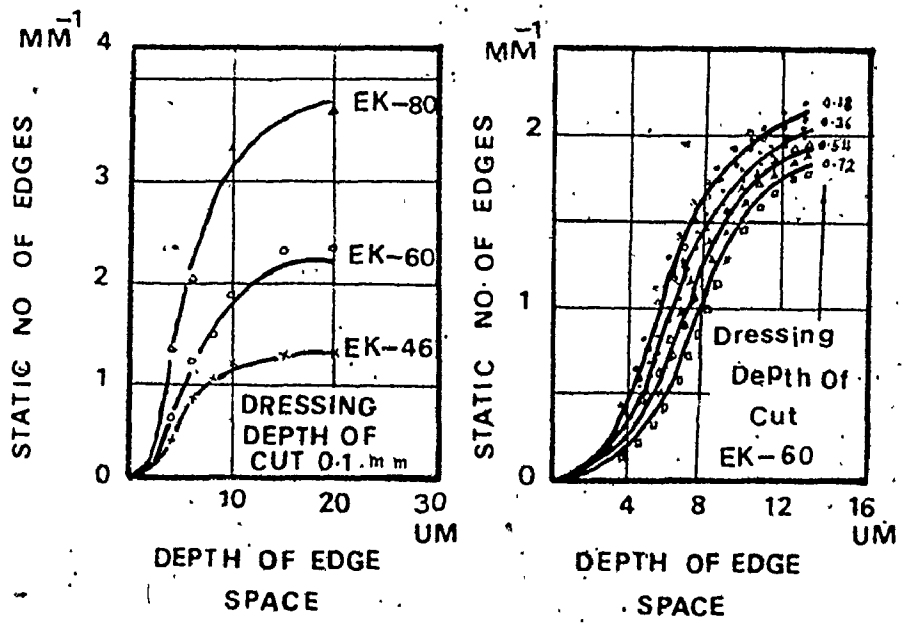

Figure 20. Static number of edges as a function of depth of edge space [24].

A distinction between the total number of cutting points existing in the edge space of the wheel (static number of cutting edges) and the part of these cutting edges actually doing the cutting work (dynamic number of cutting edges was made.

The important kinematic characteristics of the grinding process were formulated as functions of essential grinding parameters. Those which were used are:

a) Number of engaging (dynamic) cutting edges per unit of the wheel surface

$$N_{dyn} = A \left[\frac{2.C_1^{P/q}}{K_S}\right]^{\alpha} \left[\frac{V_W}{V_S}\right]^{\alpha} \left[\frac{a}{D}\right]^{\alpha/2}$$

b) Average value of maximum cross section at the end of contact length

$$\overline{Q}_{max} = \frac{2}{A} \left[\frac{K_S}{2.C_1^{P/q}}\right]^{\alpha} \left[\frac{V_W}{V_S}\right]^{1-\alpha} \left[\frac{a}{D}\right]^{\frac{1-\alpha}{2}}$$

c) The depth to which the engaging grinding edges extend into the edge space

$$z_e = \left[\frac{2}{C_1 \cdot K_S}\right]^{\frac{1}{P+1}} \left[\frac{V_W}{V_S}\right]^{\frac{1}{1+P}} \left[\frac{a}{D}\right]^{\frac{1}{2(P+1)}}$$

d) Geometrical contact length between wheel and work piece

$$\ell_K = [a.D]^{\frac{1}{2}}$$

e) Average chip length

$$\bar{\ell}_{sp} = \frac{1}{1+\alpha} [a.D]^{\frac{1}{2}}$$

f) Average value of the maximum undeformed chip thickness

$$\bar{h} = \frac{1}{A^P} \left[\frac{2}{C_1 . K_S}\right]^{\frac{1}{P+1}} \left[\frac{V_W}{V_S}\right]^{\frac{1}{P+1}} \left[\frac{a}{D}\right]^{\frac{1}{2(P+1)}}$$

g) Static number of cutting edges per unit of the wheel surface

$$N_{stat} = C_1 . K_S . Z^P$$

h) Static number of cutting edges per unit of length

$$S_{tat} = C_1 . Z^q$$

where:

V_W = work speed [mm/s]

V_S = wheel speed [mm/s]

a = depth of cut [mm]

D = equivalent wheel diameter [mm] = $d_w . d_s / (d_w \pm d_s)$

d_s = wheel diameter [mm]

d_w = work diameter [mm]

C_1 = static edge density [mm^{-3}]

K_S = factor considering the mean edge shape perpendicular to the cutting direction

Z = depth of edge space

P, q = exponential coefficients considering the edge distribution in the periphery of the wheel

α = comprehensive exponent = $q/(P+1)$

A = integration constant

The mechanism of chip formation is described in Figures (21) and (22).

In the first phase of contact, no chip formation takes place. As the depth of penetration of the cutting edge in the workpiece increases the workpiece material is deformed at first elastically and then plastically under the cutting edge. The energy created by friction and plastic deformation is converted immediately into heat. The amount of heat increases as the contact length increases leading to the reduction of resistance of the material. As a result, after reaching a certain temperature the process of plastic deformation is converted into a process of flowing chip formation.

The researchers concluded that the conventional chip formation such as encountered in metal cutting operations could not occur with the negative rake angle of about -85° normally encountered in grinding. It was suggested that chip could form; however, if the temperature was sufficiently large for visco plastic deformation. In that case the high negative rake angle is actually necessary and the temperature is constant and independent of cutting speed (Figure 23).

Based on the mechanics of chip formation, the authors explained a number of practical phenomena in the grinding process and derived the following force equation:

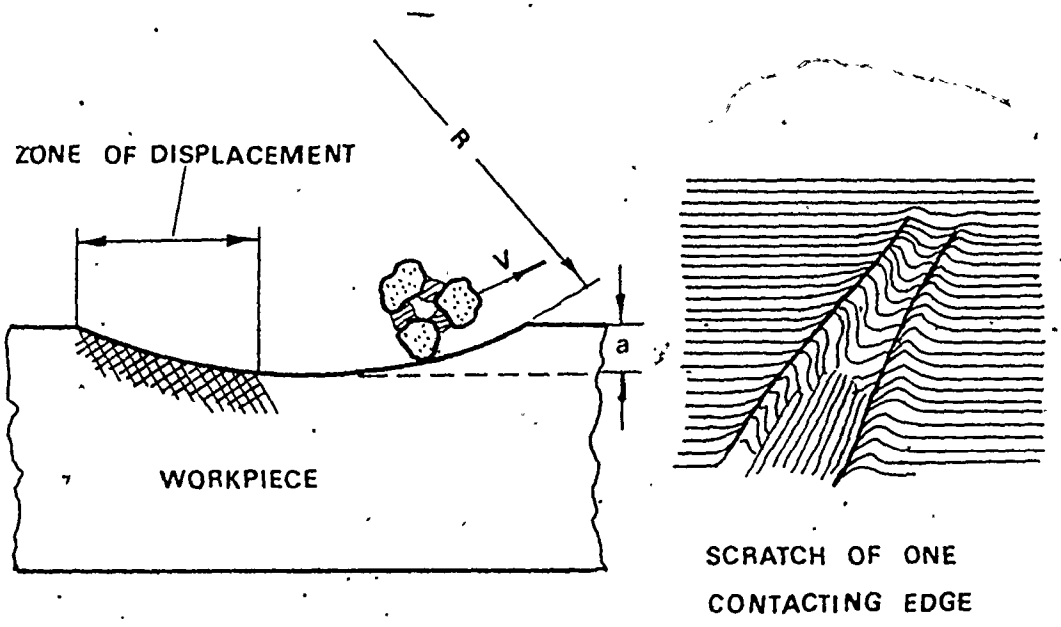

Figure 21. Plastic contact at first contact between cutting edge and work [24].

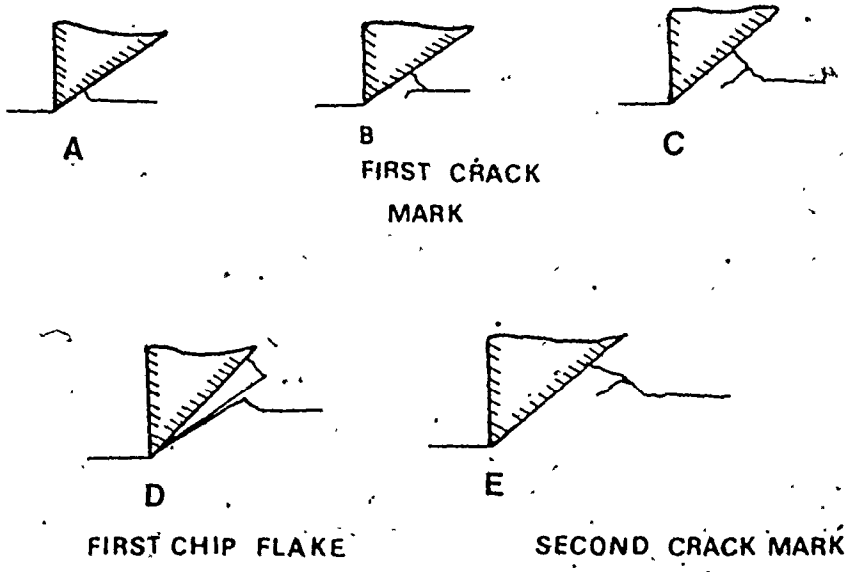

Figure 22. Chip formation at negative rake angle (γ-68) and low

$$F_n = K.A_1(n) \cdot \left[\frac{C_1^2}{\text{tank}}\right]^{\frac{1-n}{3}} \left[\frac{V_W}{V_S}\right]^{\frac{2n+1}{3}} [a]^{\frac{n+2}{3}} [D]^{\frac{1-n}{3}}$$

The interpretation of force equation confirmed a number of practical facts (Figure 24).

As the exponential factor n is always smaller than 1, the grinding forces increases degressively versus the speed ratio V_W/V_S, the depth of cut and the equivalent wheel diameter. The influence of edge density factor C_1 also corresponds to the practical given facts. The cutting forces increase with greater C_1 value, i.e. with finer grain or finer dressed wheels.

Köing and Lortz [25] developed a measuring system for characterizing the topography of a grinding wheel, using the stylus method, measuring in the circumference direction. The number of active cutting edges was combined with the dynamic chip thickness as well as shape and angle of cutting edges and their distance from each other.

The most important knowledge resulted was that only a small part of the dynamic cutting edges contributes to the actual chip formation process as it can be seen from Figure 25.

A three-dimensional analysis of the structure of the cutting area is also made by Köing and Lortz [26]. By tracing in circumferential as well as in transverse direction, they obtained interrelation between the cumulative static cutting edges and the radial depth of penetration as it is shown in Figure 26. With the help of measuring devices and corres-

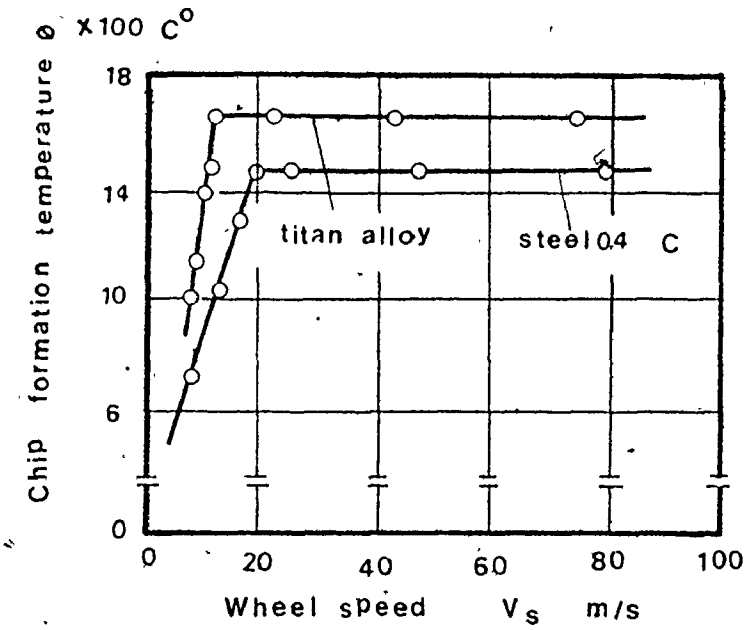

Figure 23. The relationship between chip formation temperature and wheel speed [24].

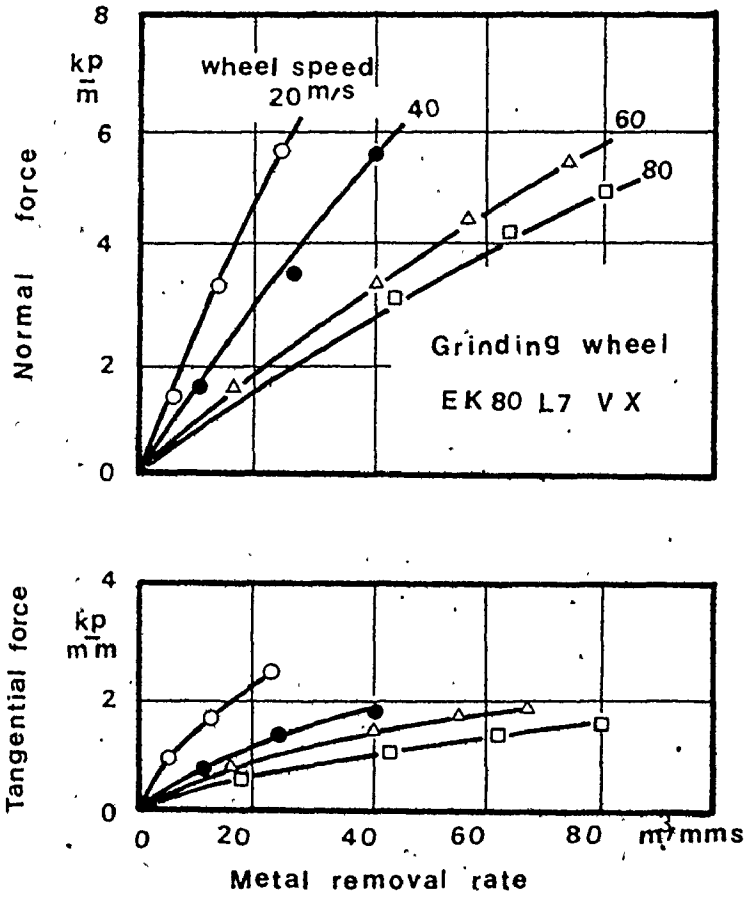

Figure 24. Cutting forces as a function of metal removal rate [24].

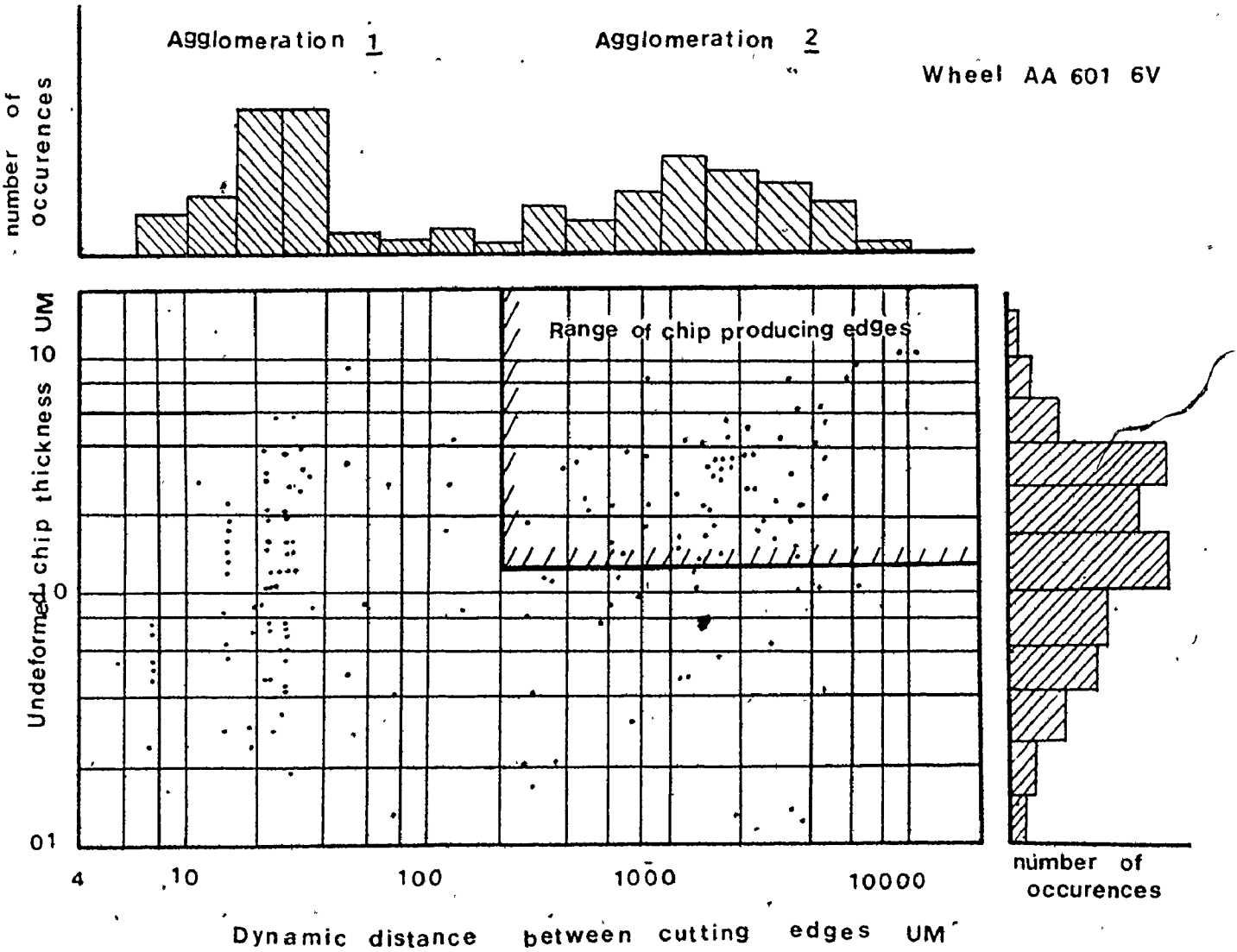

Figure 25. Effective cutting edges under consideration of kinematic and mechanical relationships [25].

ponding evaluation system, it was possible to calculate experimentally, the dynamic cutting edges as well as the chip thickness and the dynamic cutting edge distance.

Using statistical principles it was possible to extend all the considerations of a two-dimensional area to a three-dimensional space (Figure 27).

An example of a technological relationship between grinding wheel topography and the obtained result was shown in Figure 28, using a G-grade soft wheel.

It was noted that the number of three-dimensional cutting edges increases at the beginning of the grinding process and reaches its maximum value about 8 seconds after dressing. As a result of mechanical overloading of the active cutting edges the grains are dulled which is followed by the breaking away of the bonding bridge and decreasing of the number of cutting edges.

Dressing, hardly showed any influence on the cutting edges after 40 seconds of grinding time.

With the change of the number of cutting edges, the normal force also changed. When more active edges came in contact with the work piece, there was an increase in the normal force.

During the decrease of the number of active cutting edges, wear flat on grains increased and, eventually self-sharpening took place.

The number of active edges and work piece roughness

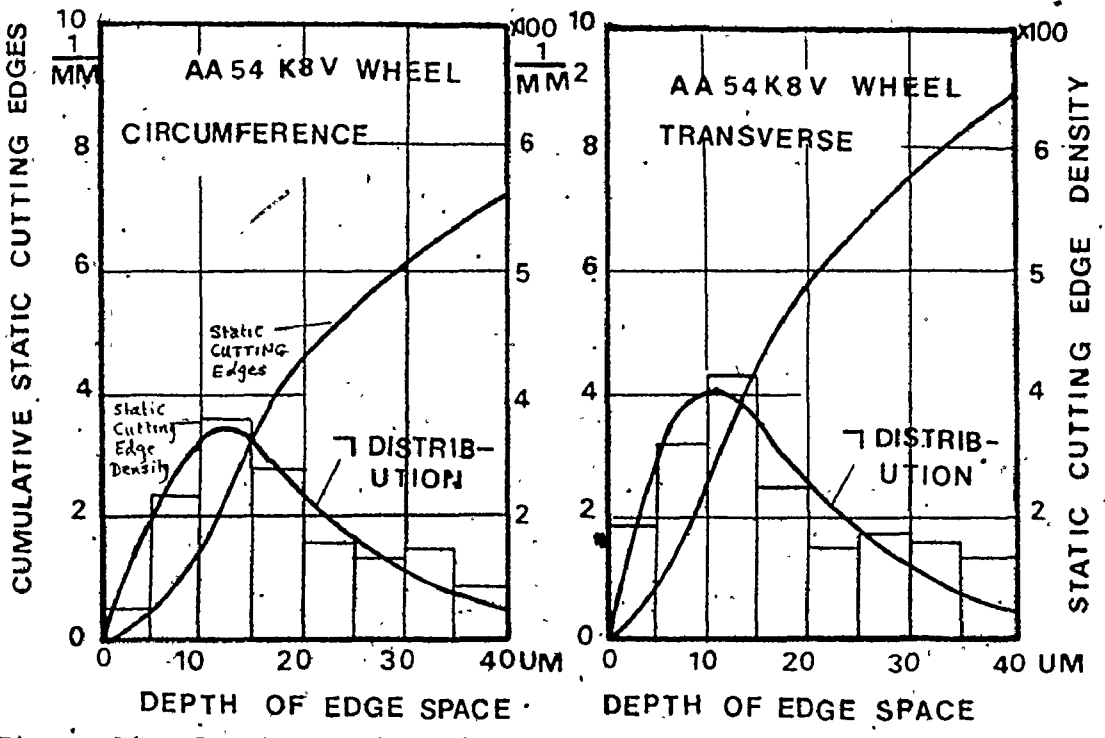

Figure 26. Static cutting edges as a function of depth of edge space [26].

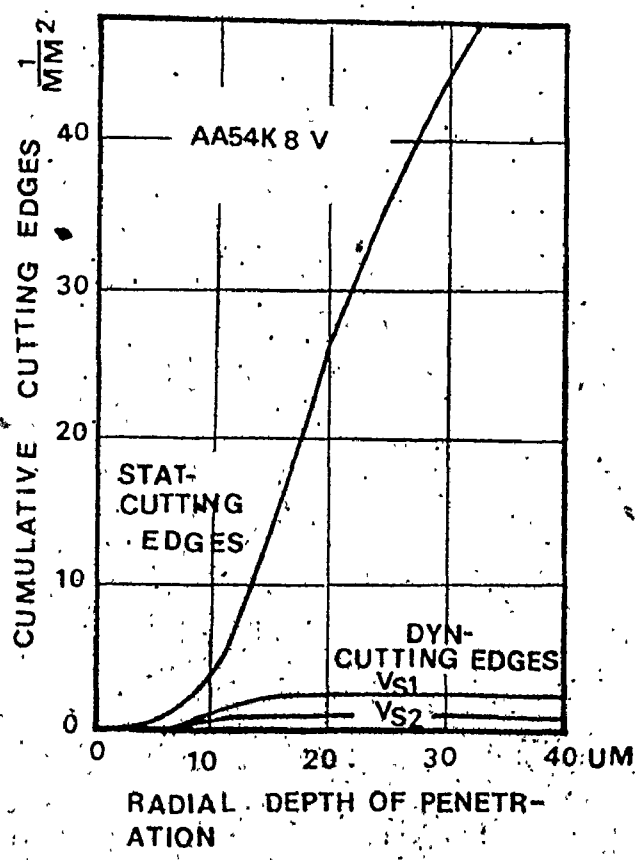

Figure 27. a

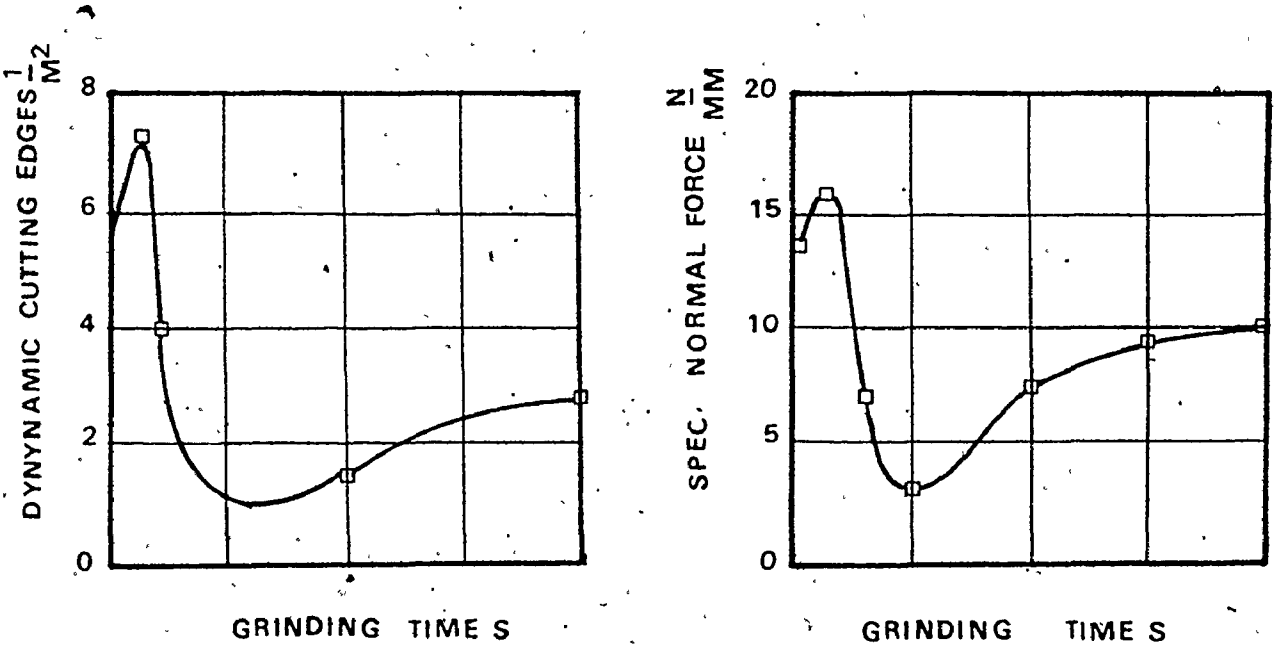

GRINDING WHEEL AA G V

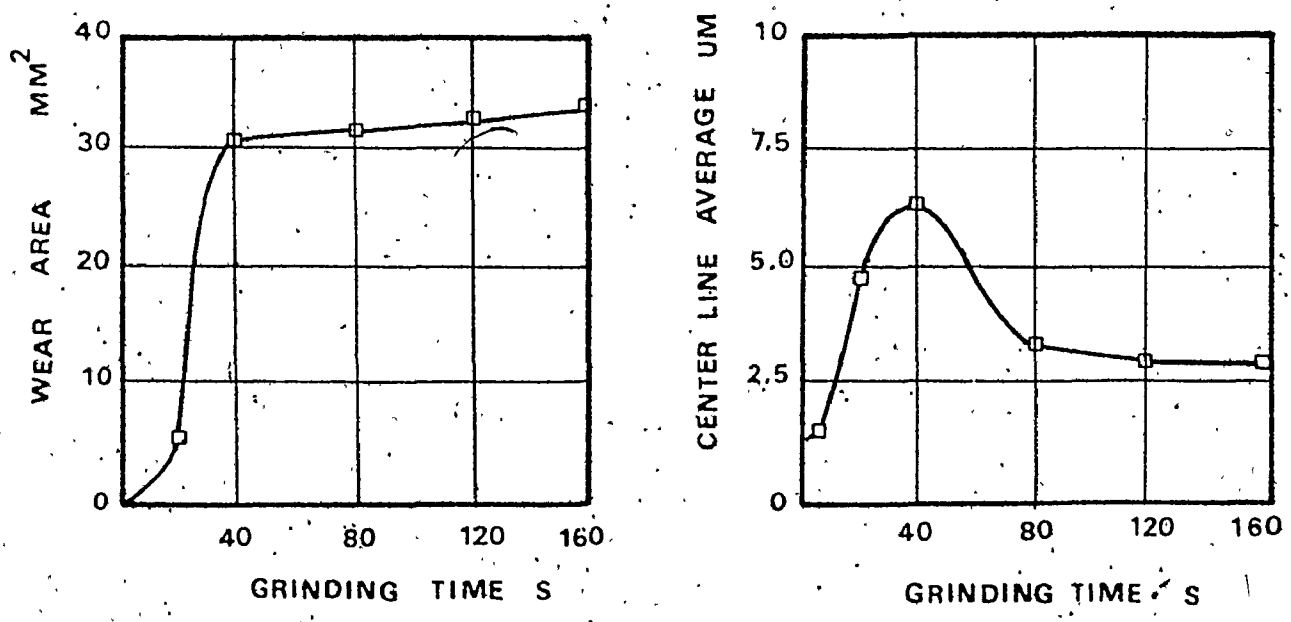

Figure 28. Development of the interrelations between grinding wheel and work piece during grinding time [26].

CHAPTER 3

TEST CONDITIONS

3.1 Equipment and Materials

3.1.1 Machine and Accessories

The experimental apparatus used in this investigation is shown in Figure 29. All tests were carried out on a THOMSON surface grinder Model 3B, with the following modifications:

1) A specially designed head stock, 10 HP with a two-speed electric motor; conventional speed, 1800 r.p.m. and high spped, 3600 r.p.m. This in combination with a 14 inch diameter grinding wheel, gives 6,600 ft/min. and 13,200 ft/min. peripheral grinding speeds respectively.
2) A special cooling system, in Figure 30, consists of 16 gal/min. at 150 psi pump. To improve the cooling efficiency a deflector is used on the coolant nozzle which eliminates the boundary air layer around the grinding wheel and thus enables the coolant stream to reach the wheel surface shown in Figure 31.
3) A special arrangement of table driving pump with an 3600 r.p.m. electro-motor, 5 HP which gives maximum table speed up to 130 ft/min.

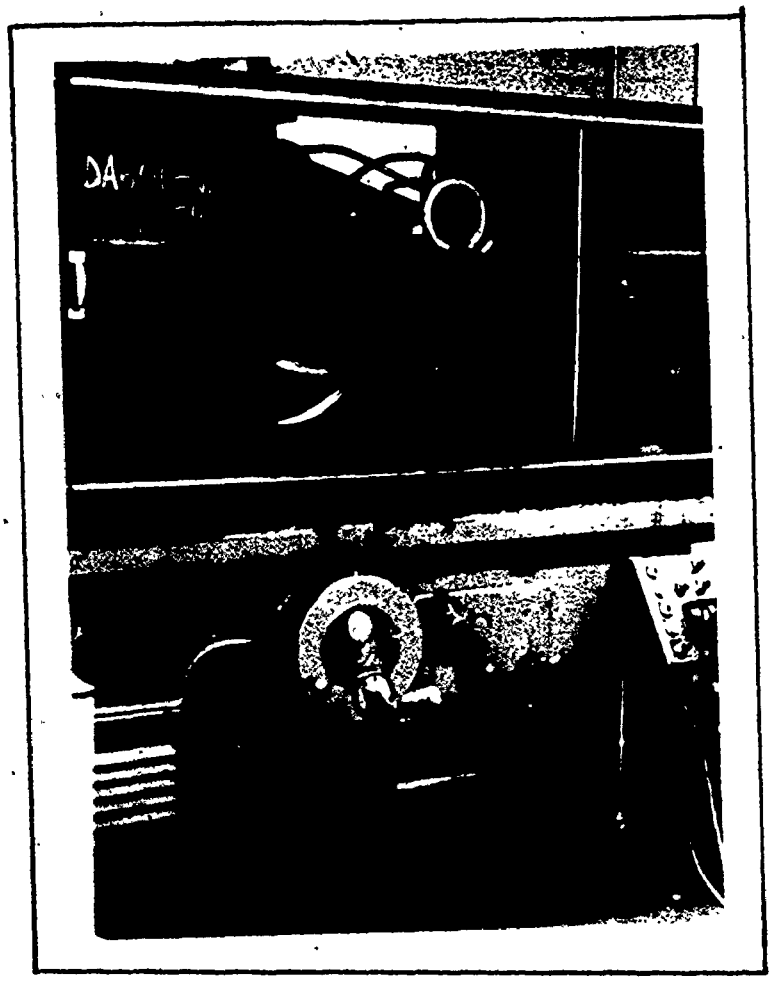

Figure 29. Thomson Surface Grinder Model 3B.

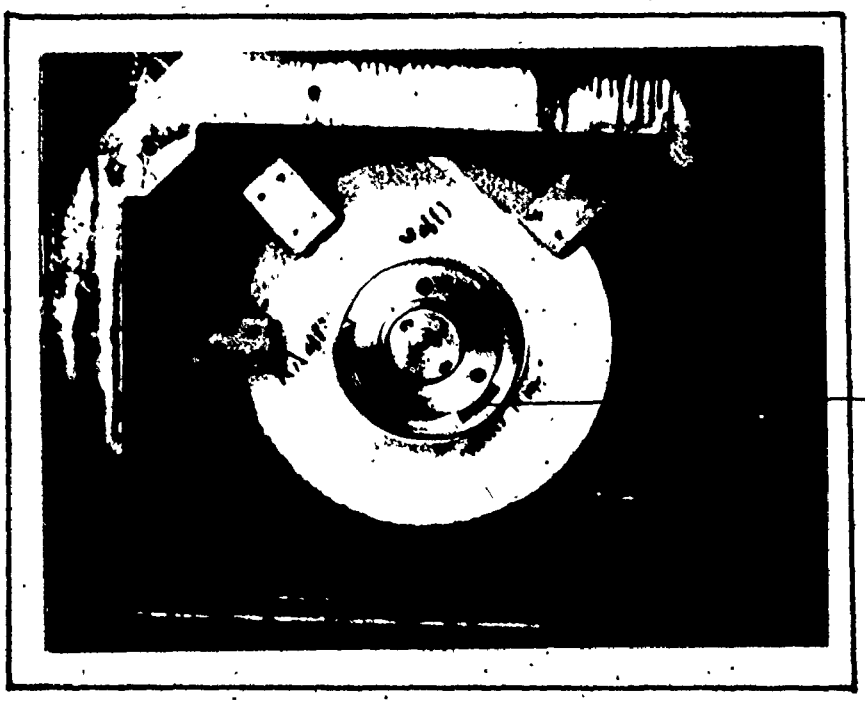

Weights for Dynamic Balance of Grinding Wheel.

4) A special wheel guard made of steel plate 0.5 in. thick and lined with an 0.5 in. thick layer of polyurethane in (Figure 32).

5) A special enclosure over the table for containing all the spray of the increased amount of coolant in (Figure 29).

3.1.2 Wheel Size

All tests were run using a wheel, 14 inch diameter; 1 inch wide, and a 5 inch bore on a 1/4 inch wide work piece under plunge cutting condition (with no cross feed).

3.1.3 Work Piece Materials

Tool steels M_2 and 52100 steel were selected for the tests described here. M_2 is rather common molybdenum high speed steel and it may be considered as an average representation as regards to grindability of tool steels. 52100 steel is an AISI high Carbon Chromium Steel. Work piece dimensions were 6 inches long X 2 inches wide and 2 inches high. The work piece materials together with their chemical composition and room temperature hardness are listed in Table 1.

3.1.4 Grinding Wheels

A number of grinding wheels were used for this investigation. Two different grain types were used, denoted

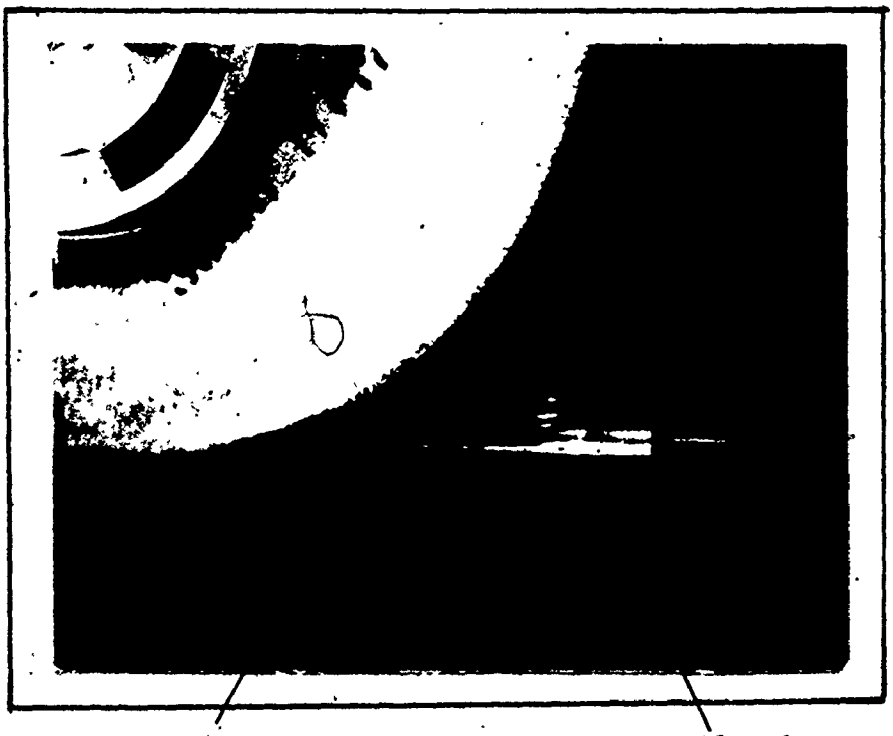

Figure 31. Coolant-Nozzle With Deflector.

Figure 32. Special Wheel Guard.

here as A and B. Three hardness grades are tested which differ in the amount of vitreous bonding material. The 60 grain size corresponds to a mean grain diameter of about 0.01 inch. The grinding wheels used are described in Table 2.

The range of hardness as expressed by the J, M and P grades has been chosen as they represent the range of gradings used in centerless and cylindrical grinding, and it excludes the ~~also~~ common soft grades, H and G.

3.1.5 Coolant

Cimperial 20 soluble oil at 20:1 concentration with water.

3.1.6 Dressing Conditions

The wheel was dressed before each test by a single point diamond tool without any spark-out and with dressing depth of cut a_d = 0.001 in., dressing lead = 0.01 in/rev., wheel speed V_s = 6600 ft/min.

3.1.7 Constant Cutting Prameters

The wheel speed and table speed, during the majority of the tests, were kept constant at 6600 ft/min. and 100 ft/min. respectively.

Material	Chemical Composition,%	R_c
M_2	0.85C, 4.5Cr, 5.00V, 12.5W, 0.6M_o, 5.0C	61
52100	1.00C, 0.35M_o, 0.30si, 1.4Cr, Bal F_e	62

Table 1. Workpiece Materials

Type of Grains	Hardness Grade	Grain Size
A	J	60
A	P	60
B	J	60
B	M	60
B	P	60

Table 2. Description of Wheels

3.1.8 Balancing of the Grinding Wheel

In spite of all precautions taken during the manufacture of the grinding wheel, it is never perfectly balanced. An unbalanced wheel produces a centrifugal force which induced a relative vibratory movement between the wheel and the work piece. The amplitude of this movement depends on the rigidity, size and design of the grinding machine and leads to the formation of work piece and wheel waviness generated on their circumferences; thus, the level of unbalance in the wheel has a large influence on the quality of the work being ground.

In order to avoid these forced vibrations due to the wheel unbalance, the wheel was carefully, dynamically balanced at the beginning of its test to a vibration amplitude of less than 5×10^{-6} in.

Two equal weights were mounted on the wheel flange (Figure 30) in such a way that the resultant force is equal in magnitude and in opposite direction with the unbalanced weight. A velocity pick-up transducer was used to measure the amplitude of the vibration on the screen of an oscilloscope.

3.2 Force Measurements

3.2.1 Dynamometer

A high quality 3-component dynamometer has been designed and constructed, capable of measuring the forces

of a bound to hundreds of pounds. The load-sensitive elements are piezo-electric force transducers, in the form of thick washers, which are rapidly finding their way into research and development measurements as standard equipment.

3.2.2 Piezo-Electric Transducers

The transducer is designed to decompose a force acting in any direction into three components perpendicular to one another. For each of the three force components, a proportional charge signal is produced in the measuring element. These charge signals are fed to the charge amplifier where they are converted into voltage which may be indicated or registered as desired.

Because of its design, this force-measuring element is very rigid. Consequently, it has a high natural frequency. For this reason, it can be applied to objects to be measured without noticeably affecting their elastic properties.

3.2.3 Calibration

The dynamometer was calibrated, while mounted on the table of the machine, vertically up to 40 lbs. using dead weights and horizontally up to 60 lbs. using a spring-type pull scale. Both the vetical and horizontal systems were completely linear and there was negligible interaction between horizontal and vertical forces.

3.2.4 Dynamometer Specification

The sensitivity is 0.625 lb/mv in the normal direction and 0.286 lb/mv in the tangential direction. The cutting forces signal was recorded by means of an ultra-violet (u.v.) recorder, provided with a pre-amplification range of 1 to 1000 times, resulting in sensitivities of the record obtainable in a range of 150 lb/in. up to 0.1 lb/in. A magnetic chuck with 6 inch width x 12 inch length was mounted on the top of the dynamometer.

3.2.5 Basic Circuit

The basic circuit of the measuring installation is illistrated in (Figure 33). The three load cells were placed on a triangular shape and were connected in parrallel. This way has the advantage that both vertical and horizontal components of the forces can be recorded correctly irrespective of the grinding position along and across the table of the dynamometer and the out-put voltage represents the sum of the charges at the input of the charge amplifier.

The transducers were connected to three charge amplifiers, whereby the electrostatic charge (PC) generated by a quartz measuring transducer was converted into a proportional voltage. A power supply was used to give an input current to the charge amplifiers and take the out-put signal. A D-C off-set was used to adjust the input voltage to the u-v recorder and an amplifier to amplify the signal

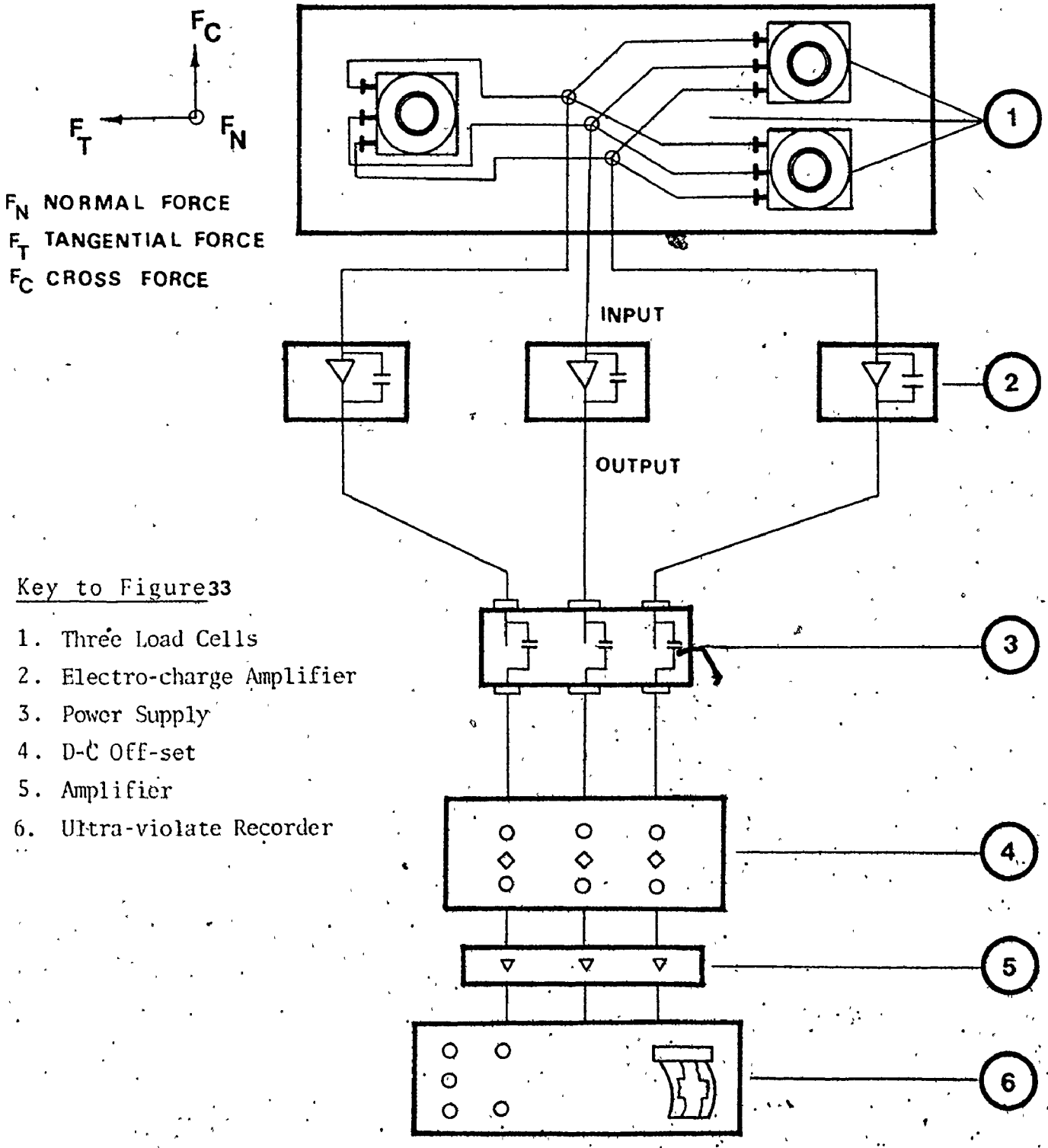

Key to Figure33

1. Three Load Cells
2. Electro-charge Amplifier
3. Power Supply
4. D-C Off-set
5. Amplifier
6. Ultra-violate Recorder

F 33. of the measuring installation.

before recording it.

The experimental set-up of the measuring circuit is shown in Figure 34.

3.3 Wheel Wear Measurement

An accurate assessment of the progressive radial wear sustained by the wheel was obtained using the "razor-blade" technique.

Reciprocating plunge grinding of a work-piece specimen of less width than the grinding wheel results in a groove being worn on the periphery of the grinding wheel of the same width as the specimen, (Figure 36).

The depth of the wear groove was measured by first duplicating the wheel profile on the edge of 0.001 in. steel shim, by plunge grinding, and then measuring the height of the step using the tool maker microscope, (Figure 35).

3.4 Thermal Damage Observations

A thermal damage to the work piece surface was observed during the grinding tests.

The onset of burning is characterized by temper colors on the work piece. In addition to this, a flash or ridge of material forms along the edge of the work piece, indicating that some of the material to be removed is ploughed aside by the grains instead of being formed into

Figure 34. Experimental Set-up.

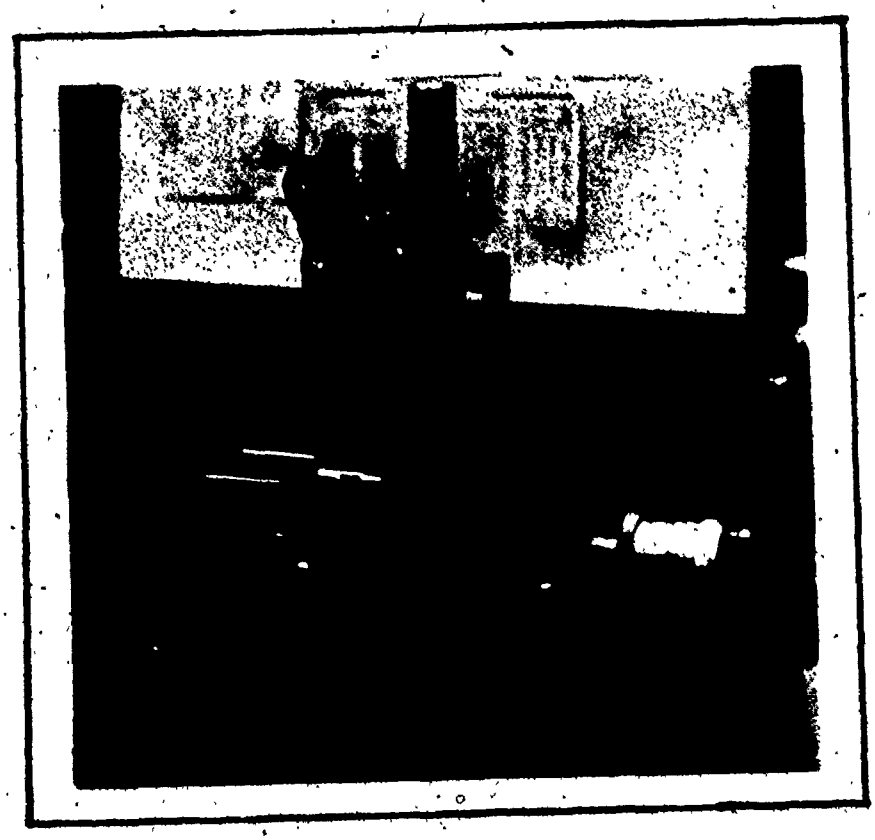

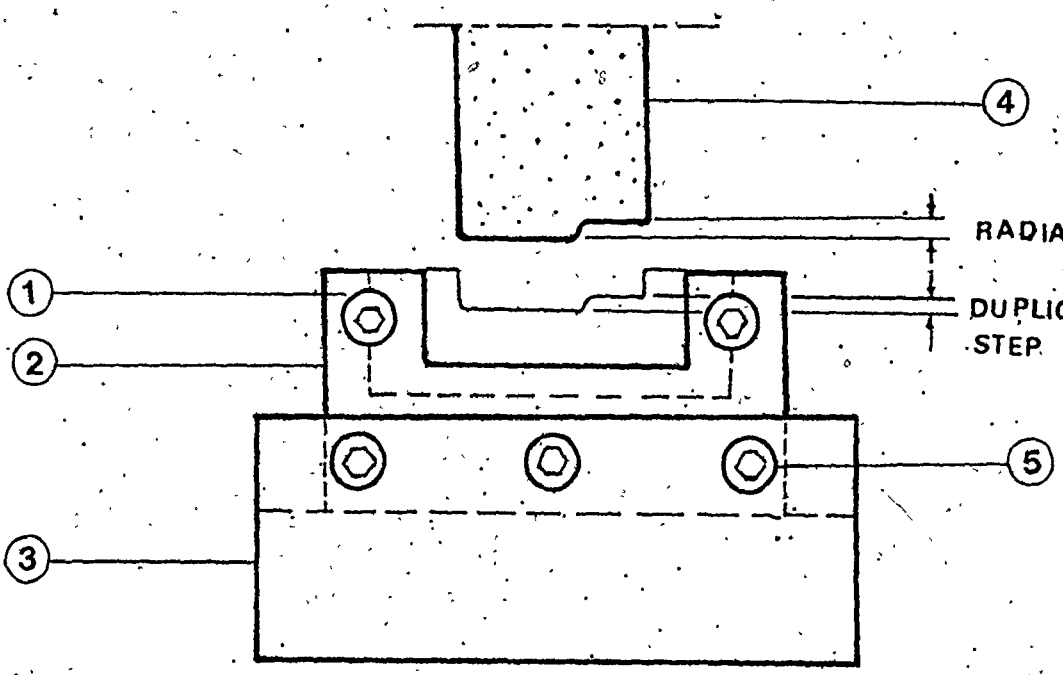

FRONT VIEW

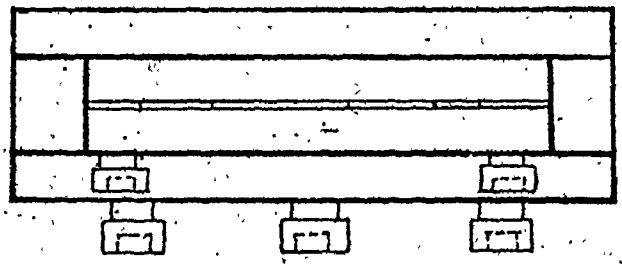

TOP VIEV

Key to Figure 36

1. Steel Shim
2. Holding Plate
3. Fixture Base
4. Grinding Wheel
5. Fixing Bolts

chips. Metallurgical examinations of burned work piece surfaces [8] have shown that the surface layers are over-tempered and softened. The burn color is the result of surface oxidation at high temperature.

Discoloration of the work piece surface is considered as an initial damage while burn is a severe damage for steel work piece materials.

CHAPTER 4

SCANNING ELECTRON MICROSCOPE OBSERVATION

4.1 Introduction

During recent years the use of the scanning electron microscope (SEM) in grinding research has become a widely recognized technique.

The ability of abrasive grains in a wheel to provide sharp fracture facets at micro and submicro levels during dressing with a dressing tool and also in the actual grinding operation (self-sharpening action), controls to a large extent the efficiency of the grinding operation.

Knowledge of the geometry of the grinding grain, surface topography of grinding wheels and of the form of chips collected from the cutting process, obtained by scanning electron microscope observations, is essential for the development of the grinding process.

The great advantages of the SEM as compared with the optical microscope are: high depth of focus, large range of magnification (up to 50,000X) and excellent dispersive power.

4.2 Scanning Electron Microscopy

Specimens for examination were prepared by mounting them on standard specimen stubs using an amorphous adhesive.

In order to render the surface of the specimens electrically conductive , a thin layer of 4% palladium-gold was vacuum evaporated onto it. Micro photographs were obtained by the SEM, Cambridge Model U-3, equipped with specimen stage which rotates and tilts.

The experimental techniques adopted in this work, fall into three categories: firstly, observation of wheel surface topography using a test specimen which was cut out from the surface of the grinding wheel; secondly, observation of grains collected in the trav connected to the table; and thirdly, observation of the chips formed during grinding process and collected from the table.

4.3 Results and Discussion

Upon completion of a series of grinding tests the specimens were examined on the SEM. The results of these examinations are summarized in the following figures.

4.3.1 Wheel Surface Topography

Figure 37 shows a stereo view microphotograph of A-J wheel surface. Many bonded grains are observed in different parts of the Figure. The bonding material surrounds the individual grains and links them together by connectors called posts. Dark portions indicate the pores.

The magnified portion of the dressed and ground

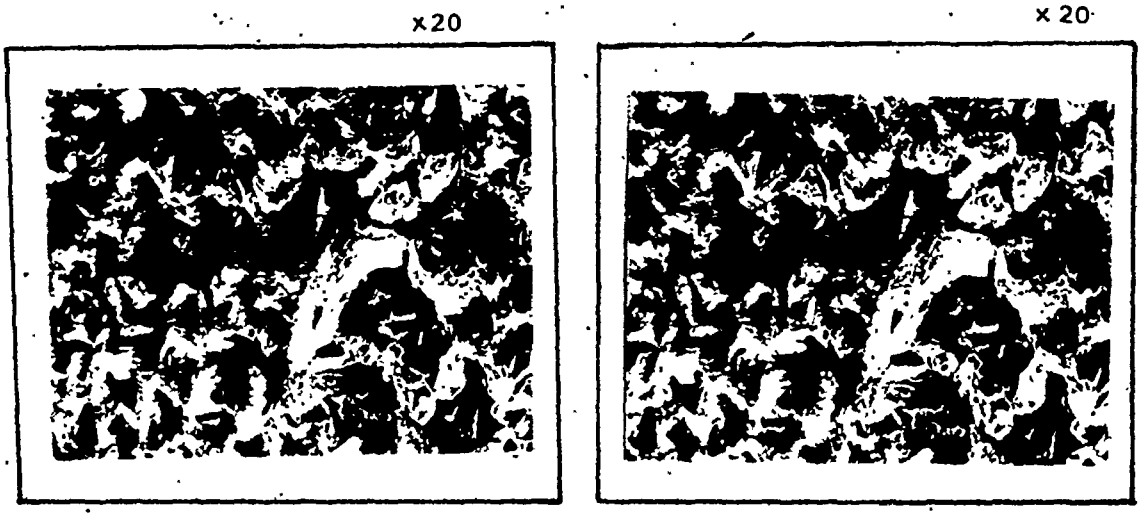

Figure 37. Stereo View Microphotograph of A--60--J Wheel Surface.

areas of the wheel surface are shown in Figure 38. It can be seen that the size of pores between the grains becomes larger with the ground area due to the wear of the grinding wheel and a corresponding loss of some grains. The microphotographs also show some of the chips being adhered to the grains of the surface which did the grinding; however, not much difference can be seen for both surfaces. Figure 39 and 40 show the microphotograph of A-P wheel surface. Comparing Figure 38 and Figure 40, the difference between grade J and P of the same wheel can be seen in terms of the amount of bond and porosity.

The grade of a grinding wheel is a measure of how strongly the grains are held by the bond. Figures 41 and 42 show the difference in wheel hardness of B wheels. It is seen that the amount of bond is much greater with P grade than with M grade. This amount of bond controls the rate at which fracture wear occurs [9].

The structure of a grinding wheel refers to the relationship of abrasive grains to bonding materials and of those two elements to the voids between them. Figures 43 and 44 illustrate the meaning of grinding wheel structure. The spaces in grinding wheel provide room for chips to escape during a cut. Figure 44 also shows the development of wear flats on the grains after grinding for 450 passes.

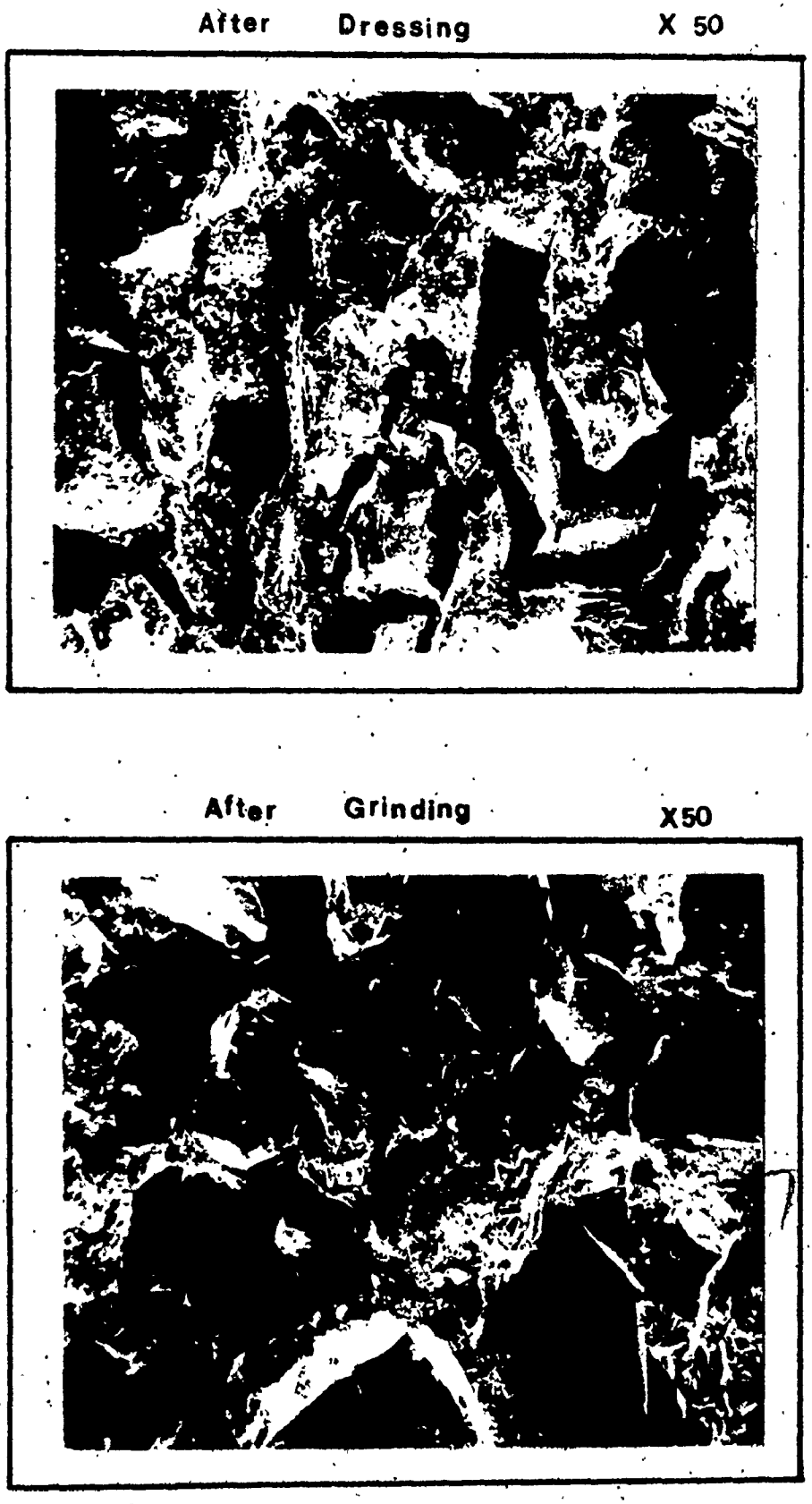

Figure 38. Microphotograph of A--60--J Wheel Surface With Higher Magnification (After Dressing and After Grinding).

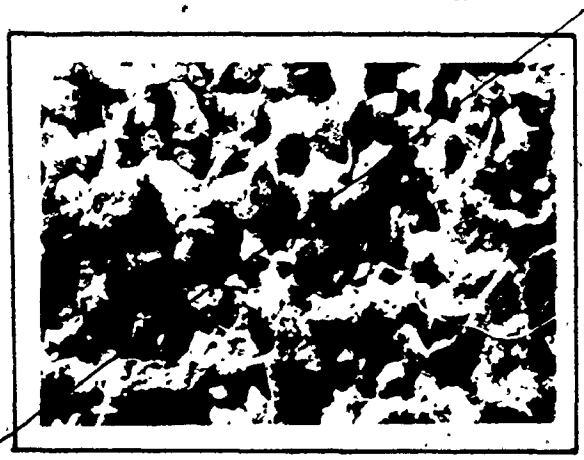

Figure 39. Microphotograph of A--60--P Wheel Surface, After Dressing (on the Left) and After Grinding (on the Right).

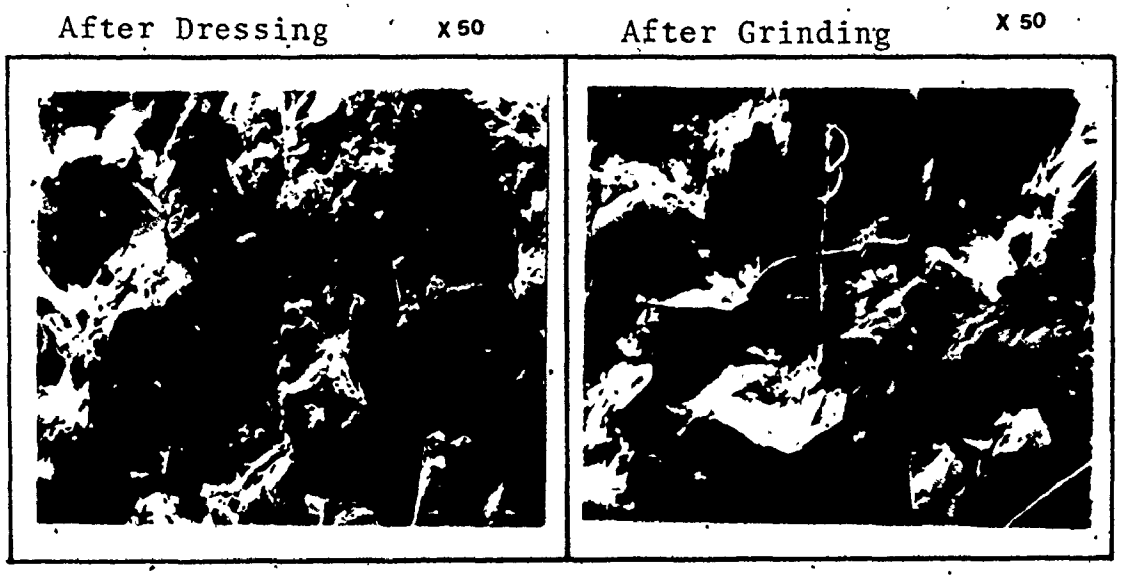

Figure 40. Microphotograph of A--60--P Wheel Surface With Higher Magnification.

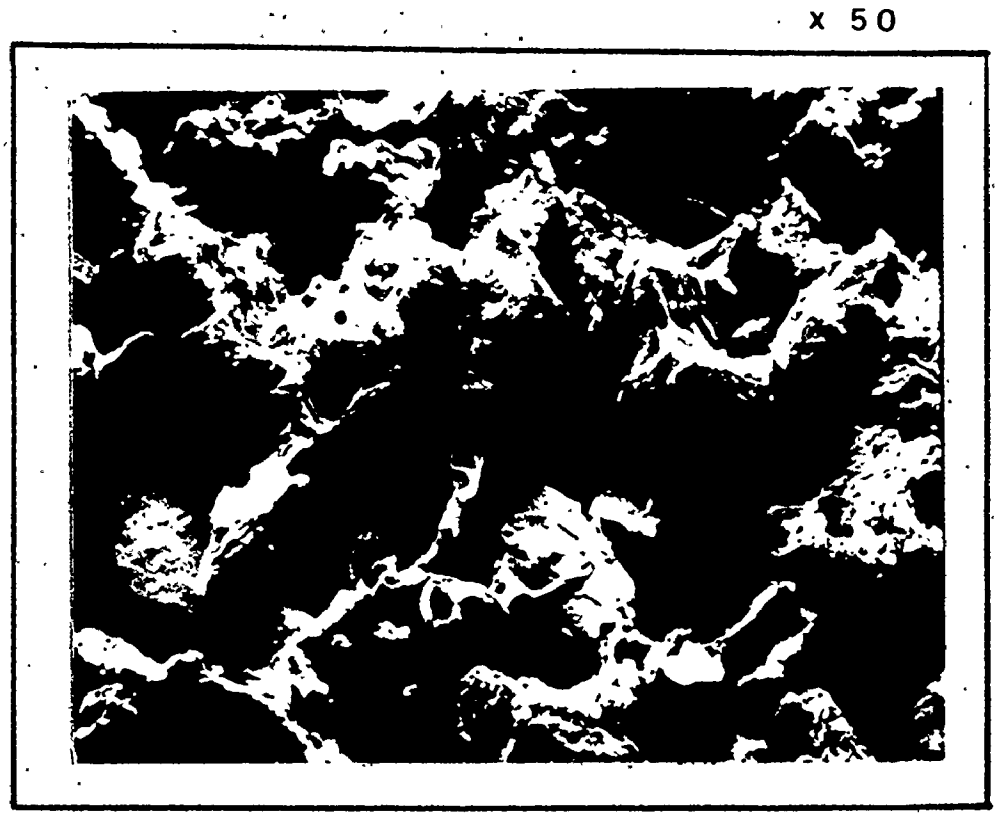

Figure 41. Microphotograph of B--60--M Wheel Surface After Dressing.

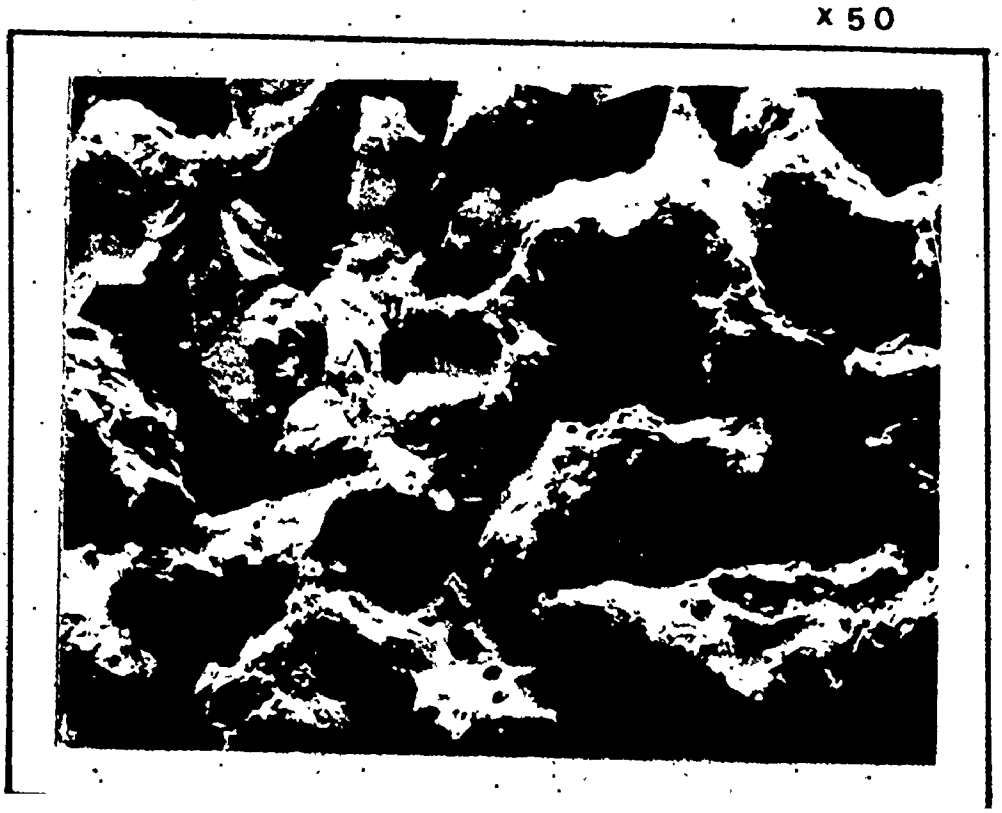

Figure 43. Microphotograph of B - 60 - M Wheel Surface After Grinding for 450 Passes. Work Material 52100. Down Feed 0.001 inch, Wheel Speed 6600 ft./min. and Table Speed 100 ft./min.

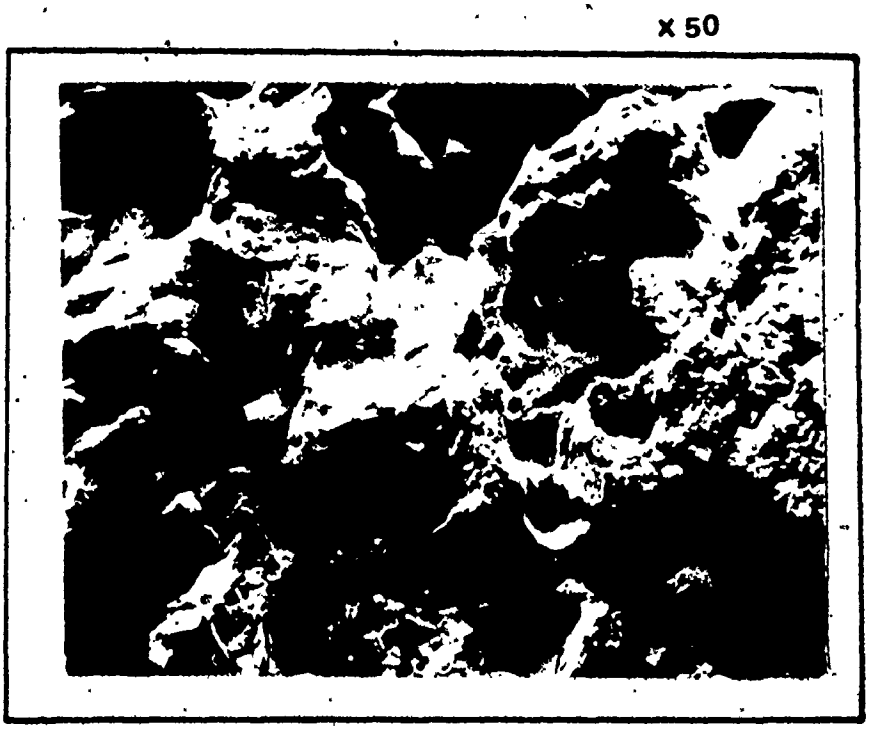

Figure 44. Microphotograph of B - 60 - P Wheel Surface After Grinding Work Material M_2.

4.3.2 Cutting Grains

In Figure 45 the simplified model of the three types of wear on grinding wheels is presented. When bond bridges (C) are broken, the grain concerned is separated from the body of the wheel. Partial fracture of the grain is illustrated by (B). Attritious wear of a grain may occur at the top of grains rubbed by metal as illustrated by (A). The former two are defined as the fracture wear of grinding wheels. The relative chances of bond fracture and grain fracture are largely affected by the hardness of wheels or by the relative strengths of grain and of bond bridges which hold the grain. The attritious wear should always occur, whether the wheel is soft grade or hard grade and may widen the contact area between grains and metal.

Figure 46-A shows that a single grain consists of several individual cutting edges which, according to the cutting conditions, engage the workpiece at varying strengths. This is in agreement with Figure 46-B which illustrates the average grain shape which has been determined according to statistical algorithms [25].

The surface deformation of single grain is shown in Figure 47. Localized melting and plastic flow of ($Al_2 O_3$) are observed in Figure 48.

Figure 49 shows a crack on the surface of a grain. This is the beginning of the grain fracture wear mechanism.

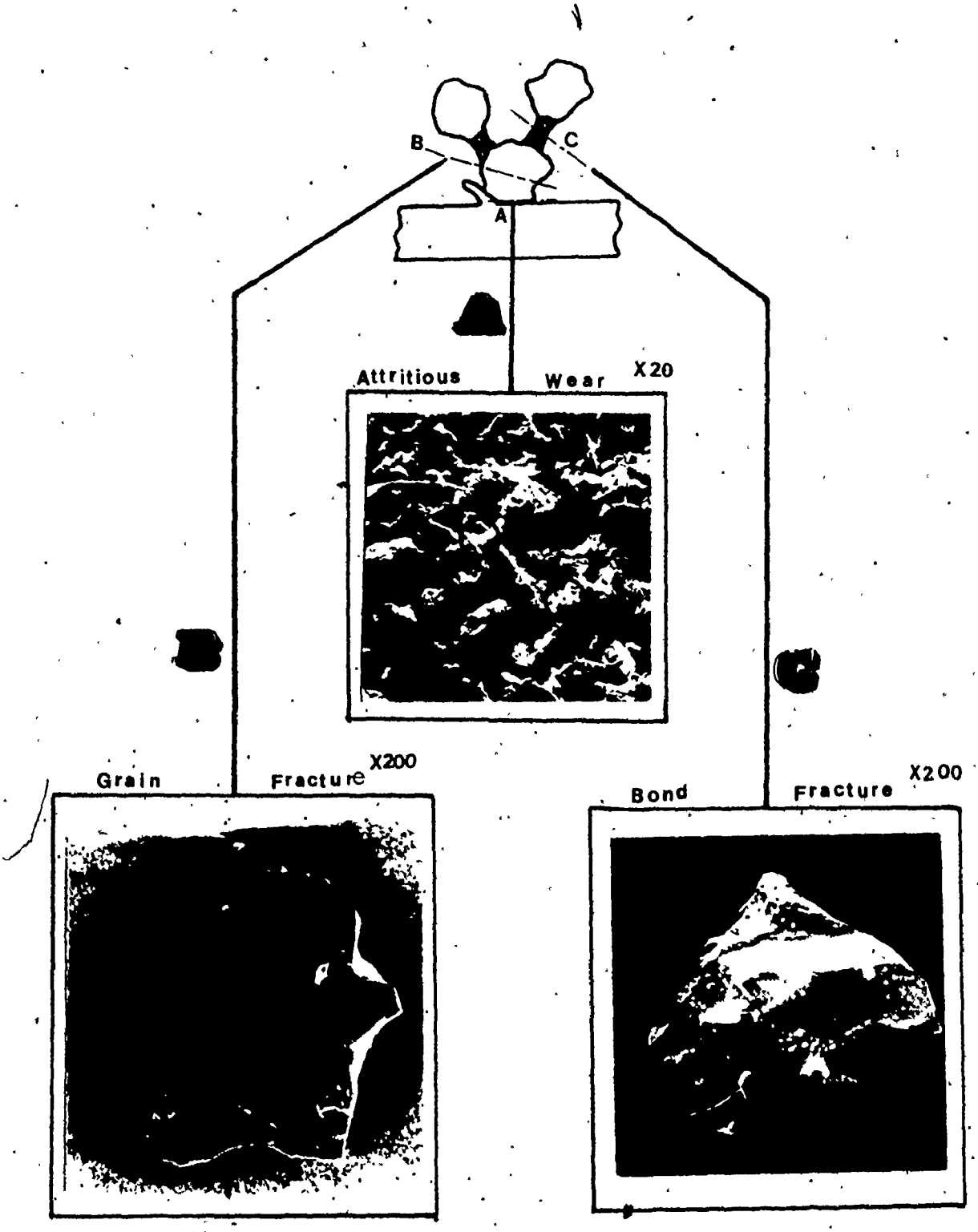

Figure 45. Wheel Wear Mechanisms.

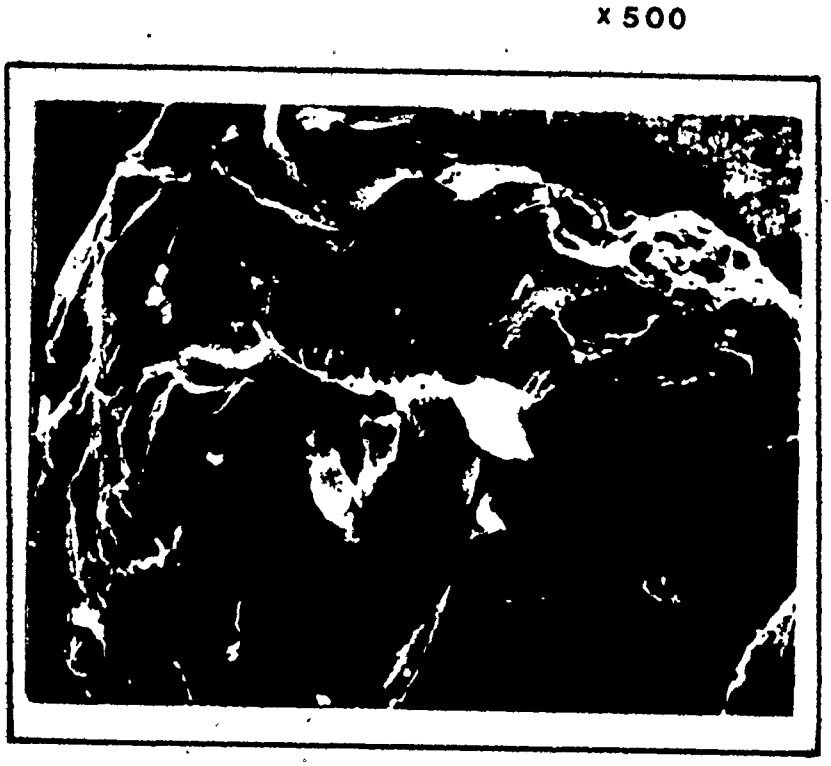

Figure 46-A. Surface of a Single Grain of Wheel A - 60 - J Collected After Grinding for 225 Passes.

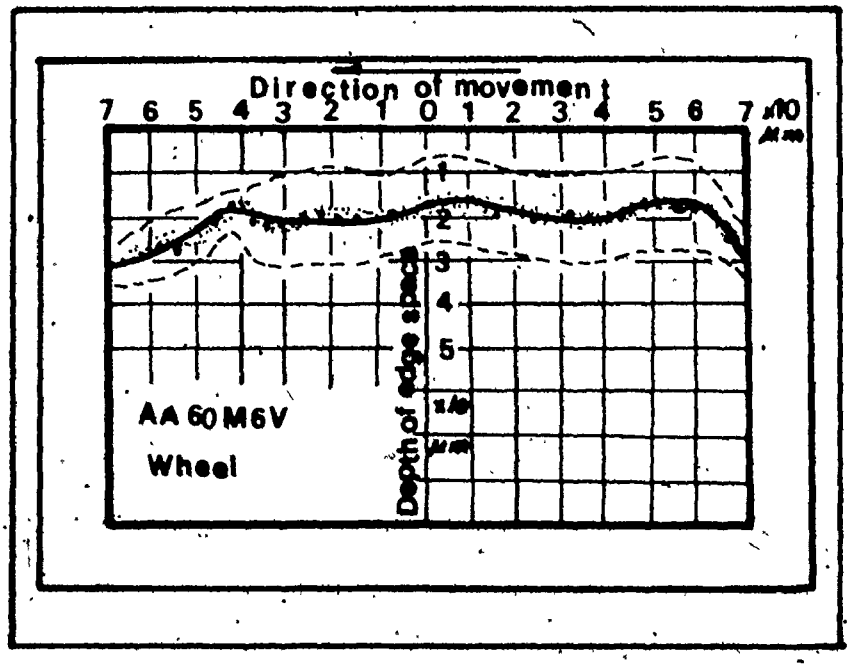

Figure 46-B. Average Grain Shape [Ref. 25].

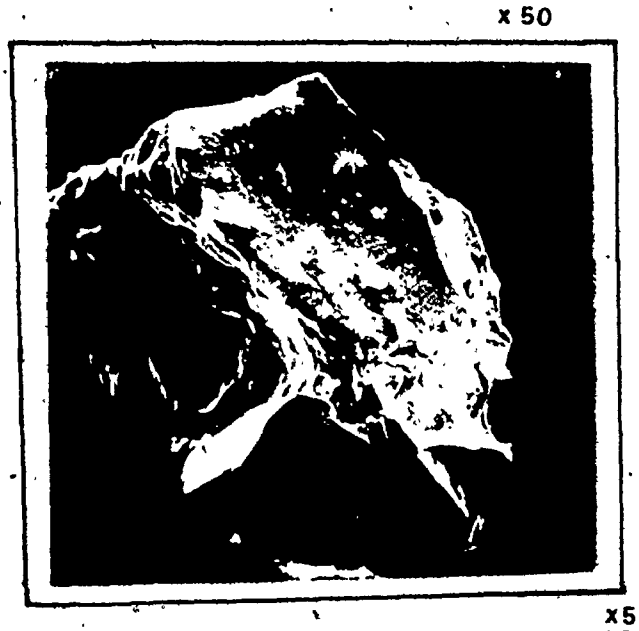

Figure 47. Surface Deformation of a Single Grain of A - 60 - J Wheel as Caused by Dressing.

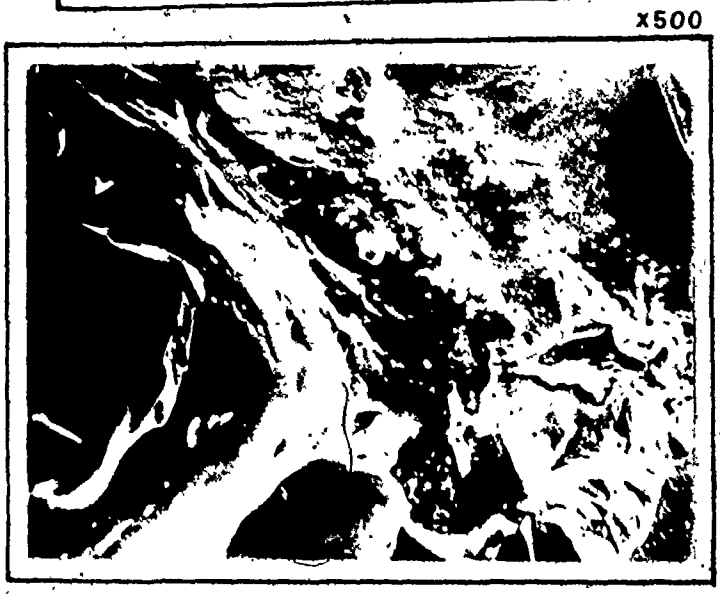

Figure 48. This Figure Presents the Magnified Portion in the Central Part of Figure 47.

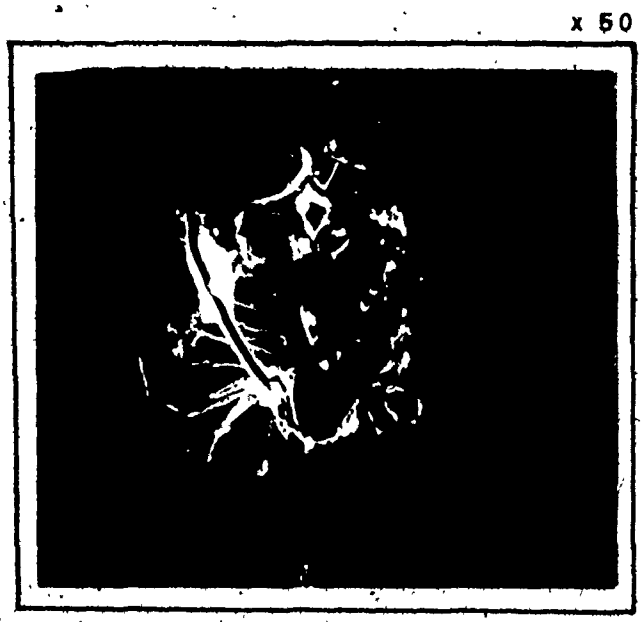

Figure 49. Grain Fracture of Wheel B - 60 - M.

The influence of dressing depth of cut on the size of the grains removed from the wheel surface is illustrated in Figure 50. At small depth of cut, tiny fractures occur, producing grains with crushed flat tops. At larger depth of cut, more and more grains break out of the bond.

4.3.3 Formed Chips

Figure 51 illustrates the forms of chips for material M_2 and 52100 respectively.

Chips were collected from the table during measuring the cutting forces with increasing down feed.

From grinding mechanics [29], the average value of the maximum underformed chip thickness ($\bar{h}$) and the average chip length $\bar{l}_{sp}$ can be given by

$$\bar{h} = 2K \frac{V_w}{V_s} \sqrt{\frac{a}{D}} \quad \ldots.1$$

$$\bar{l}_{sp} = \sqrt{\frac{a}{D}} \quad \ldots.2$$

From equations 1 and 2 it is seen that as the down feed, a, increases the chip thickness and chip length increase and consequently the force increases.

A sequence of microphotographs of material M_2 and 52100 at various down feeds are shown in Figures 52 and 53.

It can be seen that with the increase of down feed

x 95

Dressing Depth of Cut 0.001 inch.

x 95

Dressing Depth of Cut 0.0005 inch.

Figure 50. Grains of B - 60 - J.

M_2 Steel.

52100 Steel.

Fi[illegible] 51. [illegible] of [illegible]

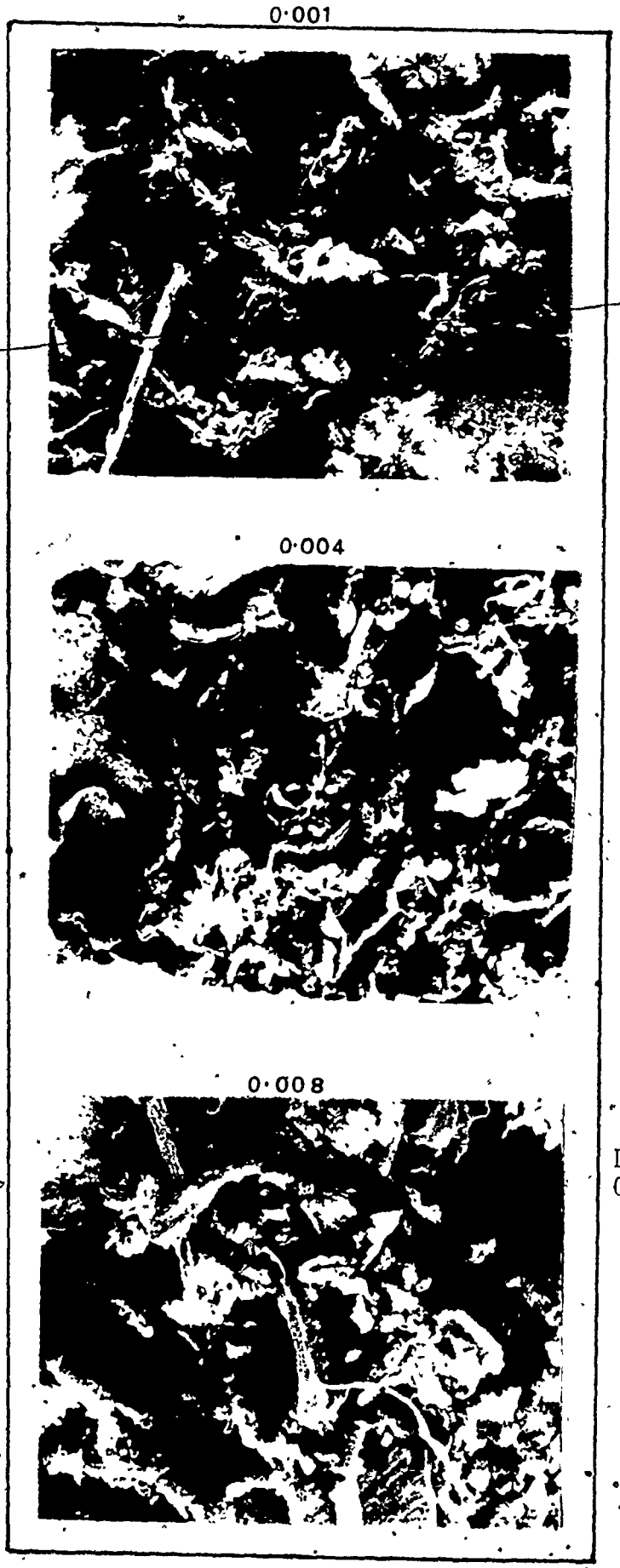

Figure 52. Chip Form of M_2 Steel When Grinding With

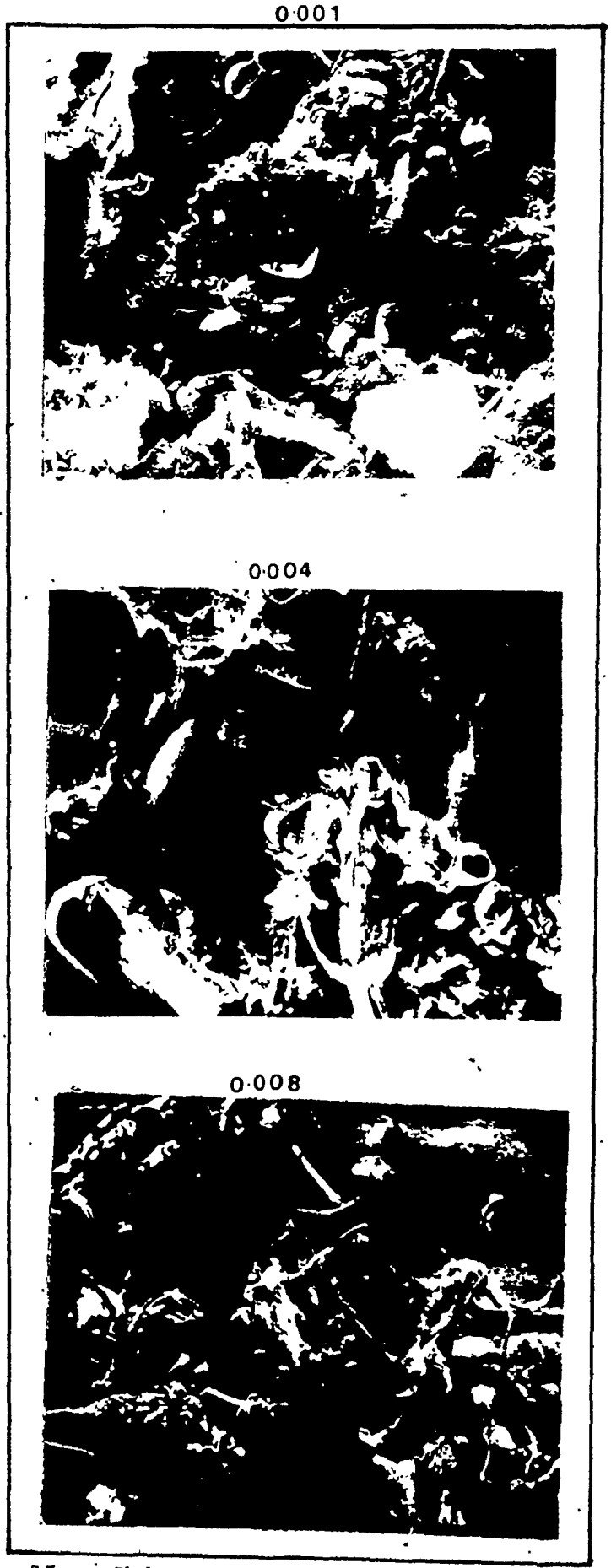

x 95

Down Feed:
0.001 inch.

Down Feed:
0.004 inch.

Down Feed:
0.008 inch.

Figure 53. Chip Form of 52100 Steel When Grinding With M - 60 - J

both the chip thickness and chip length increase and consequently the forces increase. Thus, the geometry of the grinding grain, the surface topography of grinding wheels, and the form of chips are investigated.

CHAPTER 5

EXPERIMENTAL PROCEDURE AND ANALYSIS OF THE RESULTS

5.1 Tests for Cutting Forces and Maximum Metal Removal Rate

5.1.1 Introduction

The cutting forces are used as a means to record the cutting ability of the grinding wheel.

Cutting forces were measured in two directions: the normal cutting force F_n, perpendicular to the work piece surface, and the tangential cutting force F_t in the direction of the table motion.

5.1.2 Test Procedure

Cutting forces F_n and F_t were recorded with various down feeds. The width of the cut was maintained at about 0.4 in., and the specific cutting forces F_n, F_t given as results related to 1 in. wheel width.

The sequence employed in each test was to start, after dressing, with down feed a = 0.001", grind 10 passes and record the last 4 passes, then another 10 passes with a = 0.002" and record the last 4 passes and so on. This was done until such a value a_{lim} of down feed was reached, where with the further increase of a the forces did not increase any more, indicating the breakdown of the bond material and an instant-

aneous increase of the wear.

This is taken as the maximum possible load for the given wheel and there is a corresponding metal removal rate to be obtained by:

$$\bar{Z}_{lim} \text{ in.}^3/\text{min/in.} = a_{lim}(\text{in}) \times V_w (\text{ft/min}) \times 12$$

where V_w is the table speed.

During this test surface damage to the work piece was observed as indicated by discoloration of the ground surface (mild, initial damage); or burn (severe damage).

In some cases burn was obtained already at values of (a) less than (a_{lim}). In other cases it coincided with the maximum possible depth of cut.

While interrupting the test to observe the surface damage of the work piece the chips were collected from the top of the magnetic chuck and chip form was checked as it was seen in Chapter 4.

It is important to realize that the total depth ground in this test was between 0.10 in. and 0.36 in. for work piece material M_2 (more difficult to grind) and 0.20 up to 0.66 in. for work piece material 52100.

Corresponding total volumes ground are 0.6 to 2.16 and 1.2 to 3.96 $\text{in.}^3/\text{in.}$

This volume of metal removed conveys a true picture of the grinding wheel cutting capability.

5.1.3 Results and Discussion

The measurement of cutting forces, employing a piezo electric dynamometer, provides the opportunity for relating the wear of grinding wheels to the grinding forces.

Figure (54) shows two records of grinding forces [29]. The record on the left shows constant forces during a grinding pass. The record on the right shows a case where the wheel is overloaded and it wears off rather fast during the pass and the forces decrease continuously from the beginning of the pass. The grains were immediately broken out of the bond by the overload and this is considered as the maximum possible load.

Forces measured at increasing down feed a for all tested combinations of wheel grades and work piece materials are given on individual graphs. (Figures 55, 56, 57, 58 and 59).

The observation of the thermal damage to the ground surface is shown in the upper portion of each graph. Maximum normal forces F_n max, reached (such at which massive grain break out occurred as explained in the above statement) and corresponding down feeds are summarized in Figure (60).

Considering the lower part of the diagram it is seen that values $\bar{F}_n$ max are almost the same for both M_2 and 52100 work piece materials for every wheel.

This is due to the fact that breakout of the grains depends on force only.

This force $\bar{F}_n$ max. increases, in general, with the

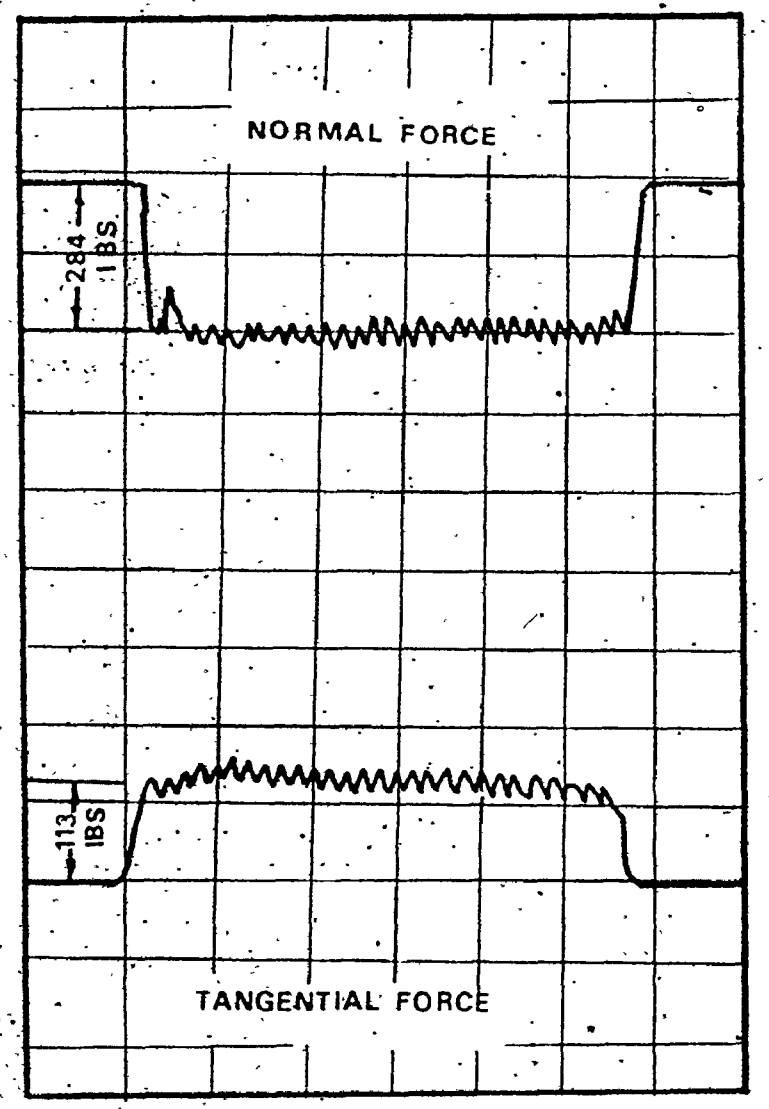

DOWN FEED: 0.001 INCH/PASS

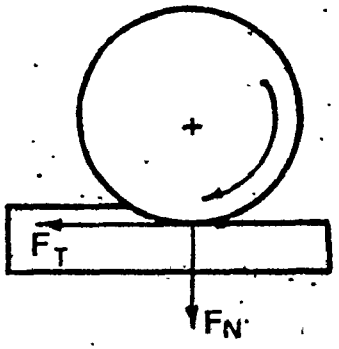

Forces acting on the work piece

F_t - tangential force

F_n - normal force

MATERIAL:
52100 STEEL

GRINDING WHEEL: B-J

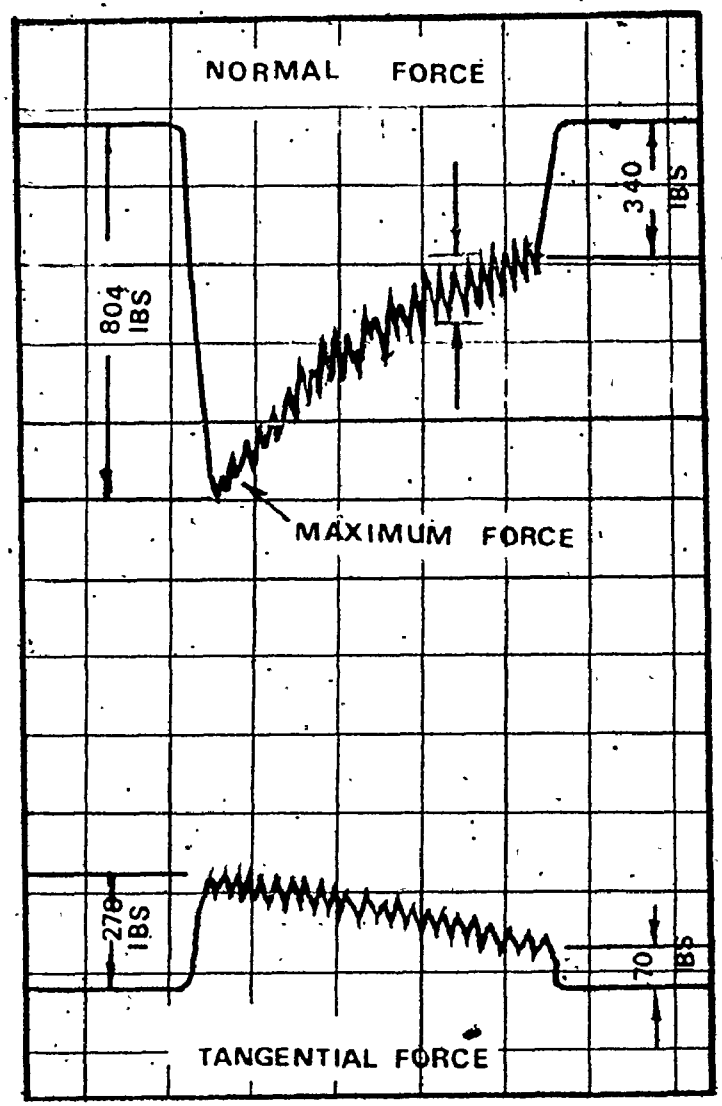

DOWN FEED: 0.007 INCH/PASS

Figure 54. Records of the cutting forces when measuring the maximum removal rate.

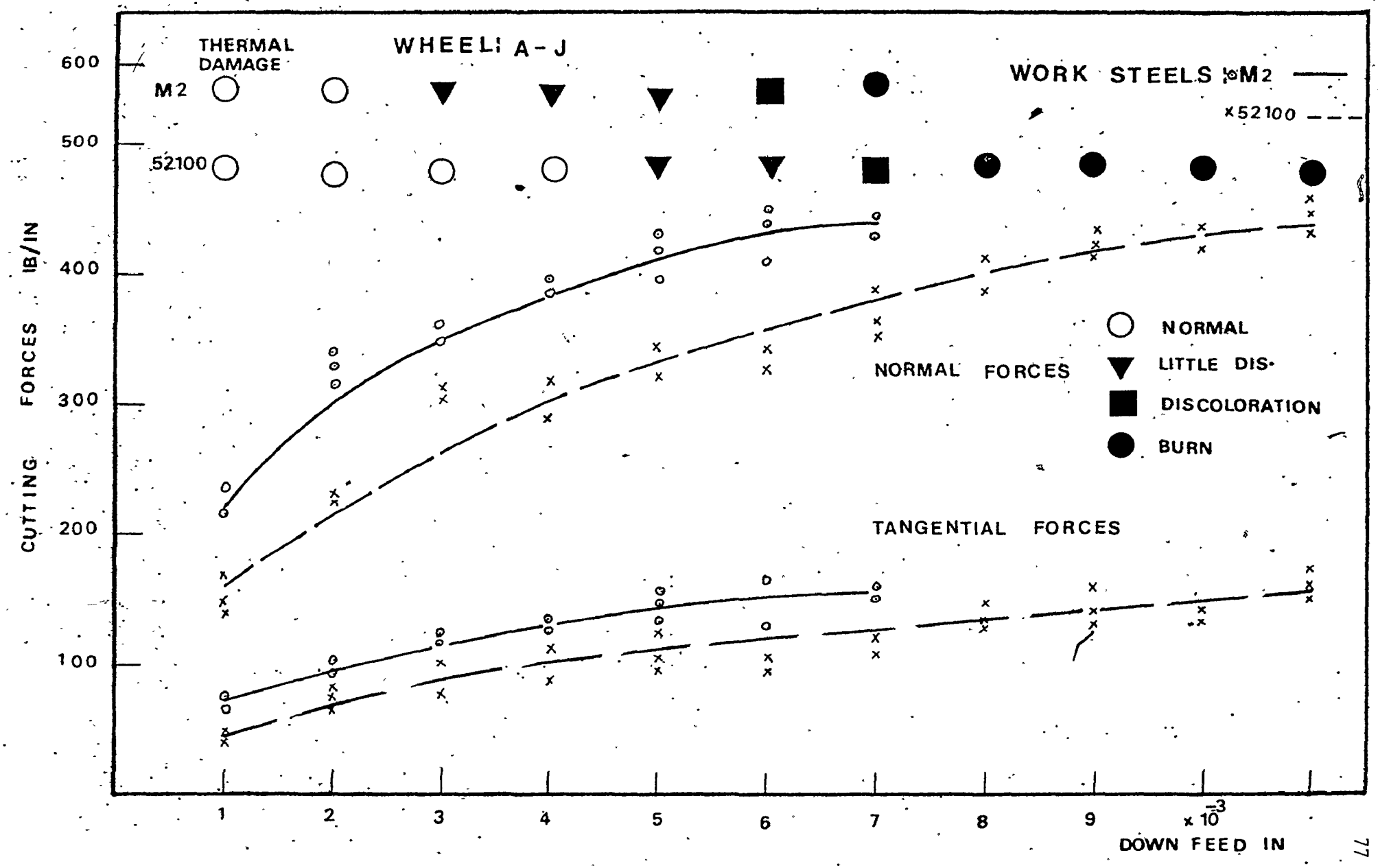

Figure 55. Cutting forces versus down feed for A-60-J wheel.

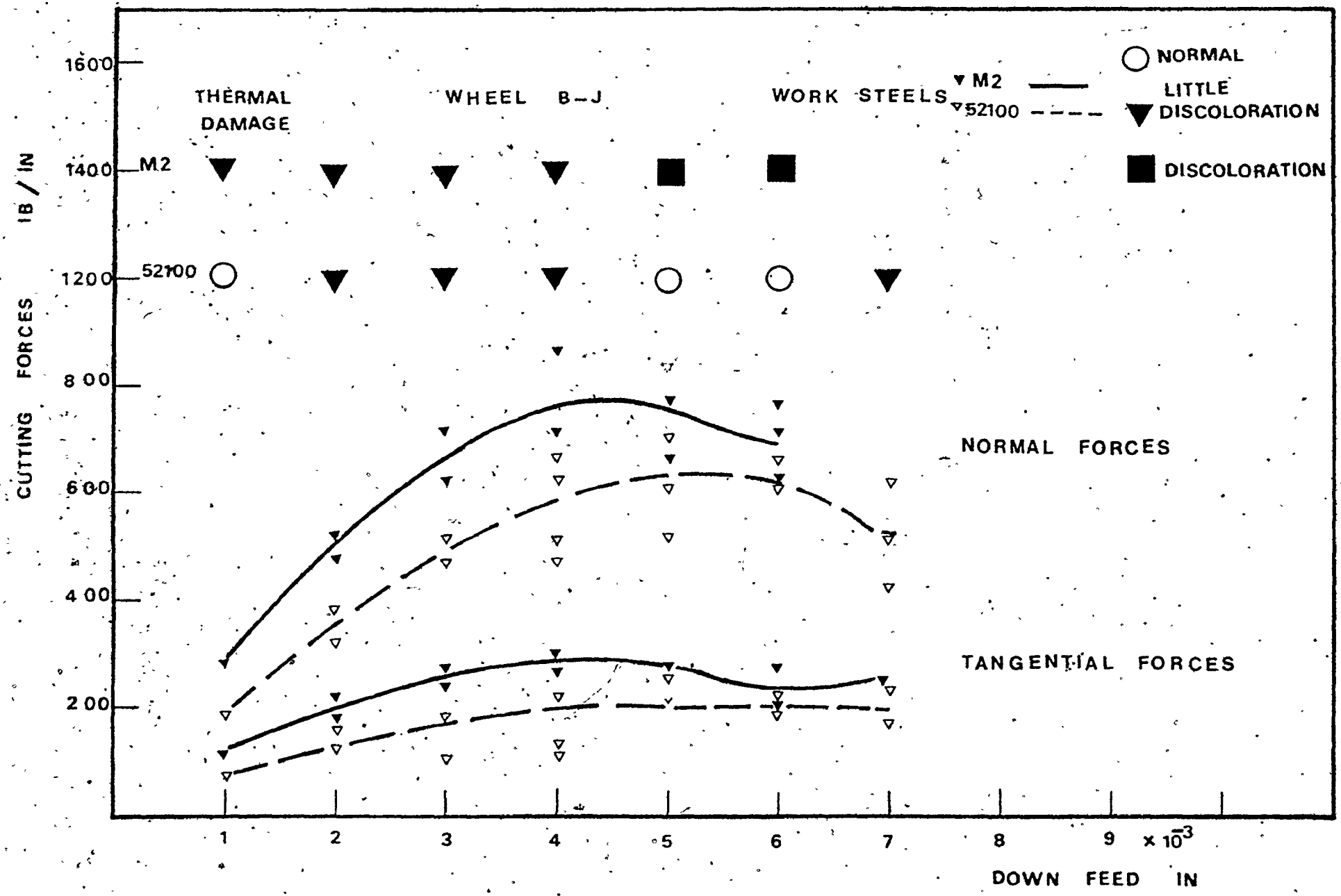

Figure 56. Cutting forces versus down feed for B-60-J wheel.

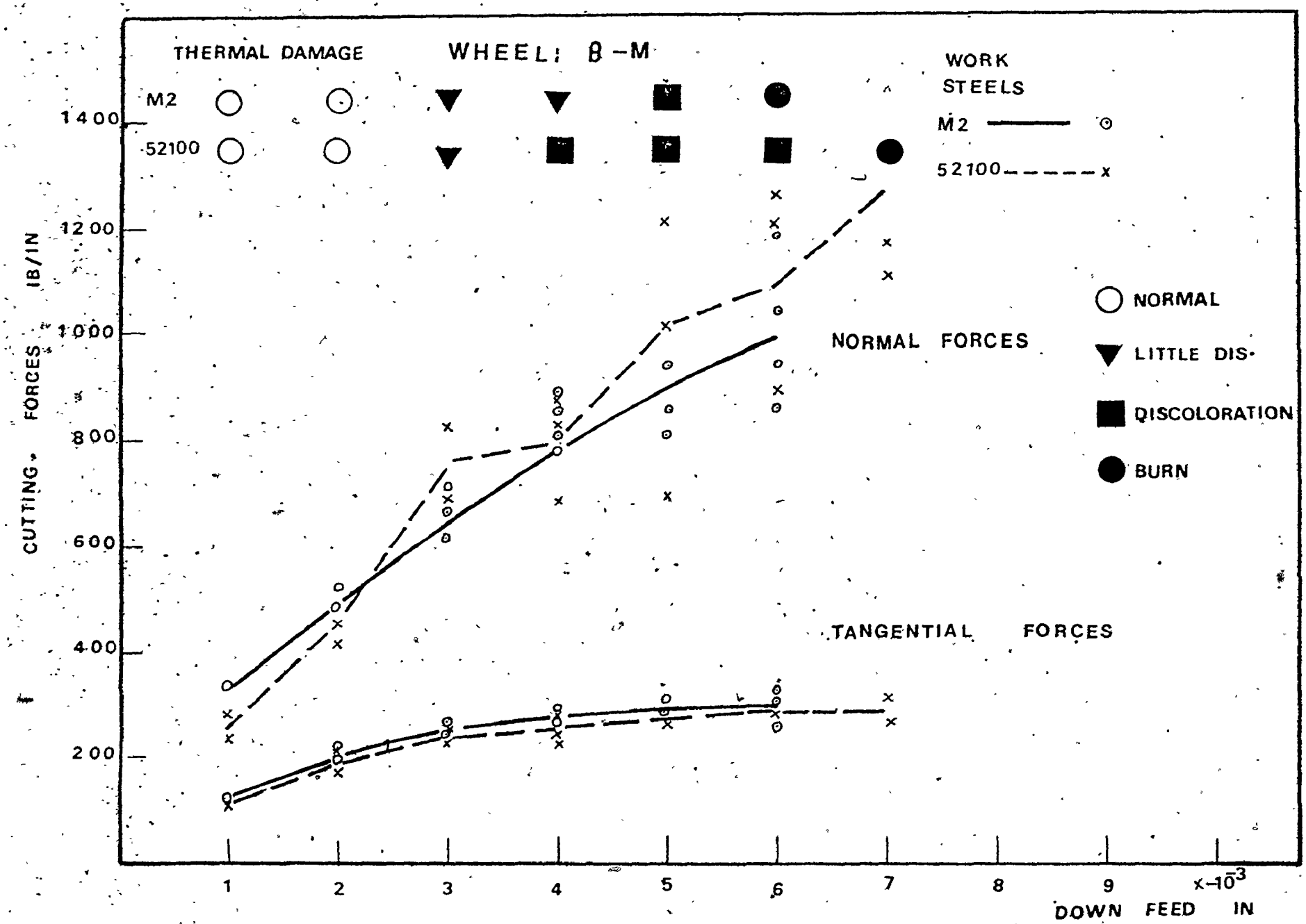

Figure 57. Cutting forces versus down feed for B-60-M wheel.

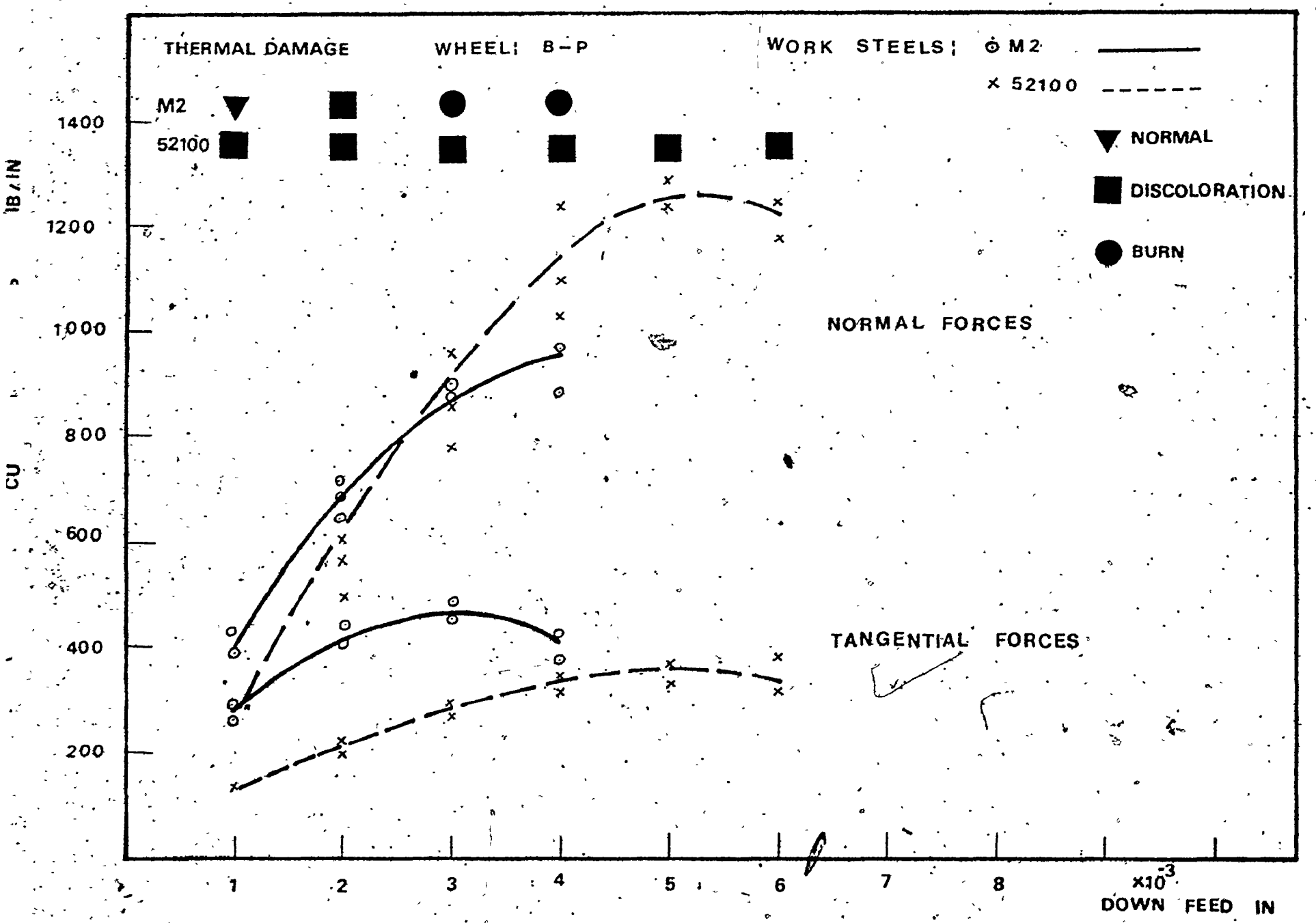

Figure 58. Cutting forces versus down feed for B-60-P wheel.

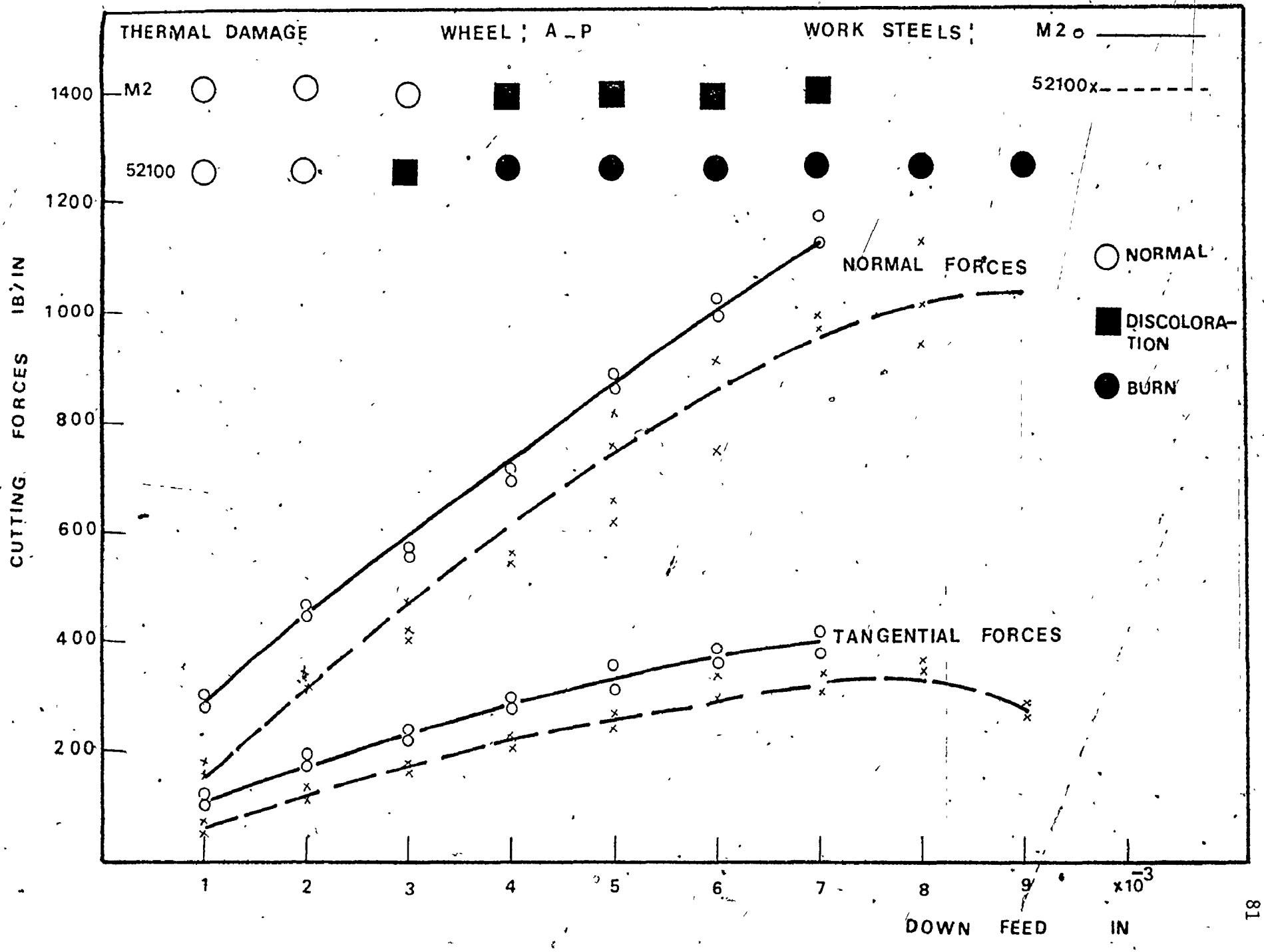

Figure 59. Cutting forces versus down feed for A-60-P wheel.

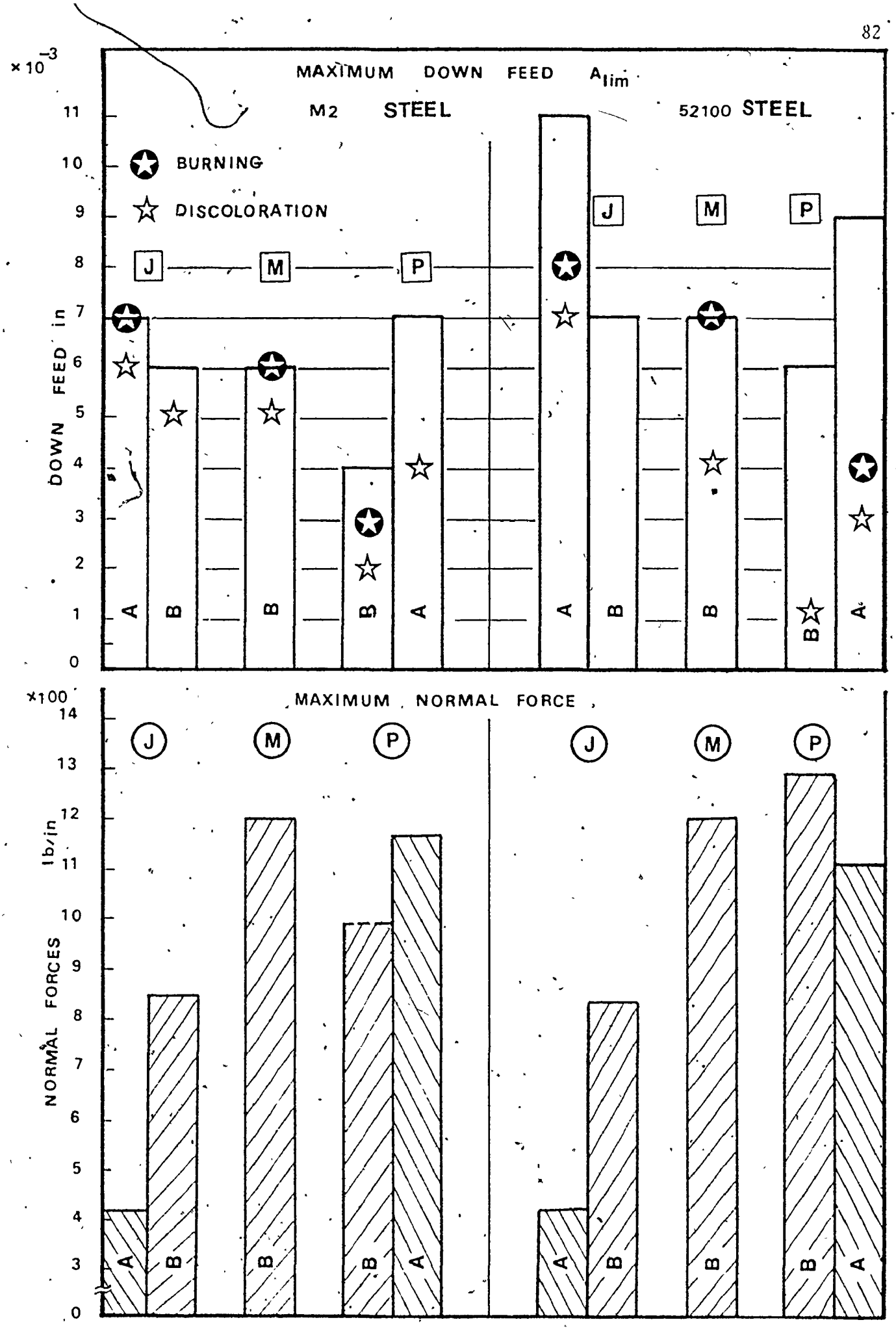

Figure 60. Summarized figure of maximum forces and maximum down feed.

increasing of wheel hardness, from J to M to P for wheels B and from J to P for wheels A.

In the J and P grades where we have both makes of wheels (A and B), the A wheels are softer, i.e., produce smaller forces.

In the upper part of the same diagram Figure (60), corresponding values a_{lim} are given as well as values of down feeds at which discoloration and further burning occurred.

Checking on the B group of wheels it is found that for grades J and M, the same value of a_{lim} = 0.006 in. applies for M_2 steel and a_{lim} = 0.007 in. for 52100 steel. For grade P the value of a_{lim} = 0.004 in. with M_2 and a_{lim} = 0.006 in. with 52100 steel.

Checking on the A group of wheels it is found that for grades J and P, the same value of a_{lim} = 0.007" applies for M_2 steel and a_{lim} = 0.009 in. for 52100 steel.

This is explained when the graphs mentioned above are inspected showing that forces for every down feed increase with increasing wheel hardness.

Obviously, with soft wheels grains break out when they develop rather small wear flats while duller and duller grains (with larger wear flats) hold in harder wheels. Thus at the same down feed a forces develop in proportion to the strength of the bond.

Malkin [4] found that harder wheels have more active grains, larger wear flat areas and hence require larger

grinding forces. On 52100 steel forces were generally smaller than on M_2 steel and therefore higher a_{lim} values were reached.

In this respect the A group of wheels act sharper than B wheels.

As regards surface damage, both a slight one, as characterized by discoloration of ground surface (light or heavy discoloration), and the more serious burn occur at lower down feeds as wheels get harder. This can be seen from the upper part of Figure (60).

In many instances the maximum load as expressed by the maximum down feed a_{lim} can not be used and the rough grinding output is limited by burn occurring at lower down feed.

Thus practical maximum down feeds for wheels B-P is 0.003 in. instead of 0.004 in. on M_2 steel. The practical maximum down feed for wheels A-J, B-M and A-P are 0.008", 0.007" and 0.004" using 52100 steel.

Again in this respect the A group of wheels is superior.

In general, it may be stated that softer wheels are capable of a larger metal removal rate. This is due to the fact that self sharpening is predominant with soft wheels while hard wheels are cutting under blunting action with excessive wheel loading.

5.2 Tests for Grinding Wheel Wear. The G Ratio

5.2.1 Introduction

In order to establish an accurate method for measuring the radius wear, plunge grinding tests were performed and a reference surface of the wheel was used for measuring the radius wear.

All the tests were carried out with a specific width of the wheel surface, leaving the rest of the surface not taking part in the grinding process, as reference for measuring of the wear. After each stage of the test surface reproduced on a thin steel plate (0.001 in) by plunging the wheel surface onto the plate. The difference Δr, between the reference surface and the cutting surface of the wheel represents the radius wear.

By duplicating the wheel profile onto a steel strip an accurate record of wheel wear is made without stopping the wheel, and with only a short interruption of the grinding test.

The steel strips were collected and measured using the tool maker's microscope after the test.

Five readings were taken for each strip and the average recorded.

The wear volume can be calculated from the equation

$$V_{wear} = \pi . D . W . \Delta r$$

where D = the wheel diameter

W = the cutting width

Δr = the radius wear

The results of the grinding wheel wear measurements are illustrated by means of a dimensionless number called the "grinding ratio" which is defined as the ratio of volume removed to the volume of wheel wear. G ratio is the generally accepted parameter for measuring wheel wear.

$$G = \frac{V_{metal}}{V_{wear}}$$

where V_{metal} = volume of metal removed

V_{wear} = volume of wheel wear

5.2.2 Test Procedure

The dressing operation was performed with a single point diamond dressing tool at traverse feed of 0.010 in./rev. and with dressing depth of cut 0.001 in. before each test.

The normal and tangential force components were recorded at the last 4 passes of every 15 passes, and the radial wheel wear was obtained by interrupting the grinding after every 45 passes so that the thin steel strip could be fed radially into the wheel and the height of the recess in the wheel surface (ΔR) could be produced on the steel strip.

The difference in height of the work piece before and after 45 passes was measured and indicated by (Δx).

During the test the surface damage of the work piece

was visually examined as indicated by discoloration of the ground surface, or by burn. Chatter marks generated on the surface of the work piece were also observed.

Debris was collected every 45 passes in a box-like container placed in the grinding zone.

Abrasive grains and chips were examined using the Electro scanning microscope. Results of this examination were discussed in Chapter 4.

The nonuniformity of wear which causes the unbalance of the grinding wheel was estimated in terms of the amplitude of forced vibration and was plotted superimposed on the average force value.

In the recent tests in order to obtain a measurable value of wheel wear using 52100 steel, the tests were carried out using down feed 0.002 and 0.001" for M_2 steel.

The individual radial wheel wear (ΔR) every 45 passes was obtained and the individual grinding ratio G was calculated. Also accumulated radial wear ($\Delta \bar{R}$) was measured and the accumulated grinding ratio was calculated.

The details about the total depth Δx ground in a couple of these tests are given in Appendix III, together with the total wear and the resulting grinding ratio.

$$G = \frac{L\ \Delta x}{\pi\ D\ \Delta R}$$

where L = 6 in. is the length of the work piece and D = 14" is the diameter of the grinding wheel.

These tests were continued for longer grinding

operation (450 passes) at constant down feed.

It should be mentioned here that the total depth Δx was approximately 0.45 in. for M_2 steel with constant down feed 0.001 in. and 0.90 in. for 52100 steel using constant down feed 0.002" (corresponding to total volume ground 2.7 $in.^3/in.$ for M_2 steel and 5.4 $in.^3/in.$ for 52100). All of these tests were run at a wheel speed V_s = 6600 ft/min. and a table speed V_w = 100 ft/min.

These cutting conditions, presented above are, in the author's opinion, severe cutting conditions. Previous researchers, Malkin [4], Lal [12], have generally adopted much less severe cutting conditions which do not convey the true picture of the grinding wheel cutting capability.

5.2.3 Results and Discussion of Grinding Wheel Wear and Forces

The changes in the grinding force components and grinding wheel wear, as grinding time increases (number of passes increases), are shown on individual graphs in Figures (73) to (78) in Appendix (I).

Several criteria are used in judging the force graphs:

a) average force level of the normal and tangential components,
b) thermal damage to the work piece as indicated by discoloration of the ground surface (initial damage), or burn (severe damage).
c) nonuniformity of wear in terms of the amplitude of forced vibration.

The three criteria are presented on each graph.

The nonuniformity of wheel wear is determined from the force record as it is shown in Figure (61) and superimposed on the average force level.

The observation of the thermal damage to the ground surface is shown in the upper portion of each graph.

The cutting capability of a properly chosen grinding wheel, working in well-selected conditions, is affected by wear of two kinds:

1. Grain fracture and bond fracture. Grain fracture may or may not deteriorate the cutting capability which depends on the state of cutting edges of the part of the grain which remains bonded to the grinding wheel.
2. Attritious wear which deteriorates the cutting capability of the edges.

The cutting capability of grinding wheels may also be affected by chips trapped in the pores or wedged in the bond as it was indicated in Chapter 4.

Generally speaking, the deterioration of cutting capability of grinding wheels may appear:

1. on the work piece (discoloration or burn),
2. on the grinding wheel itself (nonuniformity of wear), or
3. may accompany the grinding (the grinding forces).

Therefore, the three criteria used in judging the graphs can be used to determine the grinding wheel capability

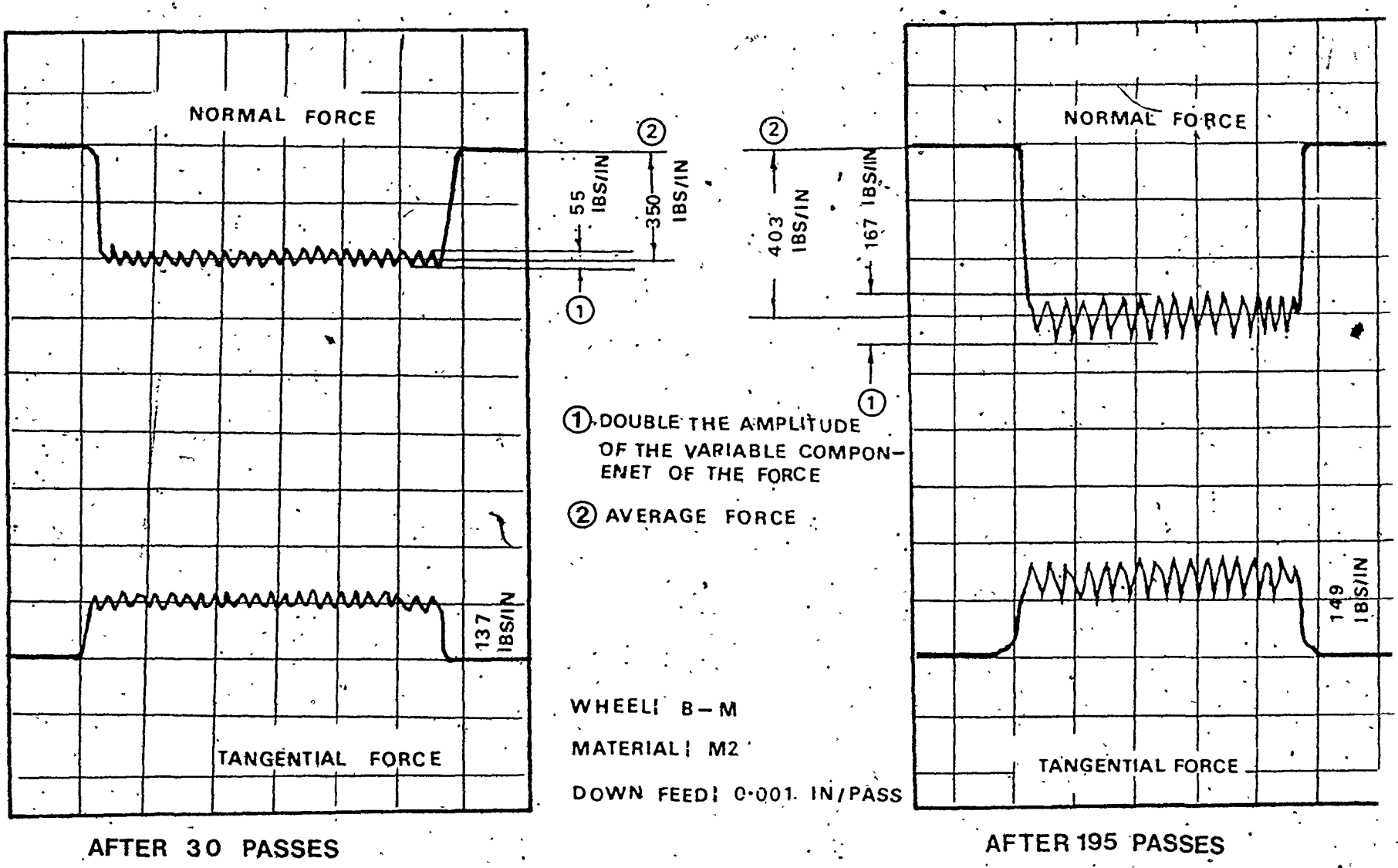

Figure 61. Records of the cutting forces when measuring the non uniformity of the grinding wheel wear.

(grinding wheel tool life).

5.2.3.1 Variation of Force Components and Wheel Wear with Grinding Time

With a view to explaining this variation, particular attention will be paid to the results shown in Figures (62) and (63).

The selection of this set of results is that they illustrate very clearly the features shown by the data obtained for all tested combinations of wheel grades and materials.

A review of the data in Figures (62) and (63) shows that these curves can be divided into four stages:

Stage A: is the non steady stage and is characterized by a rather low wear rate (high grinding ratio) and rapid increase of grinding forces with time.

Stage B: is a transient stage, in which the force holds on a high level and wear rate decreases (grinding ratio increases).

Stage C: is another transient stage, during which the wear rate increases steeply (grinding ratio decreases) and the force drops simultaneously.

Stage D: is a rather stable stage with a rather high wheel rate and low forces.

Consider the sequence of events when a wheel which has been dressed begins to grind a work piece. As the wheel begins to grind, the weakest and most damaged grits caused by the dressing operation, will be either pulled out from the

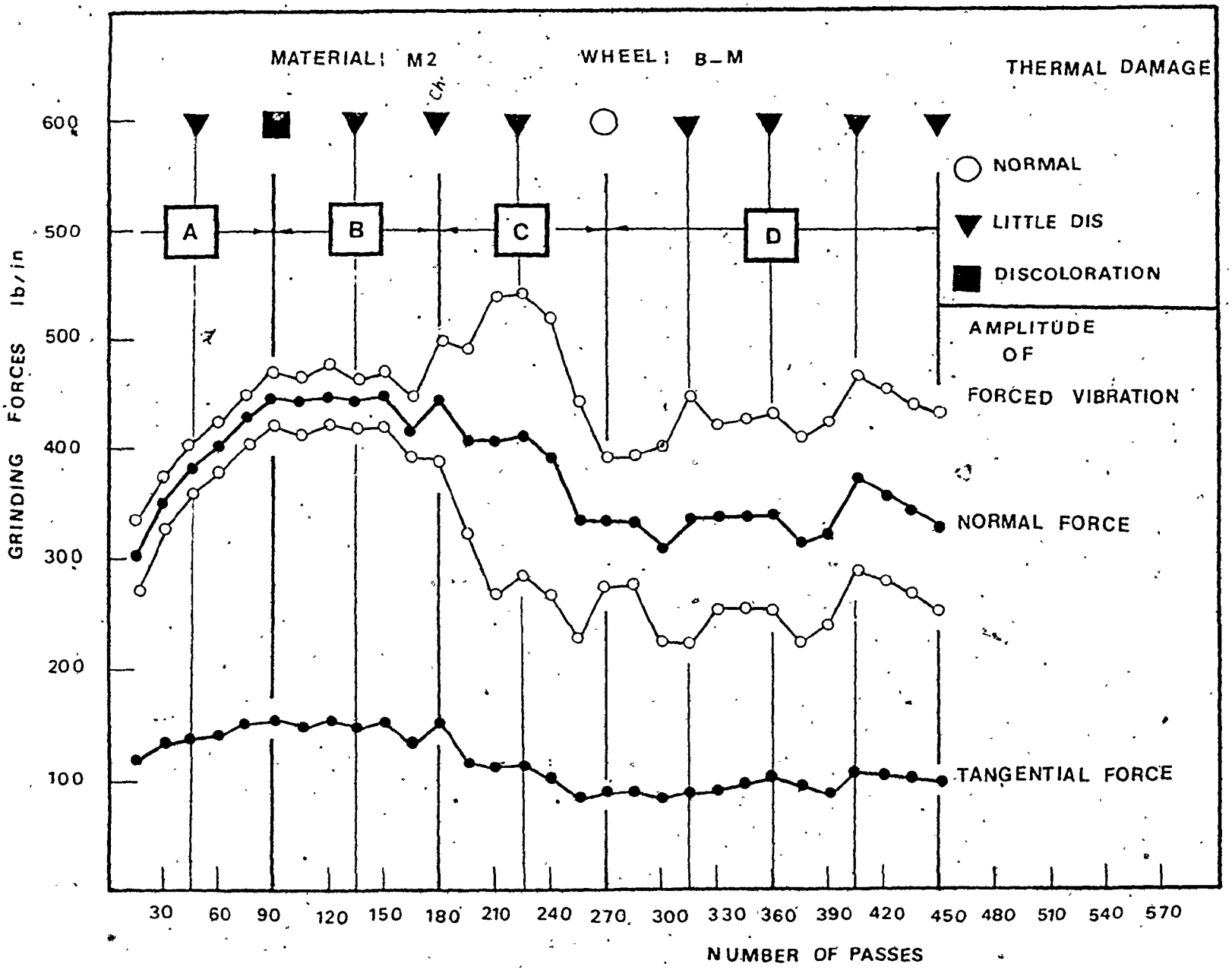

Figure 62. Variation of cutting forces with number of passes.

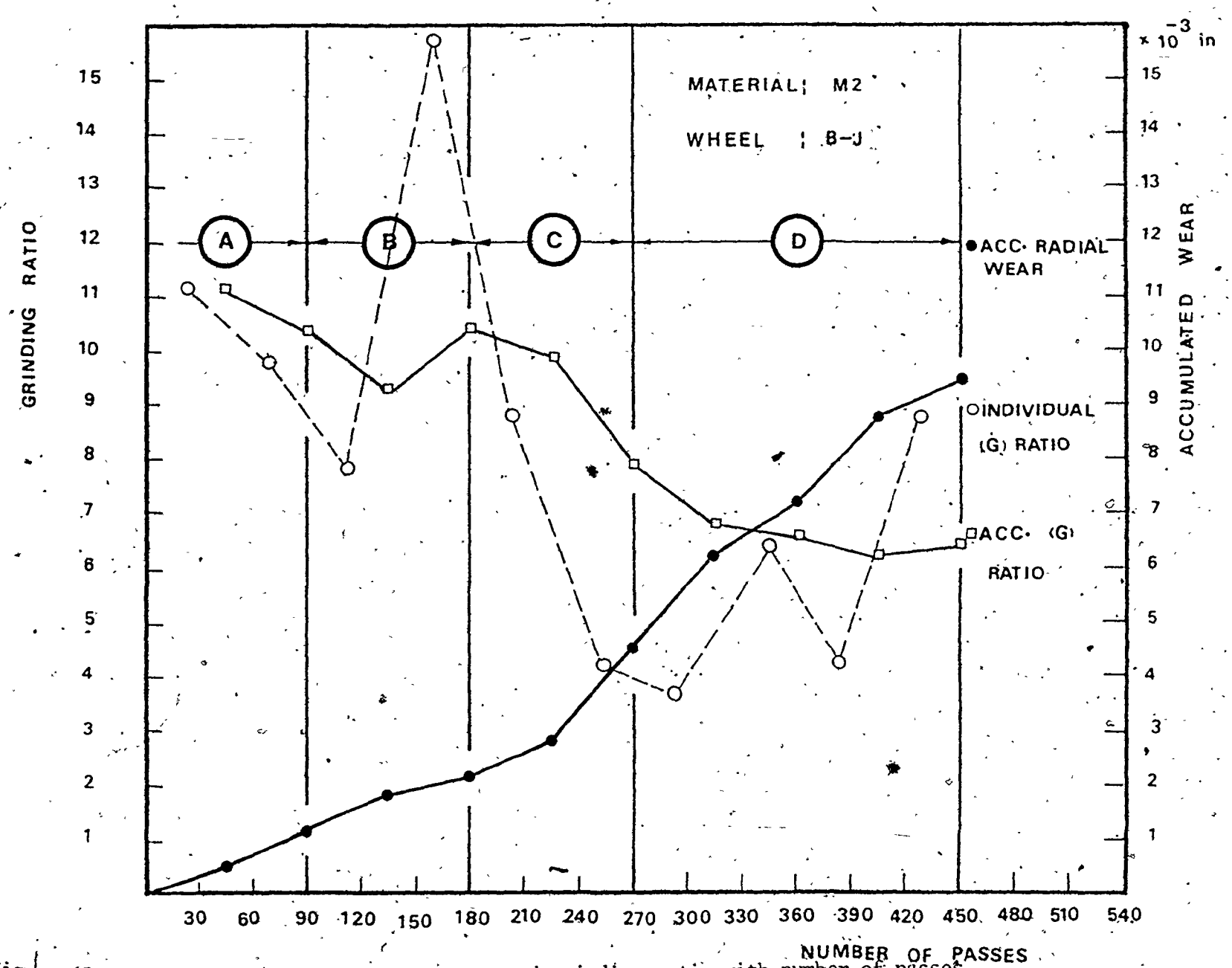

Figure 63. Variation of grinding wheel wear and grinding ratio with number of passes.

bond or will fracture. This depends on whether the grit/bond adhesion is lower or higher than the grit fracture strength. Stage (A) will be reached when the weakest grits will have been removed or fractured and those remaining on the wheel are sufficiently strong to withstand the grinding forces. During Stage (A) the grits wear by attrition at a relatively slow rate and the number of grits actively participating in work piece removal slowly increases. In this stage there is a progressive build-up of forces with normal force rising more rapidly than the tangential force. This rapid increase in the normal force is probably due to the development of wear flats and consequently the dulling of the wheel.

Stage (B) is a transient stage. This stage is characterized by the thermal damage of the work piece. With the attainment of high grit temperatures, due to the dulling of the wheel, the thermal shock which the grit sustains as it enters and leaves the wheel work piece contact area will be increased.

The opportunity for grit fracture as a result of thermal stresses increases.

It should be mentioned here that, because of the non-uniformity of wear during Stage (b) and due to the thermal stresses which cause the grain fracture, the end of this stage is characterized by the development of chatter marks caused by the unbalance of the grinding wheel.

During Stage (C), the wear rate increases steeply and the force drops simultaneously. Also, an increase of

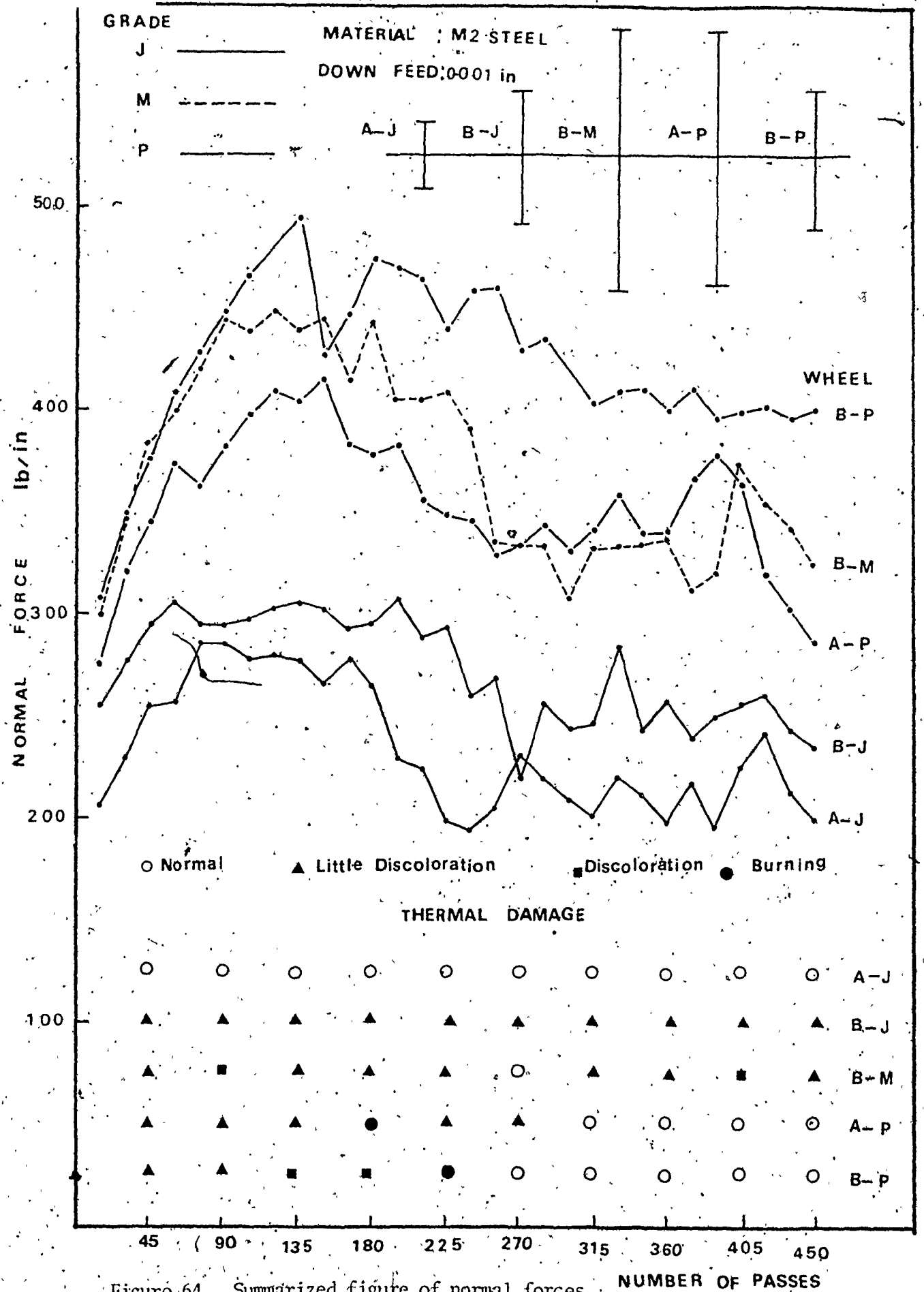

Figure 64. Summarized figure of normal forces versus number of passes for M_2 steel.

unbalance of the wheel is observed which is due to the nonuniformity of the wear over the circumference of the wheel. During this period the effect on thermal damage of the ground surface improves. This indicates that the wheel is regaining its "sharpness", or grinding capability.

The wheel finally enters a rather stable stage (D) with a fairly high wear rate and low force. It seems that a balance of self sharpening is maintained in this stage.

Thus the accompanying changes in wheel wear rate and in grinding forces with time are explained.

Conclusion

It is important to point out here that the performance of grinding wheels can be evaluated from force pattern and grinding wheel wear during this long grinding test. This test appears to present a clear picture of the wear phenomenon and could be adopted for the selection of grinding wheels.

5.2.3.2 Effect of Wheel Hardness on Force Pattern

Normal force patterns for different wheel grades of both groups of wheels (A, B), under identical grinding conditions, are presented in the summarized Figure (64), (Material M_2).

In the upper portion of the figure the maximum amplitude of forced vibration for different wheel grades are presented.

The values presented are taken from the individual graphs in Figures (73-76) in Appendix I.

In the lower part of the same figure, the thermal damage to the work piece as it was observed during the tests is illustrated.

With soft wheels A-J, B-J, it is seen that the normal forces remain constant and the grinding wheels maintain their cutting ability over a long period of grinding.

As regards thermal damage, the surface of the work piece remains normal during the test, with only a little discoloration, in the case of the B-J wheel.

The amplitude of forced vibration, Figures (73), (74) does not change except for group B where the change was slight.

The above observations give a good impression of how soon the self-sharpening phenomenon takes over from the initial dressing.

With hard wheels, A-P and B-P, an increase in the normal component of grinding force is observed during the early part of the grinding test, followed by a stabilization of forces.

This shows that self-sharpening phenomenon is not completely capable of countering wear, and wear flats are developed on the grains as mentioned in the preceding section.

Hard wheels underwent several changes during the early stages of the test due to wear of grits by attrition,

high grits temperature and thermal shocks which the grit sustains as it enters and leaves the wheel/work piece contact area. These changes in the wheel resulted in the variation of surface damage on the work piece (varying between discoloration and burning).

It is necessary to mention here that during this rather long grinding test the thermal effect does not increase but improves when reaching the end of the test. The amplitude of forced vibration changes during the test as it is seen in Figures (75), (76) in Appendix I.

In the upper portion of Figure (64) it is clear that the maximum amplitude of forced vibration increases with wheel hardness grades from J to M to P.

Force patterns for different wheel grades of both groups of wheels (A, B) when cutting 52100 steel are summarized in Figure (65).

The facts mentioned above about the behaviour of wheels with M_2 steel were found to be similar to that of the wheels with 52100 steel.

The only difference in the behaviour is that the thermal damage in the case of 52100 steel is increased.

This is owing to the fact that the down feed was increased from 0.001 in. to 0.002 in.

Conclusion

Based on force patterns and the extent of thermal

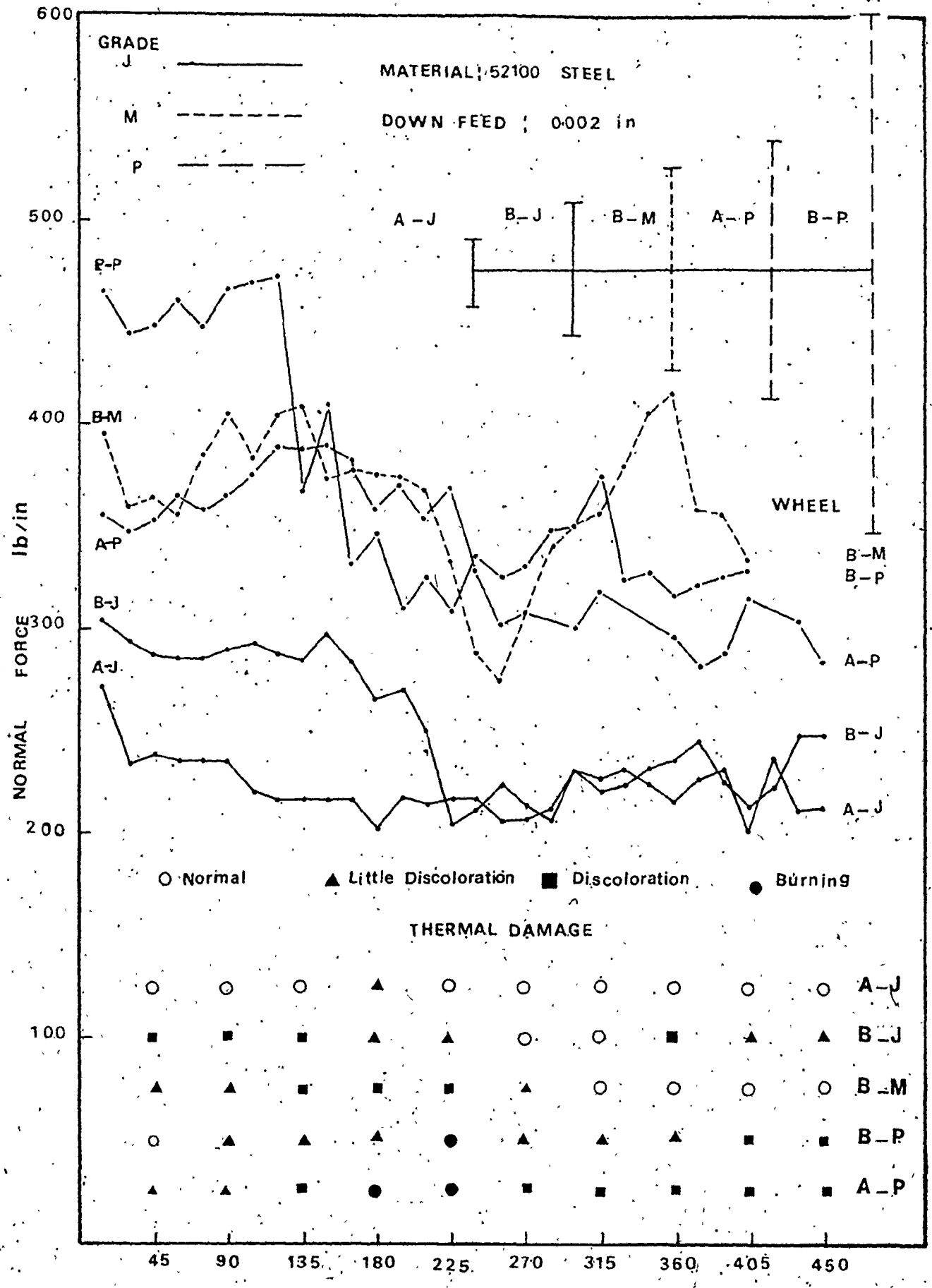

Figure 65. Summarized figure of normal forces versus number of passes for 52100 steel.

damage to the ground surface, as shown in the summarized Figures (64) and (65), it can be concluded that all tested wheels, of rather hard variety, continuously maintained their cutting capability.

The maximum normal force $\bar{F}_{max}$ reached during the long grinding operation for different wheel grades are summarized in Figure (66). This figure compares the grinding forces for M_2 and 52100 steels. It is seen that maximum cutting forces increase with increased wheel hardness for both work steels. This is clear from the fact that harder wheels, as it is shown by Malkin [4] in Figure (67), have more active grains, larger wear flat areas and hence require larger grinding forces.

5.2.3.3 The Variation in Grinding Ratio with Wheel Hardness

Grinding ratio was calculated by two methods. Firstly, based on material removed every 45 passes (Δx) and corresponding wheel wear (Δr).

$$G = \frac{L\ \Delta x}{\pi\ D\ \Delta r}$$

Secondly, based on material removed from the beginning of the test up to a time period when the number of passes is = n x 45 (where n is an integer) $\Delta\bar{x}$, and corresponding accumulated wheel wear ($\Delta\bar{R}$).

$$\bar{G} = \frac{L\ \Delta\bar{x}}{\pi\ D\ \Delta\bar{R}}$$

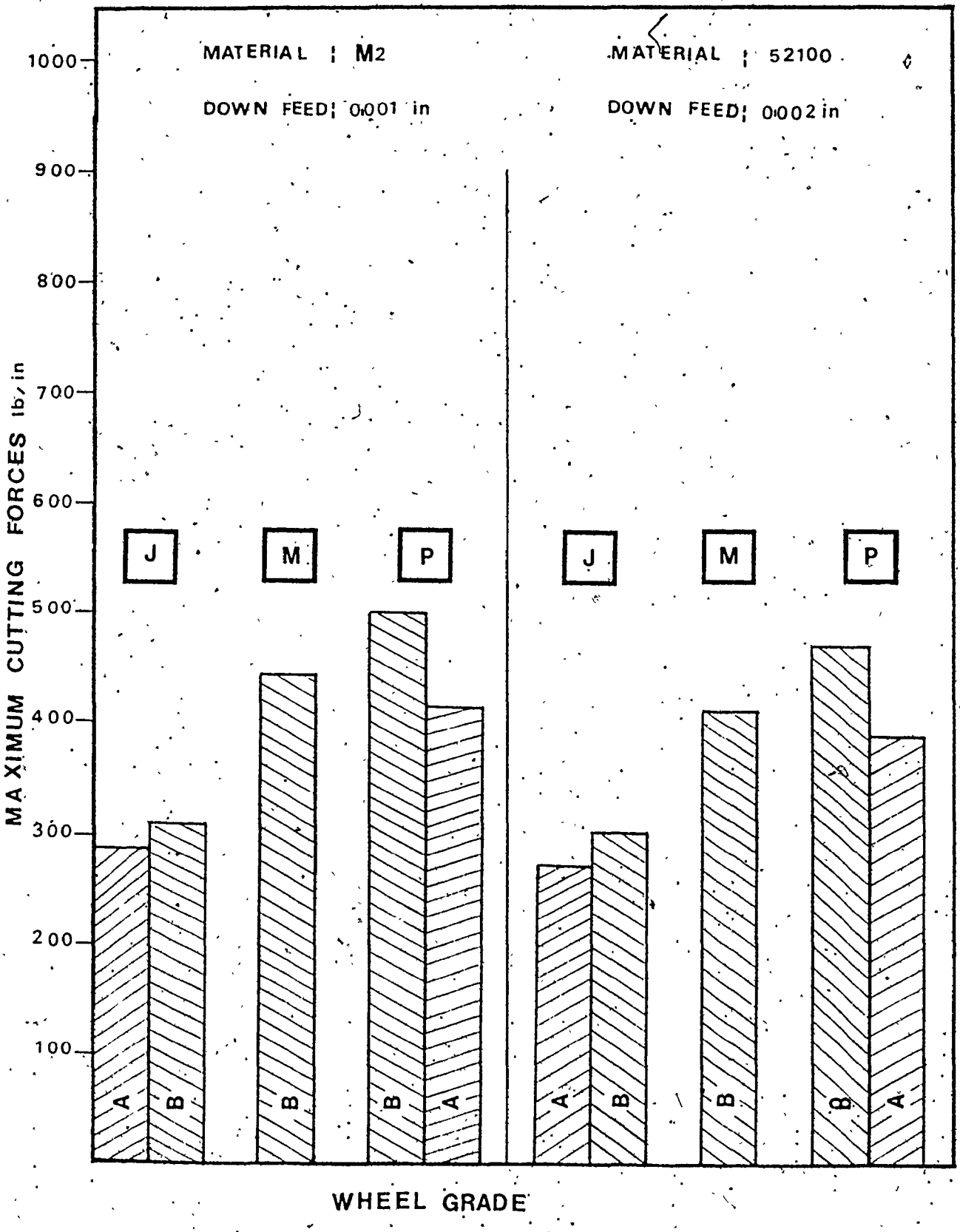

Figure 66. Summarized figure of maximum forces during the long grinding test.

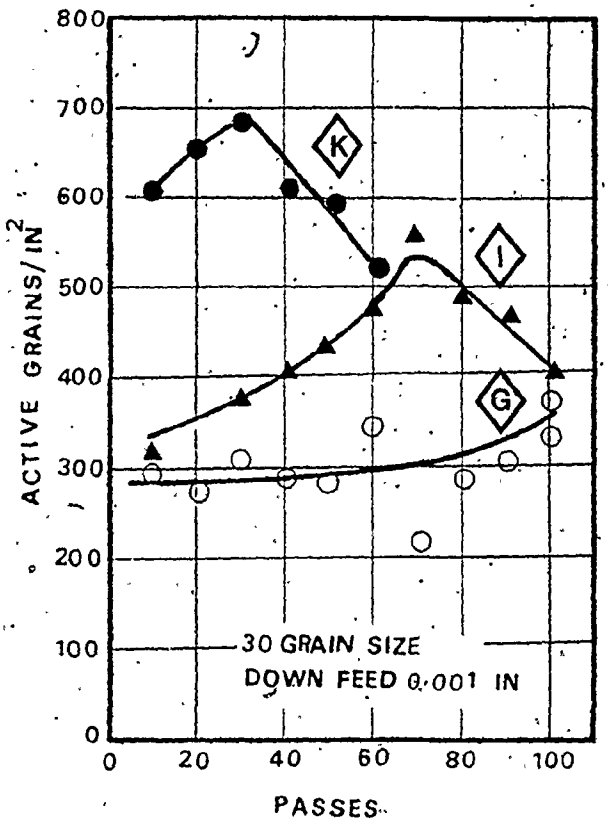

Figure 67(a) Active grains/in^2 versus number of passes for different wheel grades [28].

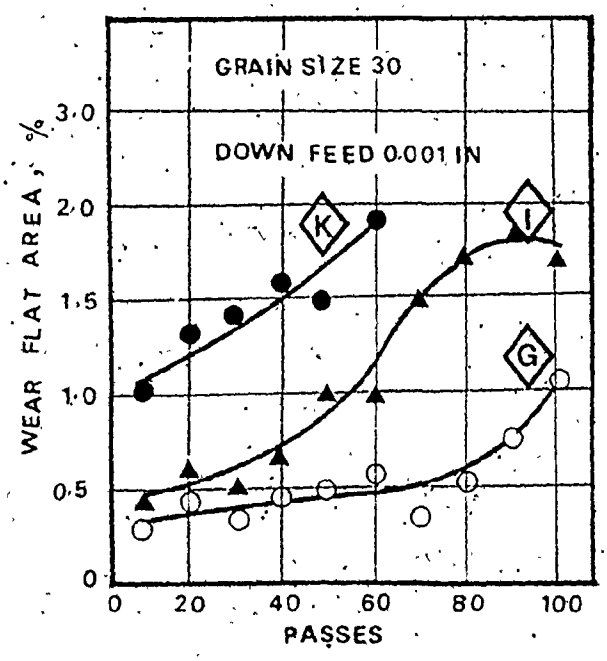

Figure 67(b) Wear flat area versus number of passes for different wheel grades [28].

A good representative of grinding ratio is that final value of the accumulated wear and it will be taken as the base of comparison.

The maximum and minimum individual grinding ratio together with the final accumulated grinding ratio for different combinations of wheel grades and work materials are summarized in Figure (68).

It is necessary to point out that the scale for G ratio is two times larger for 52100 steel than that for M_2 steel.

Checking on the B group of wheels for both steels, 52100 and M_2, it can be seen that as the hardness of the wheels increases the grinding ratio first increases and then decreases giving an optimum wheel hardness.

The highest grinding ratio is found to be 9.69 for 52100 steel and 6.43 for M_2 steel with optimum wheel hardness M for both steels.

Checking on the A group of wheels for both materials it is found that as the hardness of the wheels increases from J to P grade, the grinding ratio decreases.

It is important to mention here that the grinding ratio does not increase appreciably while increasing the wheel grade from J to M to P.

Discussion of the Results

Lure [18] found that the grinding ratio tends first to increase with the wheel hardness but then reaches a peak

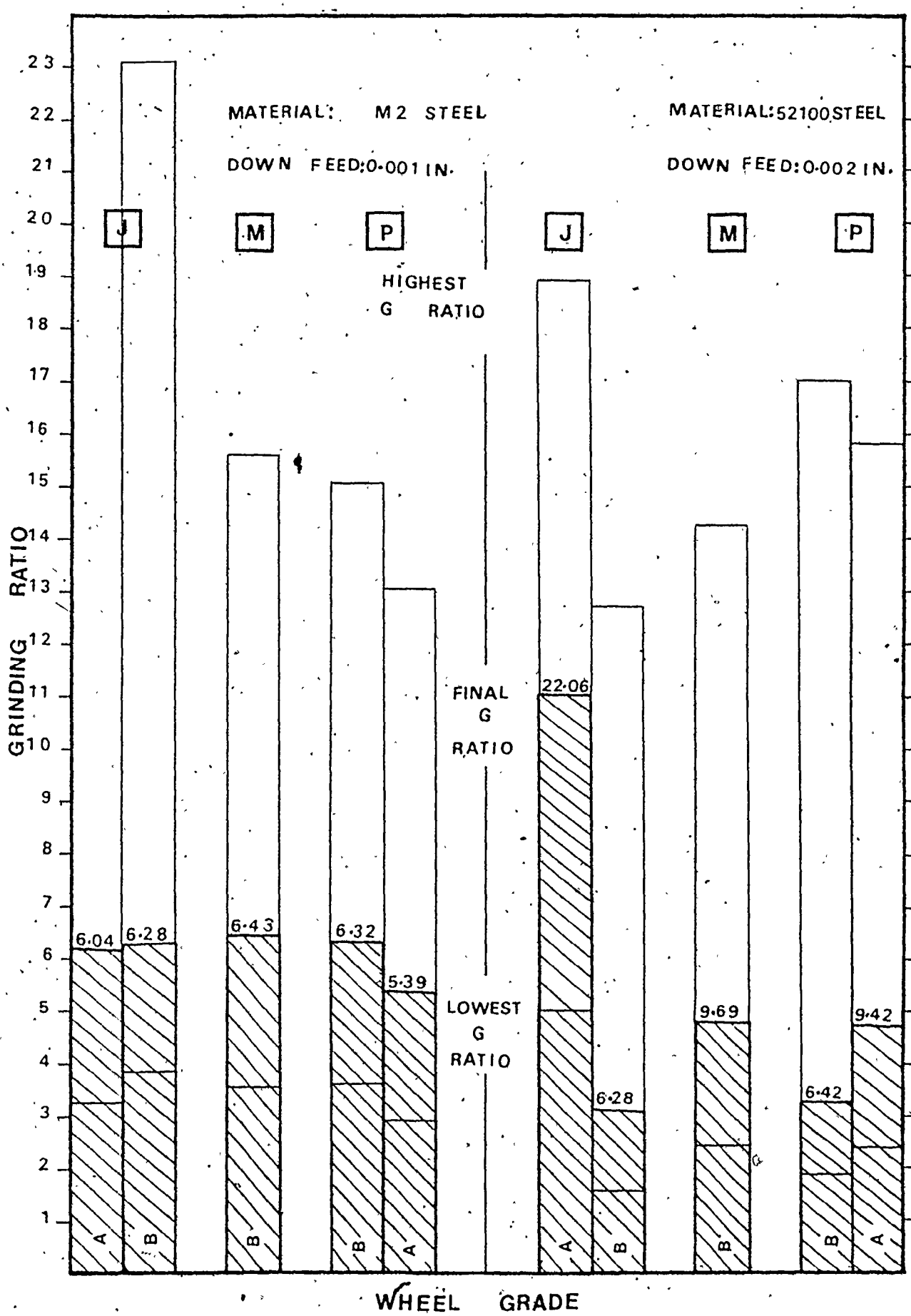

Figure 68. Summarized figure of grinding ratio versus wheel hardness.

and thereafter decreases with further increases in wheel hardness. Our results are in agreement with Lure's results. The above found phenomenon may be explained as follows: as the hardness is increased the wheel first grinds in the self-sharpening range and later in a zone of mixed conditions partly sharpening and partly blunting. In the final range blunting is predominant, material removal rate drops with excessive wheel loading and wheel wear increases. With A wheels it appears that we are on both sides of the optimum curve with A-J wheel grinding in the zone of self-sharpening and A-P wheels grinding in the range where blunting becomes progressively predominant.

Force patterns of soft wheel J for M_2 steel in Fiugures (73) and (74) show that the rise in force is small compared to hard wheels of grade P in Figures (75) and (76), (Appendix II). This suggests the occurrence of self-sharpening in soft J wheels with very little of flat formation.

The variation of radial wear with the number of passes, for A-J wheel (soft grade) and A-P wheel (hard grade), are presented in Figures (69) and (70) for both work steels.

If the screen number of the used grain is 60, then the mean diameter given by [19] = 0.7 x nominal diameter = $0.7 \times \frac{1}{60} = 0.011$ inch.

The final radial wear of A-P wheel for M_2 and 52100 steels are $\Delta\bar{R} = 0.011$ in. and 0.012 in. respectively (about 0.96, 1.1 times grain diameter). Also the final radial wear of the A-J wheel for M_2 and 52100 steels is $\Delta\bar{R} = 0.009$ in. and

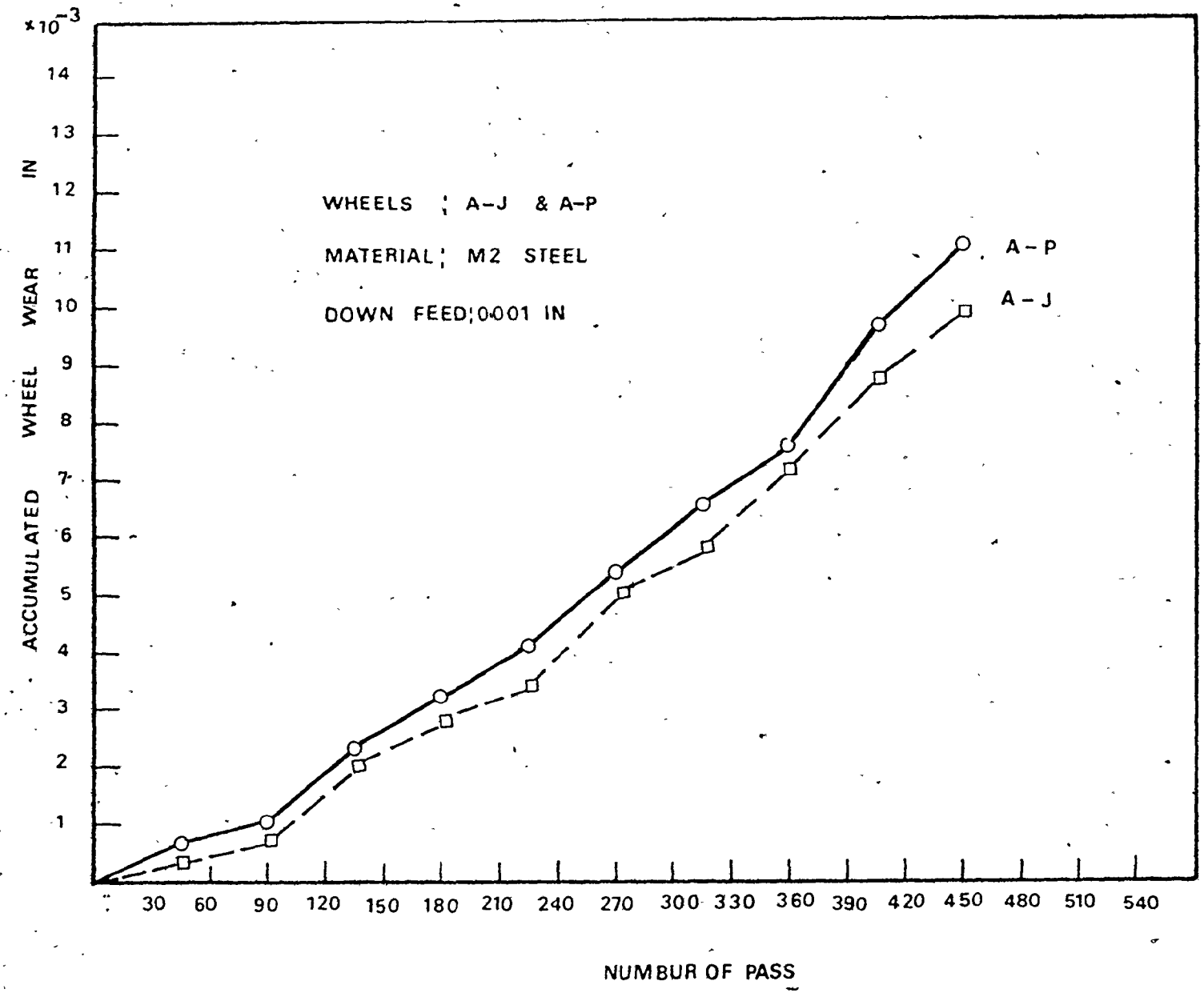

Figure 69. Variation of radial wheel wear with number of passes for M_2 steel.

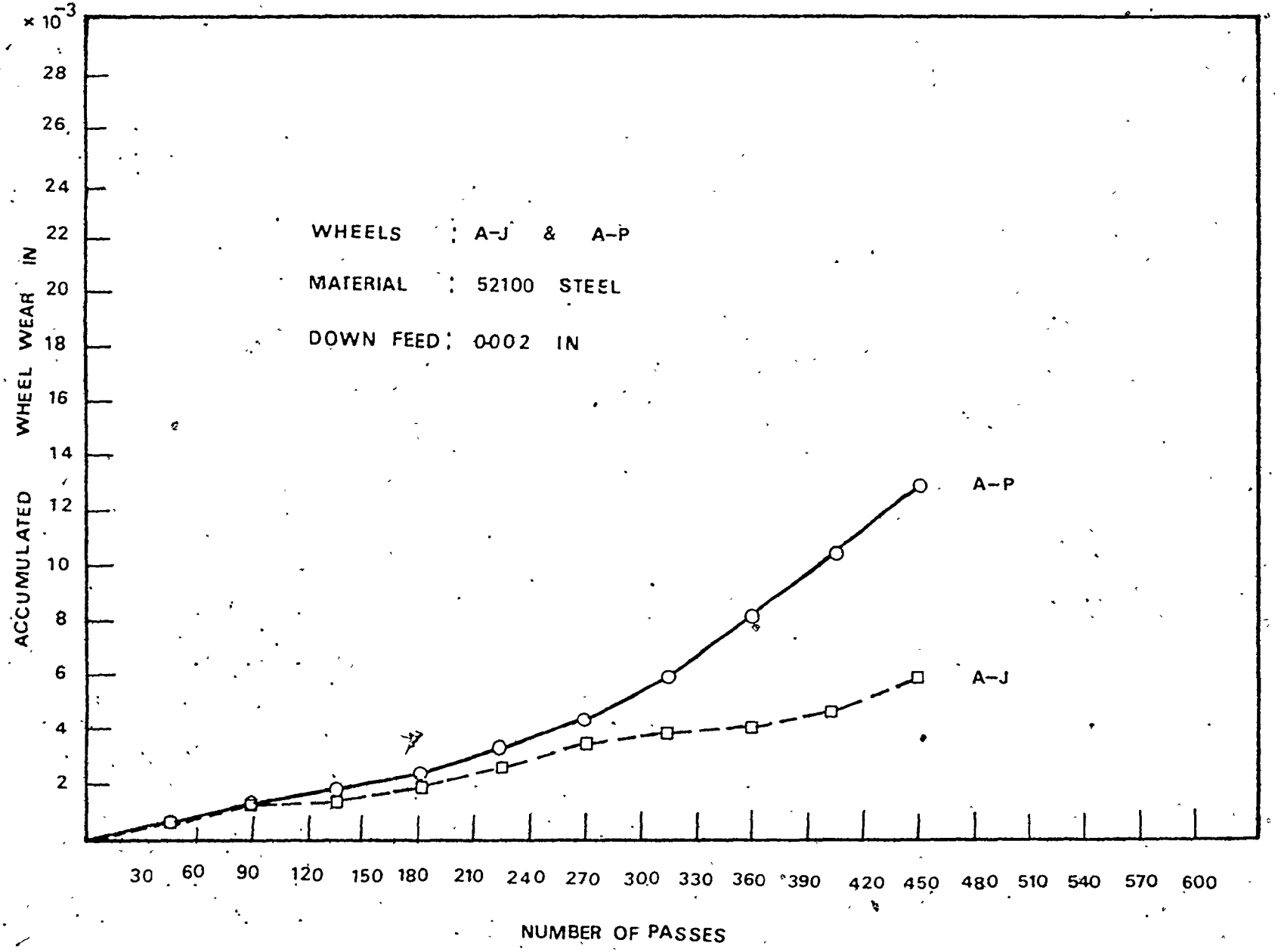

Figure 70. Variation of radial wheel wear with number of passes for 52100 steel.

0.005 in. (about 0.85, 0.47 times grain diameter).

The above results indicate that the amount of radial wear was high enough (about 0.47 to 1.1 grain diameter) to give a true picture of the wheel wear phenomenon and the grinding wheel cutting capability.

Unexpectedly, the softer wheels in these rather hard grades (J, M and P) give less wear and higher grinding ratio than the harder grades.

The results presented above are, however, different in the case of grinding wheels of the rather soft grades (G, H and J), [Ref. 27].

The difference in performance is that increasing the hardness grade in this range leads not only to higher grinding forces and a greater extent of thermal damage but also to a lower grinding ratio.

5.2.4 The Influence of the Dressing Process

5.2.4.1. Introduction

In order to enable the wheel to remove material efficiently, the bond material between the grits must be removed preferentially so that the space is available for grinding chips to be accommodated. The grits must also be fractured so as to reduce the plateau area. This is the function of the dressing operation, from which, when properly performed, the wheel emerges in an open and sharp condition.

The influence of replacing the used dressing tool (U.D.T.) with a new dressing tool (N.D.T.) as well as changing

the dressing depth of the cut on the grinding process were studied. Tests were carried out using a soft wheel (A-60-J) for both steels M_2 and 52100.

5.2.4.2 Test Results

The variation of grinding force components and grinding wheel wear with grinding time for M_2 steel is shown on an individual graph in Figures (79) to (82) in Appendix II. Normal force patterns showing the influence of changing the dressing tool, changing the dressing depth of cut and the variation of the down feed are shown in the summarized Figures (71) and (72) for both steels. Examining Figure (71) for M_2 steel it can be said that dressing plays an important role during the very early stages of the grinding operation.

The comparison of curves 1, 2 in Figure (71) shows that an increase in the dressing depth of cut results in reducing the average force during the test and the extent of thermal damage. In addition to this, forces start with a lower value indicating that smaller flats are developed.

Comparing Figures (79) and (80) and checking on the upper part of Figure (71), it is shown that the amplitude of the forced vibration is decreased, which means that the uniformity of wheel wear is improved.

The influence of increasing down feed is seen when comparing curves 2,3. In general increasing down feed increases the average force and the nonuniformity of the grinding wheel.

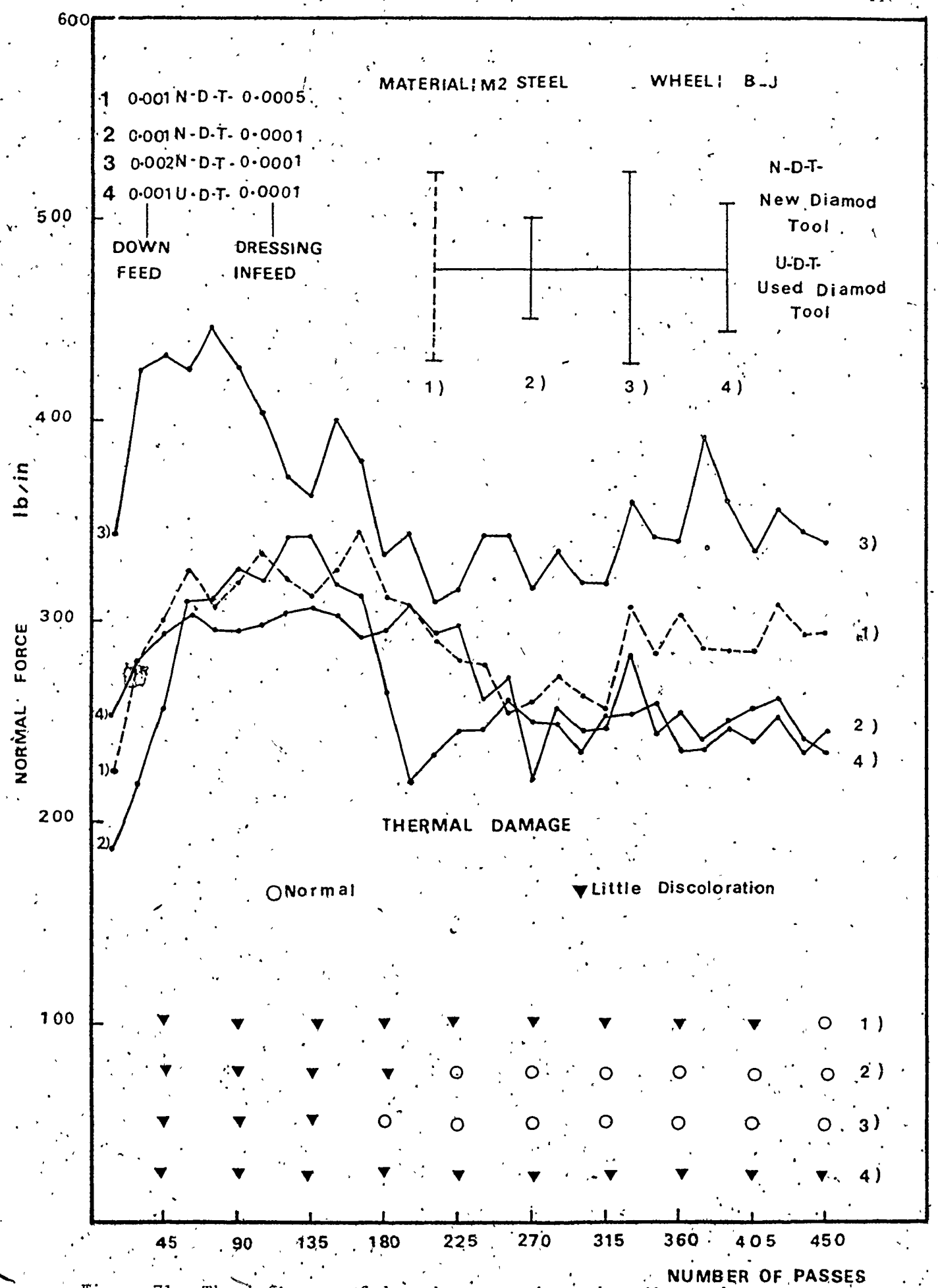

Figure 71. The influence of dressing operation using M_2 steel.

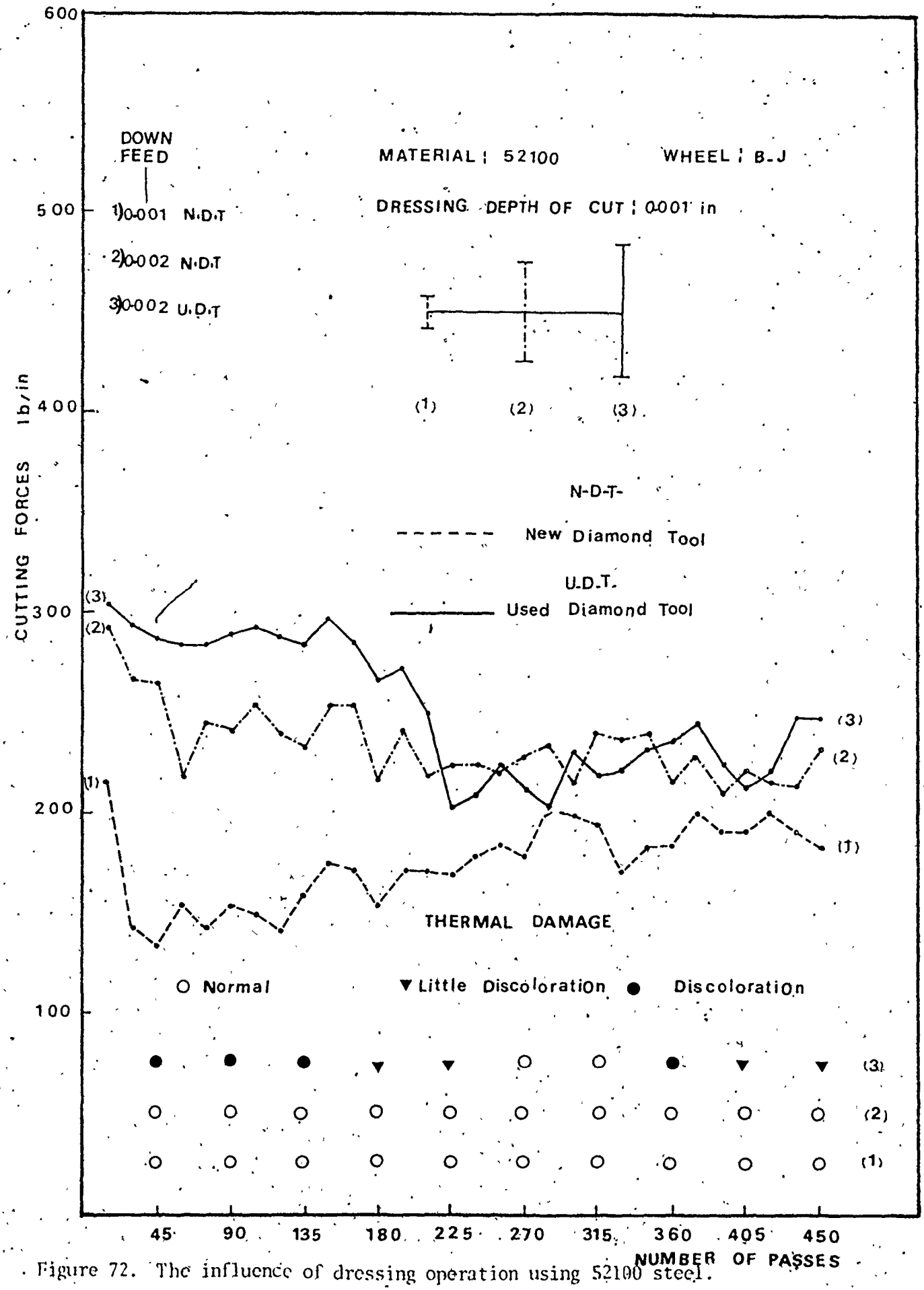

Figure 72. The influence of dressing operation using 52100 steel.

The increase of thermal damage seems to be the only influence of dressing with a worn out diamond tool. Checking the summarized Figure (72) for 52100 steel, the same influence of increasing down feed and dressing with a used diamond tool is obtained. The nonuniformity of wheel wear is affected by down feed and the quality of the dressing tool

The radial wheel wear increased from 0.011 in. to 0.015 in. and the grinding ratio decreased from 5 to 4 when the dressing depth of the cut increases in Figures (81) and (82) (Appendix II).

It can be seen from the same figures that increasing the dressing depth of the cut increases the rate of wear at the beginning of the test.

5.2.4.3 Discussion of Test Results

As the severity of the dressing increases by an increase in the dressing depth of cut, the plateau area before starting grinding will be reduced and more cracks will have been introduced into the grits so that their readiness to fracture during grinding will be enhanced.

Malkin [19] stated that the greater the dressing depth of the cut, the fewer the number of active grains.

Since the grinding force increases as the plateau area per grit increases [4] and because the plateau area is considerably smaller with a higher dressing depth of cut, it can be expected that the force will start to increase from a

lower value. Also the opportunity of severe surface damage will be lesser and this would be followed by an increase in the cutting ability of the grinding wheel.

On the other hand, if the dressing depth is reduced the plateau area becomes larger. The temperatures at the grits rapidly exceed the critical value at which grit wear becomes excessively high and work piece burn occurs.

While the readiness of cutting grains to fracture increases with increasing dressing depth of cut, it is to be expected that the radial wheel wear would be higher.

Conclusion

In agreement with Malkin [18], Pacitti [21] and Tsuwa [20], the experimental evidence presented here indicates that a fine dressing (smaller dressing depth of cut) gives a low wheel wear but results in high grinding forces and a greater tendency toward work piece thermal damage.

CHAPTER 6

CONCLUSTIONS

Results of measurements of grinding forces and wheel wear, in addition to the scanning electron microscope observations, were presented for grinding hardened tool steel M_2 and AISI bearing steel 52100. Plunge-type surface grinding tests were performed with differenent hardness grade wheels of aluminum oxide grains in vitrified bond.

In this section the main conclusions of this investigation are presented:

1. Experimental findings indicate that, as the wheel hardness increases from grade J to M to P, two criteria are found to increase: the force components (normal and tangential) and the extent of thermal damage. Contrary to common belief, the grinding ratio does not increase appreciably.

   This is different in the lower range of wheel hardness. When wheel hardness increases from G to H to J, three criteria increase: the force components, the extent of thermal damage and the grinding ratio.

2. During a long grinding operation all wheels tested (of a rather hard variety) continuously maintain their grinding capability, i.e., there was no increase in either the cutting forces or the extent of thermal

damage.

This is contrary to Malkin [4] and to what is commonly believed.

3. From the two previous conclusions it can be seen that in grinding hardened steels 52100 and M_2 under plunge-surface grinding operation, the optimum hardness grade to be used is grade J.

   This soft grade J gives the same grinding ratio as hard grades M and P while lower grinding forces and less thermal damage are obtained.

4. The method of evaluating the performance of grinding wheels from force pattern and grinding wheel wear appears to present a clear picture of the wear phenomenon and it could be adopted for the selection of grinding wheels.

REFERENCES

1. M. C. Shaw, "New Developments in Grinding", Proceedings of the International Grinding Conference, April 18-20, 1972, Carnegie Press, Pittsburgh, p. 161.

2. P. Ramachandran and S. Vaidyanathan, "Statistical Evaluation of Parameters in Grinding", Wear, 36 (1976), p. 119.

3. E. J. Krabacher, "Factors Influencing the Performance of Grinding Wheels", Trans. ASME 81B, (1959), p. 187.

4. S. Malkin, "The Attritious and Fracture Wear of Grinding Wheels", Ph.D Thesis, Massachusetts Institute of Technology, February, 1968.

5. G. B. Lure, "Evaluating the Performance of Grinding Wheels", Russian Engng., J. 47, 69 (1967).

6. H. Y. Yoshikawa, T. Sata, "Study on Wear of Grinding Wheels", Journal of Engineering for Industry, Trans. ASME, Series B, February 1963, p. 39.

7. H. Yoshikawa, "Theory of Tool Life for Grinding Wheels", Annals of the C.I.R.P., Vol. XIV, 1967, p. 347.

8. S. Malkin, W. H. Cook, "The Wear of Grinding Wheels, Part I, Attritious Wear", J.S.M.E., 1971, p. 1120.

9. S. Malkin, N. H. Cook, "The Wear of Grinding Wheels, Part II, Fracture Wear", J.S.M.E., 1971, p. 1129.

10. S. Kannappan, S. Malkin, "Effects of Grain Size and Operating Parameters on the Mechanics of Grinding", J.S.M.E., 1972, p. 1.

11. G. K. Lal, M. C. Shaw, "Wear of Single Abrasive Grain in Fine Grinding", Proc. Int. Grinding Conf., Pittsburgh, 1972, p. 107.

12. S. J. Pande and G. K. Lal, "Wheel Wear in Dry Surface Grinding", Int. Mach. Tool Des. Res., Vol. 16, 1976, p. 179.

13. G. Stetiu, G. K. Lal, "Wear of Grinding Wheels", Wear, 30 (1974), p. 229.

14. W. R. Backer and M. E. Merchant, "On the Basic Mechanics of the Grinding Process", A.S.M.E., Vol. 80, 1958, p. 141.

15. S. K. Gattcharyya and V. L. Moffat, "Characteristics of Micro Wheel Wear in Grinding", 16th International Machine Tool Design and Research Conference, U.M.I.S.T., 1975, p. 13.

16. H. Kaliszer and G. Trmal, "Force Vibration During Plunge Grinding and its Effect on Surface Topography", Proc. Int. Grinding Conf., Pittsburgh, 1972, p. 708.

17. S. Shiozaki, M. Miyshita and Y. Furukaw, "Generation and Growing Up Process of Self-Excited Chatter Vibration in Grinding", J.S.M.E., 13, 1970, p. 139.

18. J. Kaczmarek, Z. Kornberger, "Cutting Capability of Grinding Wheels Its Symptoms and Stability", Annals of the C.I.R.P., Vol. 21/I, 1972, p. 79.

19. S. Malkin, R. B. Anderson, "Active Grains and Dressing Particles in Grinding", Proc. Int. Grinding Conf., Pittsburgh, 1972, p. 142.

20. H. Tsuwa and H. Yasui, "Micro Structure of Dressed Abrasive Cutting Edges", Proc. Int. Grinding Conf., Pittsburgh, 1972, p. 142.

21. V. Pacitti, C. Rubenstein, "The Influence of Dressing Depth of Cut on the Performance of a Single Point Diamond Dressed Alumina Grinding Wheel", Int. J. Mach. Tool Des. Res., Vol. 12, 1972, p. 267.

22. A. M. Besuyen, J. Verkerk, "Scanning Electron Microscope Observations of Grinding Grains", Annals of the C.I.R.P., Vol. 20, 1971, p. 65.

23. R. Komanduri and M. C. Shaw, "A Technique for Investigating the Surface Features of a Grinding Wheel", 24th General Assembly C.I.R.P.

24. H. Optize, W. Konig, G. Werner, "Kinematics and Mechanics in Grinding with Regard to the Machining Processes", Int. Grinding Conf., Pittsburgh, 1972, p. 708.

25. W. Konig and W. Lortz, "Properties of Cutting Edges Related to Chip Formation in Grinding", Annals of the C.I.R.P., Vol. 24/I, 1975.

26. W. Konig and W. Lortz, "Three Dimensional Measurements of the Grinding Wheel Surface Evaluation and Effect of Cutting Behaviour", Annals of the C.I.R.P., Vol. 25/I, 1976.

27. M. Younis, S. Shalaby, J. Tlusty, "Basic Comparison of Grinding Wheels of Various Grains and Various Bond Strengths", Metal Working Research Group Report No. 92, Hamilton, Mechanical Engineering Department, McMaster University, October, 1976.

28. S. Kannappan, S. Malkin, "Effects of Grain Size and Operating Parameters on the Mechanics of Grinding", A.S.M.E., Paper No. 71-WA/Prod-27, 1971.

29. J. Tlusty, M. Younis, "Effect of Wheel Work piece Conformity on Performance of Grinding High Speed Steels", Proc. of the Fourth North American Metal Working Research Conference, Columbus, Ohio, 1976.

APPENDIX I

CUTTING FORCES AND WHEEL WEAR

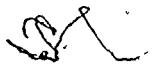

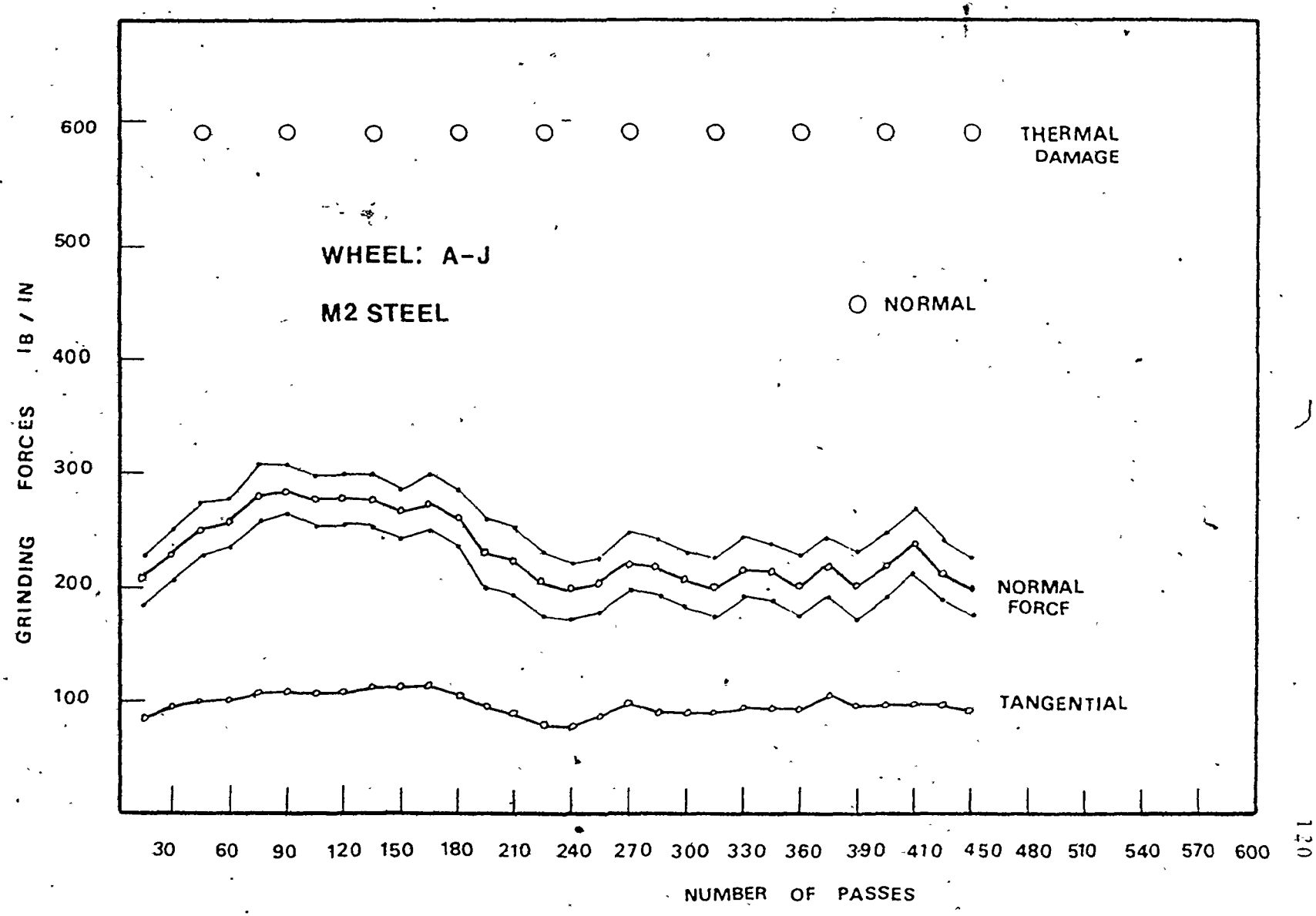

Figure 73. Cutting forces versus number of passes for A-J wheel.

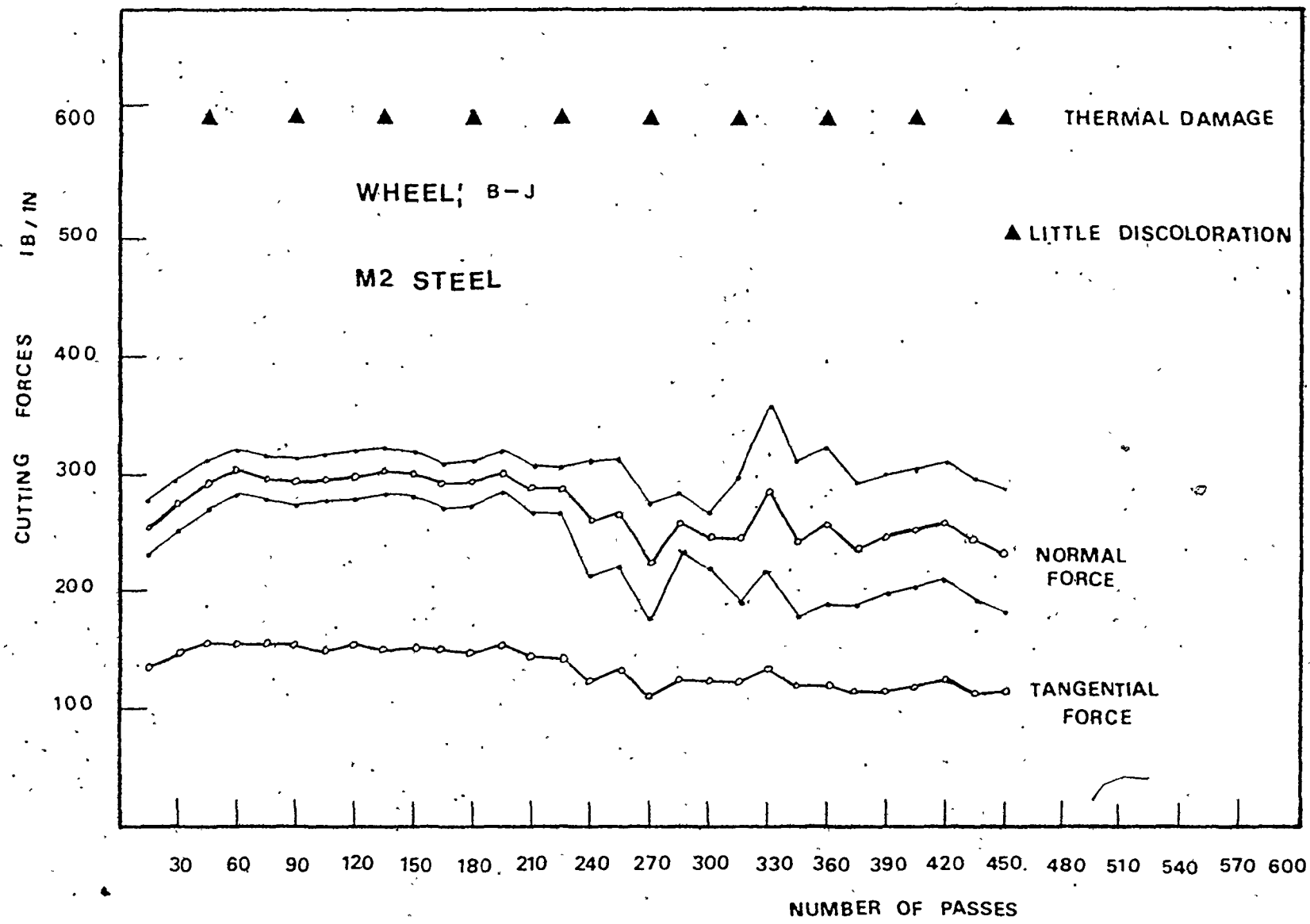

Figure 74. Cutting forces versus number of passes for B-J wheel.

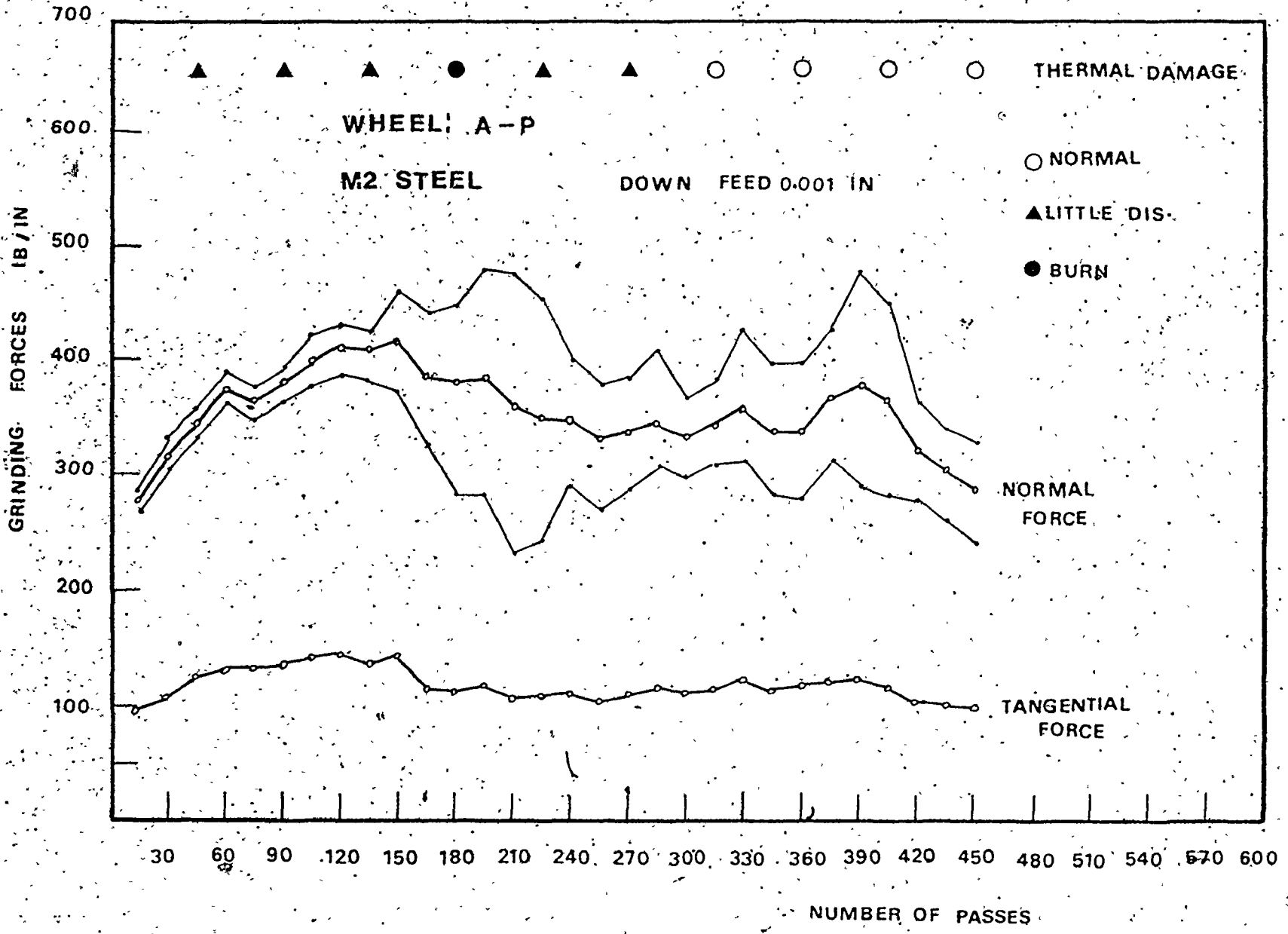

Figure 75. Cutting forces versus number of passes for A-P wheel.

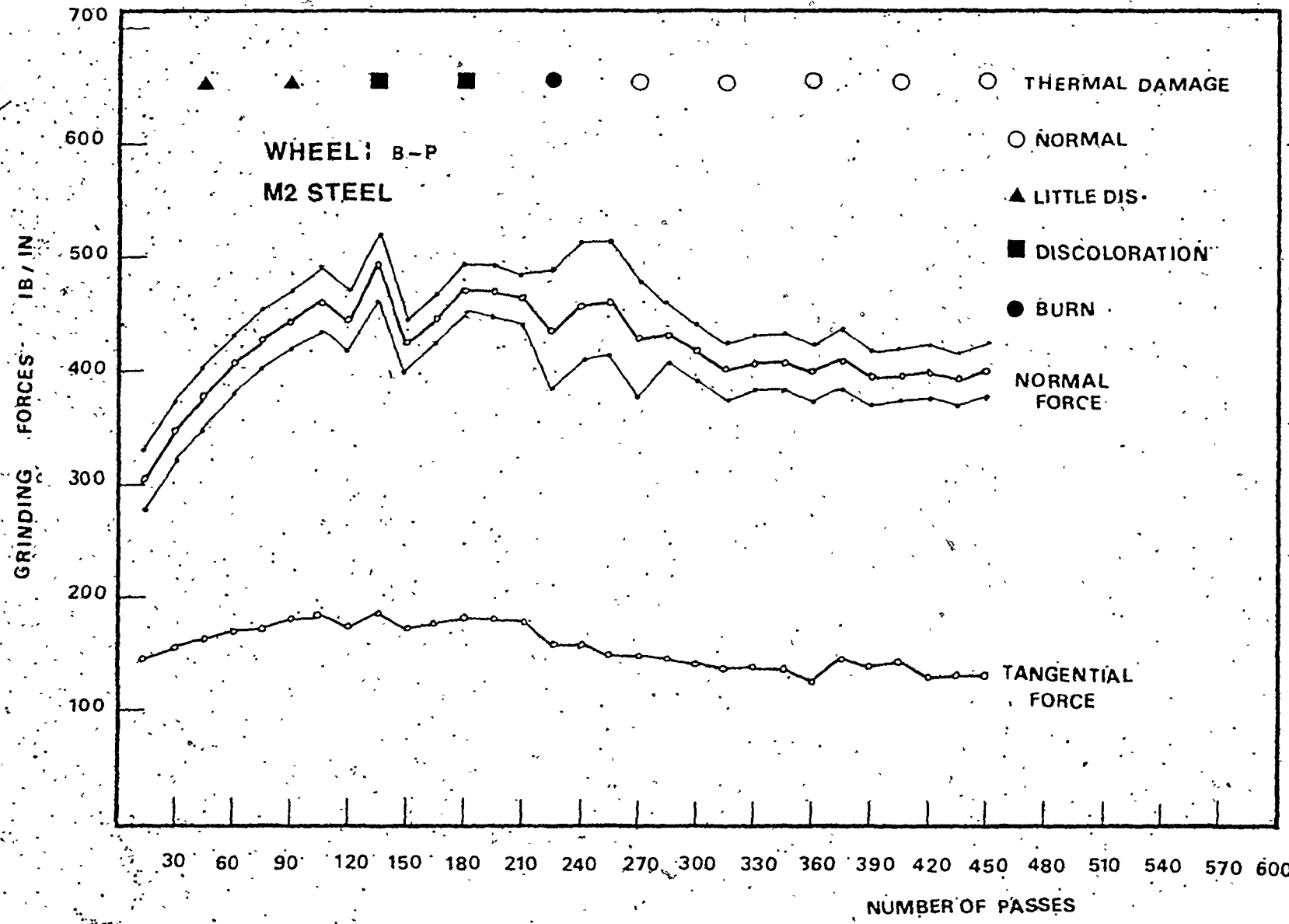

Figure 76. Cutting forces versus number of passes for B-P wheel.

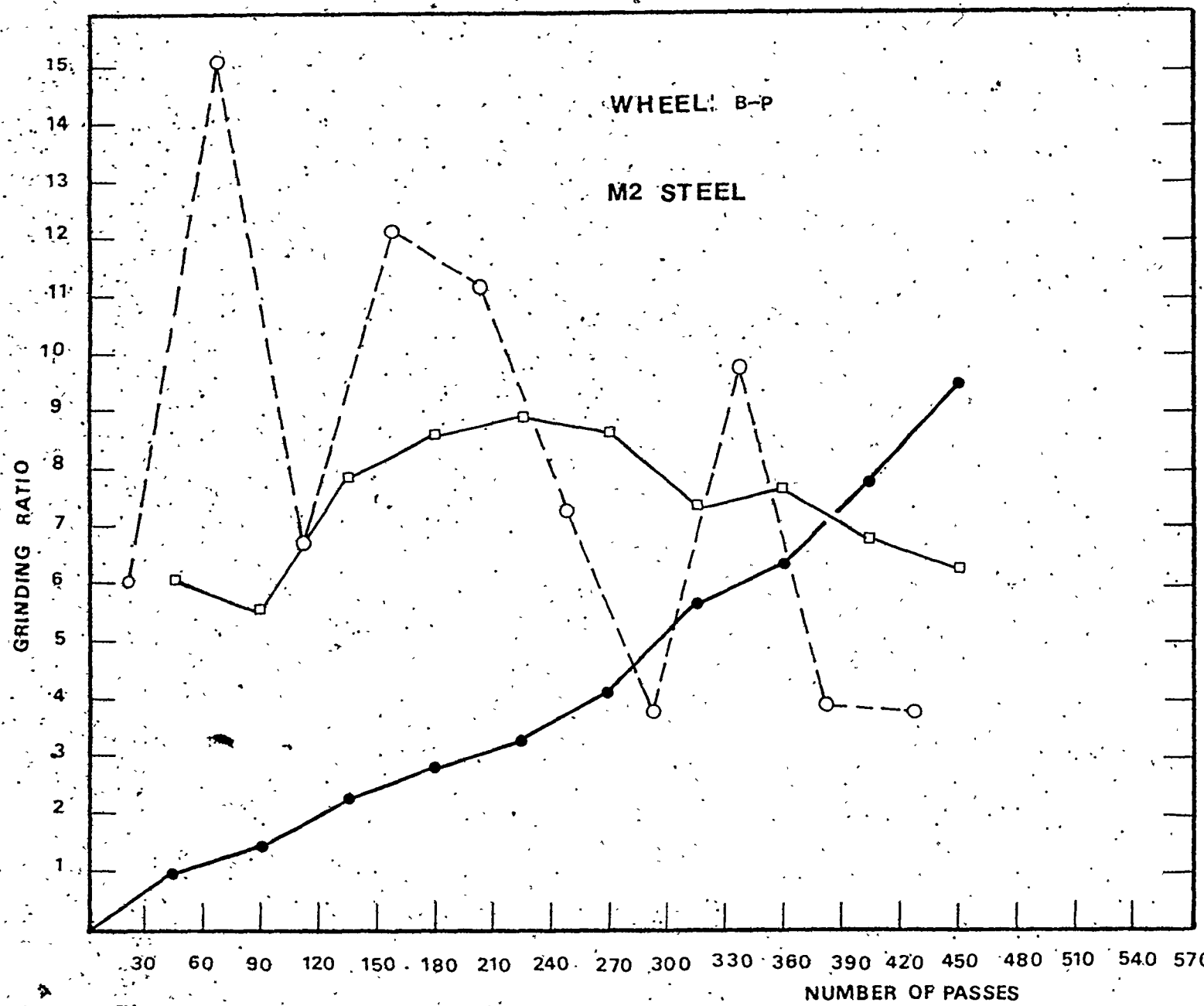

Figure 77. Grinding wheel wear versus number of passes for A-P wheel.

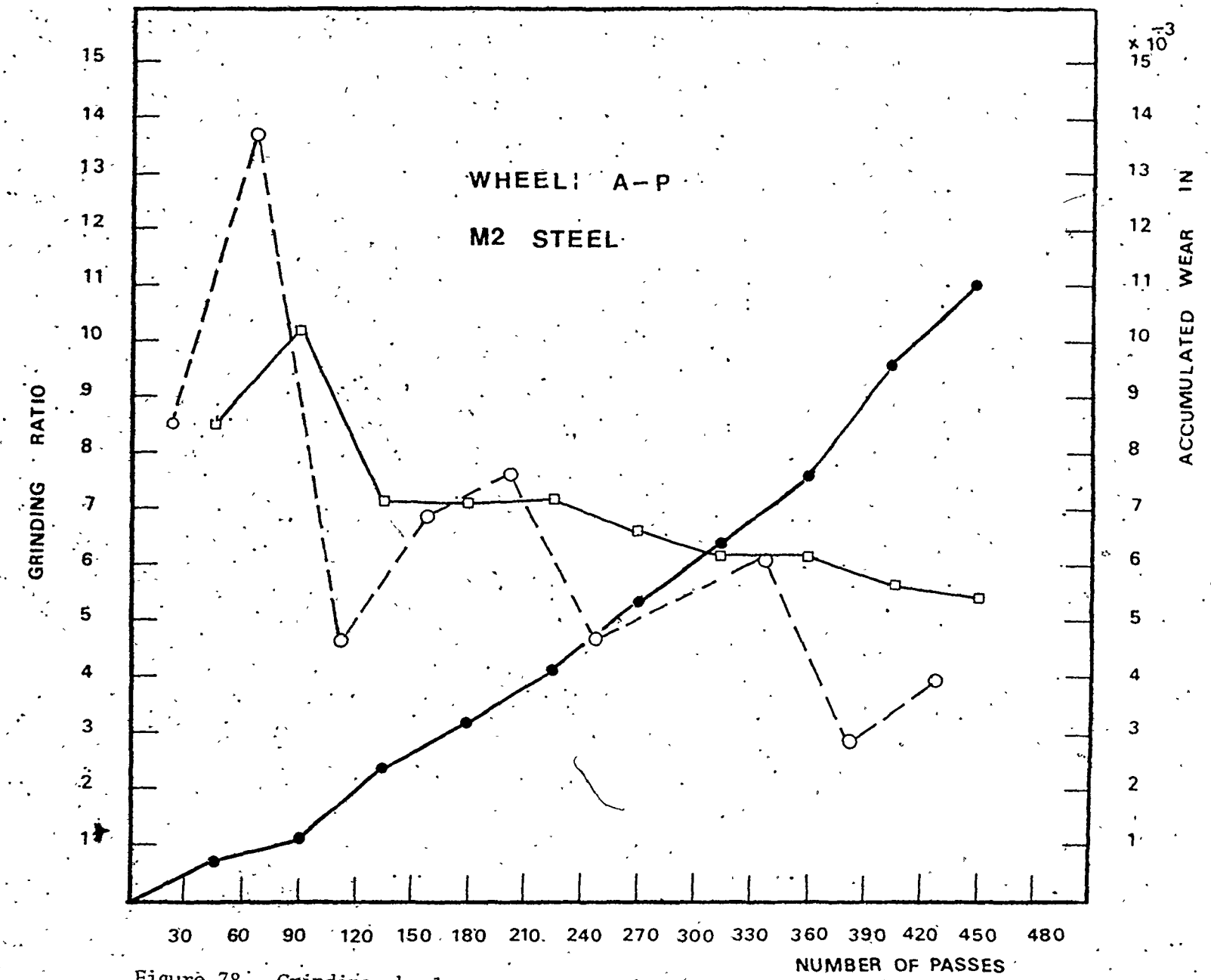

Figure 78. Grinding wheel wear versus number of passes for B-P wheel.

APPENDIX II

INFLUENCE OF DRESSING

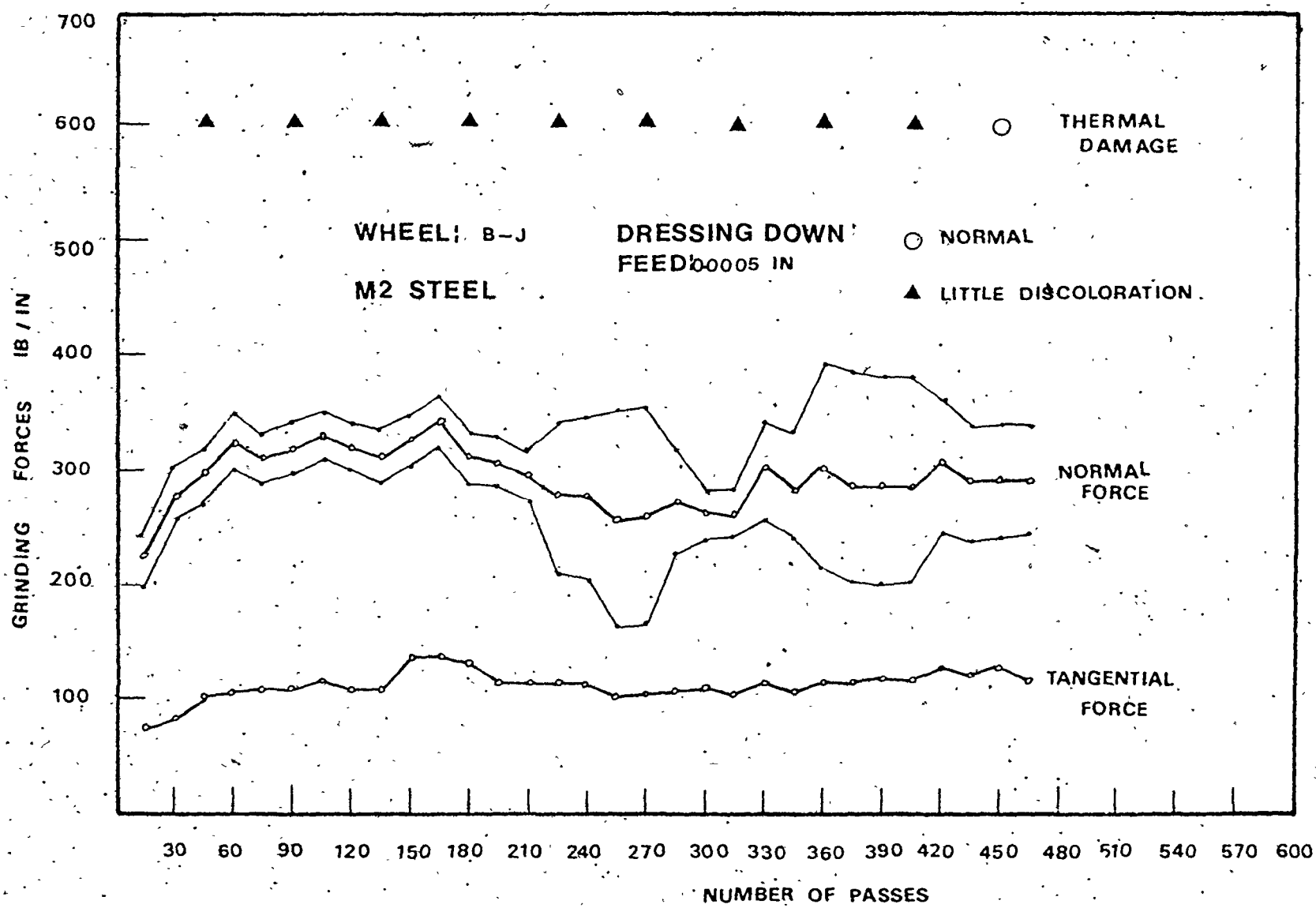

Figure 79. Cutting forces versus number of passes using fine dressing.

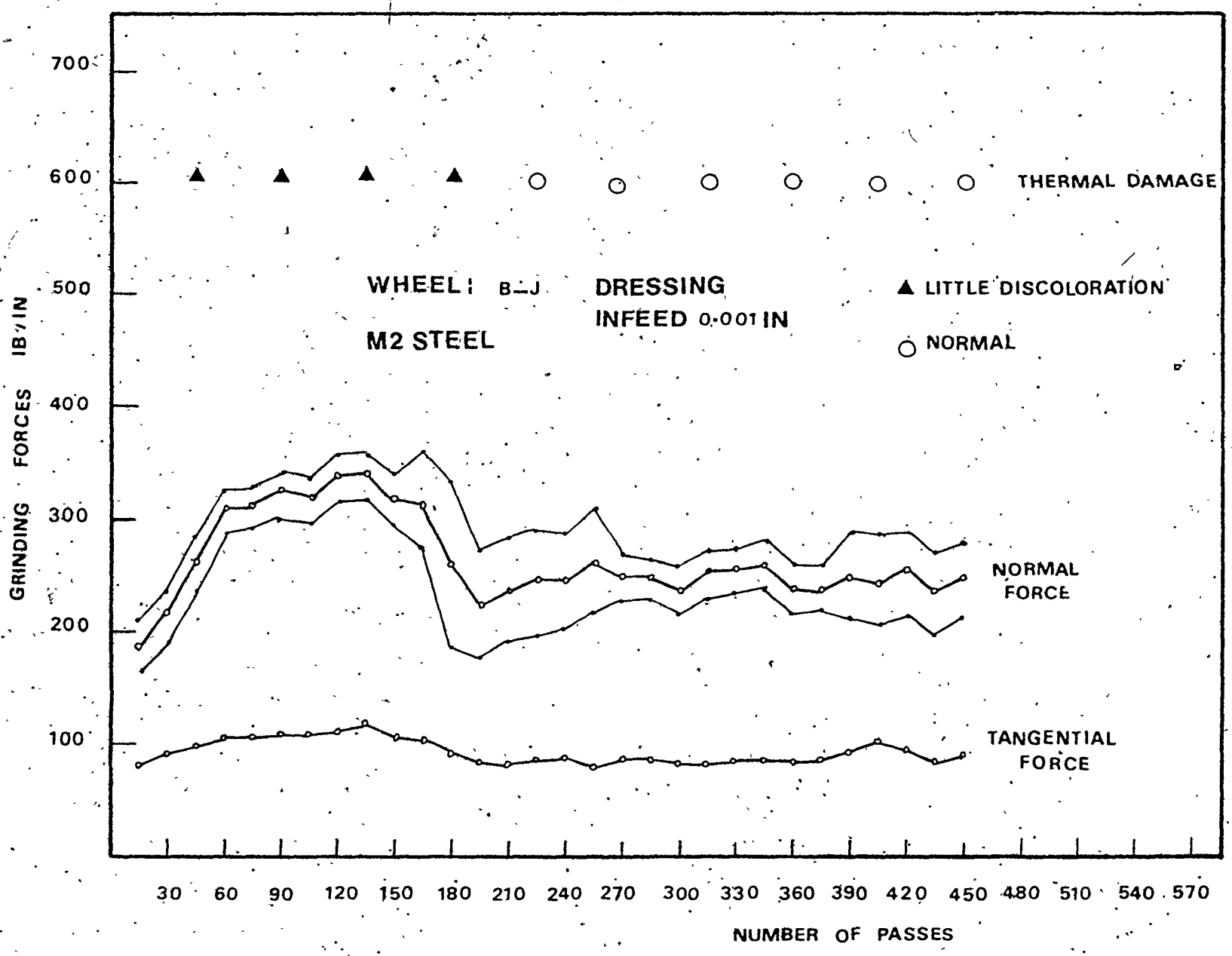

Figure 80. Cutting forces versus number of passes using coarse dressing.

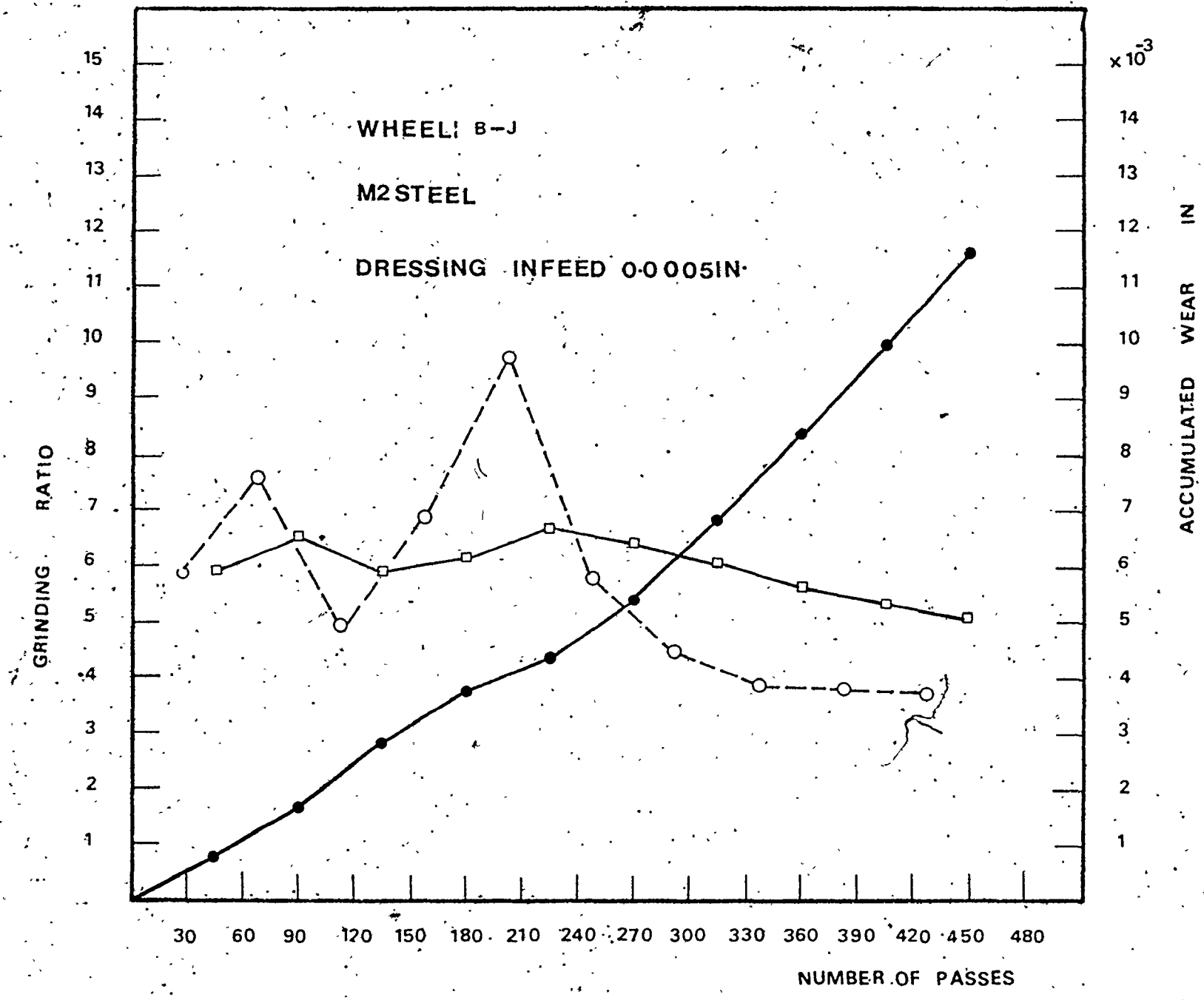

Figure 81. Grinding wheel wear versus number of passes using fine dressing.

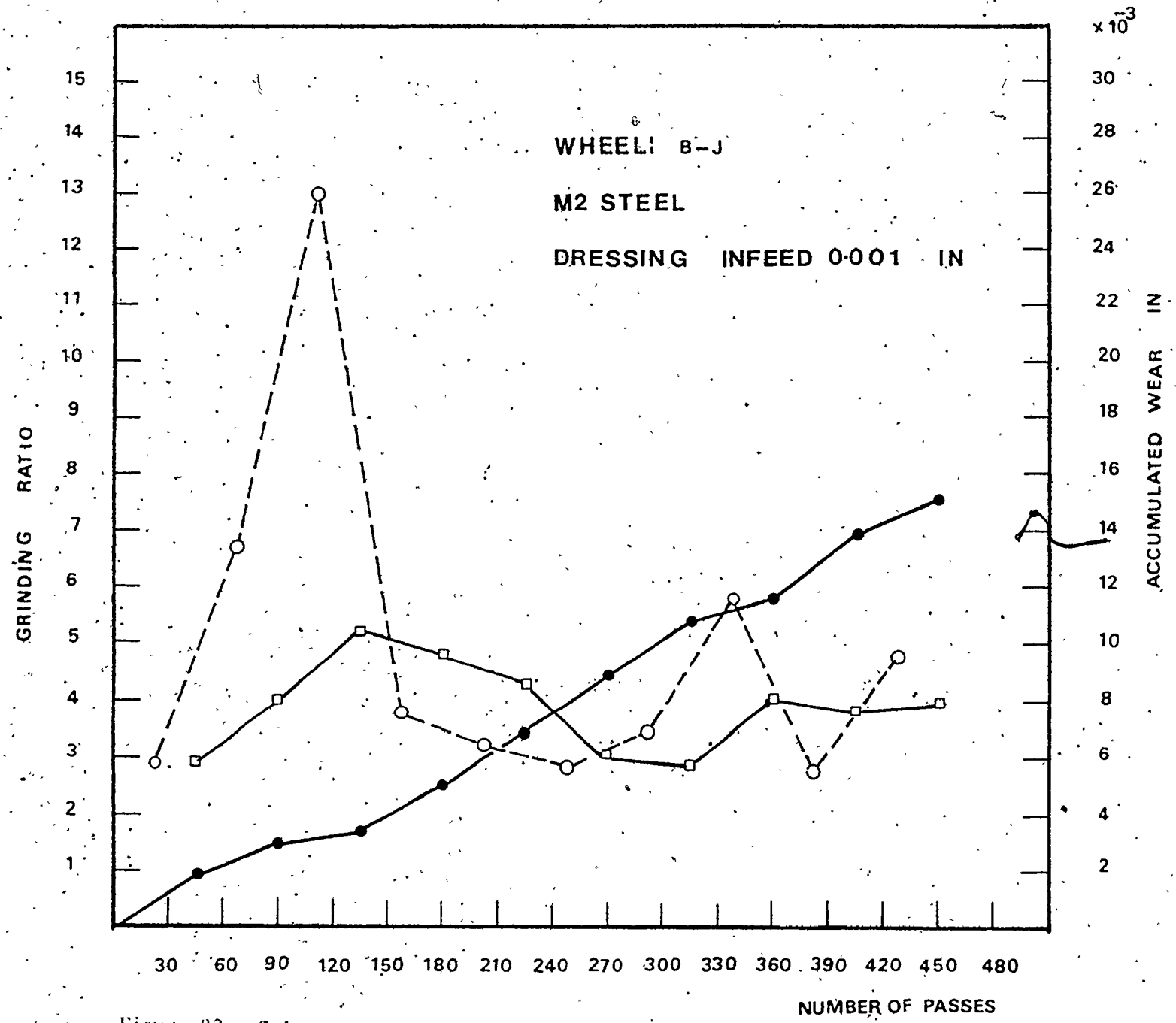

Figure 82. Grinding wheel wear versus number of passes using coarse dressing.

APPENDIX III

TABLES OF RADIAL WHEEL WEAR AND GRINDING RATIO

Grinding Wheel: A-60-J
Material: M_2 Steel
Wheel Speed: 6600 ft/min.

Infeed: 0.001 in.
Table Speed: 100 ft/min.
Test No: (8)

No. of Passes	Height of W/P Before Grinding x_1	Height of W/P After Grinding x_2	Individual Metal Removed $\Delta x = x_1 - x_2$	Accumulated Metal Removed $\Delta \bar{x}$	Accumulated Wheel Wear $\bar{\Delta R}$	Individual Wheel Wear ΔR	Individual Grinding Ratio G	Accumulated Grinding Ratio $\bar{G}$
45	1.300	1.255	0.045	0.045	0.00036	0.0036	17.06	17.06
90	1.255	1.212	0.043	0.088	0.00078	0.00042	13.97	15.46
135	1.212	1.167	0.045	0.133	0.00204	0.00126	4.87	8.90
180	1.167	1.123	0.044	0.177	0.0028	0.00076	7.9	8.63
225	1.123	1.080	0.043	0.22	0.00338	0.00058	10.12	8.88
270	1.080	1.038	0.042	0.262	0.0052	0.00182	3.15	6.88
315	1.038	0.993	0.045	0.307	0.00574	0.00054	11.37	7.30
360	0.993	0.949	0.044	0.351	0.0071	0.00136	4.42	6.75
405	0.949	0.906	0.043	0.394	0.00856	0.00146	4.02	6.28
450	0.906	0.861	0.045	0.439	0.00992	0.00136	4.52	6.04

Table 3. Radial Wheel Wear and Grinding Ratio for A-60-J Wheel.

Grinding Wheel: B-60-J
Material: M_2 Steel
Wheel Speed: 6600 ft/min.

Infeed: 0.001 in.
Table Speed: 100 ft/min.
Test No: (10)

No. of Passes	Height of W/P Before Grinding x_1	Height of W/P After Grinding x_2	Individual Metal Removed $\Delta x = x_1 - x_2$	Accumulated Metal Removed $\Delta \bar{x}$	Accumulated Wheel Wear $\bar{\Delta R}$	Individual Wheel Wear ΔR	Individual Grinding Ratio G	Accumulated Grinding Ratio $\bar{G}$
45	1.260	1.216	0.044	0.044	0.00026	0.00026	23.10	23.10
90	1.216	1.173	0.043	0.087	0.00062	0.00036	16.30	19.15
135	1.173	1.128	0.045	0.132	0.00188	0.0012	5.12	9.58
180	1.128	1.085	0.043	0.175	0.00296	0.00108	5.43	8.07
225	1.085	1.038	0.047	0.222	0.00348	0.00052	12.34	8.71
270	1.038	0.995	0.043	0.265	0.00442	0.00094	6.24	8.18
315	0.995	0.951	0.044	0.309	0.0057	0.00128	4.69	7.40
360	0.951	0.908	0.043	0.352	0.0070	0.0013	4.51	6.86
405	0.908	0.863	0.045	0.397	0.0080	0.00101	6.08	6.76
450	0.863	0.820	0.043	0.44	0.00956	0.00155	3.79	6.28

Table 4. Radial Wheel Wear and Grinding Ratio for B-60-J Wheel.